Acoustic Characterization of Left Ventricular Assist Device Function

Gardner L Yost

B.S., Cornell University, Ithaca, New York, 2012

THESIS

Submitted as partial fulfillment of the requirements

for the degree of Master of Science in Bioengineering

in the Graduate College of the

University of Illinois at Chicago

Chicago, Illinois 2015

Defense Committee

Dr. Thomas Royston, Chair and Advisor

Dr. Miiri Kotche

Dr. Geetha Bhat, Advocate Christ Medical Center- Center for Heart Transplant and Assist Devices

Acknowledgments

This existence of this project, and indeed many projects borne of its explorations, is due, almost entirely, to the efforts of two truly remarkable people: Dr. Geetha Bhat and Dr. Thomas Royston. Each the head of their departments, Heart Transplant and Assist Devices and Bioengineering, respectively, Dr. Bhat and Dr. Royston created the position in which I have worked for the past 18 months from nothing. Each has a passion for innovation, exploration, science, and the education of people around them. Working closely with each has been an honor beyond description- I have learned more fundamentally important lessons in the tutelage of Dr. Bhat and Dr. Royston than I have from any other experience in my life. I will take what they have taught me with me wherever I go, and will be forever appreciative for their kindness, support, trust, and challenges. This work was also made possible by the support of many vital staff at Advocate Christ Medical Center, including the cardiothoracic surgeons Dr. Tatooles and Dr. Pappas; Sejal Modi of Perfusion; and Roxanne Siemeck, Laura Coyle, Maureen Honnessy, Lisa Kukla, and Sudha Kurien of Nursing. Additional thanks to the members of the Acoustics and Vibrations Laboratroy at The University of Illinois at Chicago: Brian Henry, Zoujun Dai, and Ying Peng. A final thank you to Kevin Yost, my father, whose attention to detail, engineering proclivities, and curious intellect I hope will live on in his son.

Contents

List of Tables

List of Figures

List of Abbreviations or Nomenclature

RAAS: renin-angiontensin-aldosterone antagonist system

ACE: Antiogensin converting enzyme

LVAD: left ventricular assist device

CT: computerized tomography

MRI: magnetic resonance imaging

LDH: lactate dehydrogenase

DFT: direct Fourier transform

MAP: mean arterial pressure

LPM: liters per minute

HMII: HeartMate II

AUC: area under the curve

BMI: body mass index

PI: pulsatility index

RVDd: right ventricular dimension in diastole

LVDd: left ventricular dimension in diastole

BP: blood pressure

INR: international normalized ratio

SNR: signal to noise ratio

EF: ejection fraction

MR: mitral regurgitation

RV: right ventricle (ventricular)

LV: left ventricle (ventricular)

RVAD: right ventricular assist device

TID: Ter in die (three times per day)

ICM: ischemic cardiomyopathy

NICM: non-ischemic cardiomyopathy

Summary

Background: Advanced heart failure, a disease typically resultant to insufficient myocardial contractility, is characterized by reduced cardiac output. Reduced systemic perfusion in patients with advanced heart failure causes end-organ ischemia and dysfunction and ultimately results in loss of functional status. The use of left ventricular assist devices (LVADs), implantable pumps used to supplement cardiac output, has become an increasingly common and effective treatment for advanced heart failure. Although modern continuous flow LVADs improve quality of life and survival over medical management of heart failure, device malfunction remains a common concern. Specifically, thrombus formation within the device, a complication occurring in 8-12% of LVAD patients, is life threatening and often requires prompt surgical intervention. Current imaging modalities cannot penetrate the echo- and radio opaque titanium LVAD housing for clinical detection of LVAD thrombosis. Consequently, indirect markers of hemolysis and heart failure must be used for evaluation of potential LVAD thrombosis. Improved non-invasive methods for assessment of LVAD function are needed to detect device complications.

Methods: Sound produced by LVAD operation was recorded with a hand held microphone and uploaded to a personal computer for analysis. Device operation was studied in 70 patients with both axial flow and centrifugal flow LVADs in the operative, inpatient, and outpatient settings. In the laboratory, an axial flow LVAD was implanted in EcoFlex gel and incorporated into a mock-circulatory flow loop. Sound generation under varied pressure, viscosity, and impeller speed rates was studied. Spectral analysis, including peak localization, was used to evaluate samples and to compare acoustic samples.

Results: Peak frequency values measured in vivo were found to correlate strongly with both predicted values and *in vitro* measurements ($r>0.999$). Plots of the area under the acoustic spectrum curve, obtained by integrating over 50 Hz increments, showed strong correlations between *in vivo* and *in vitro* measurements ($r>0.966$). Device acoustics were related to design. Impeller design and the presence of fixed stators in the blood flow field appeared to generate design-specific acoustic signatures. These acoustic signatures were unique to each of 3 different LVAD manufacturers. The presence of simulated thrombus in laboratory experiments caused reductions in spectral amplitude with preservation of curve morphology. This same trend occurred when spectral tracings were compared for indivicual patients with thrombus who had undergone

surgical exchange of their LVAD.

Conclusions: This methodology is sensitive to acoustics generated during LVAD operation in the laboratory and clinical environments. Pump acoustics are dependent upon device design and operation parameters. Our results suggest that pump patency may be assessed using serial measurements of a patient's LVAD acoustics.

Part I

Introduction to Heart Failure and Left Ventricular Assist Devices

Chapter 1

Introduction to Advanced Heart Failure

1.1 Mechanisms and Symptomology

Advanced heart failure is a broad term for a medical condition that involves inadequate cardiac function and related physiological derangements including end-organ dysfunction, neurological complications, metabolic wasting, dyspnea, and loss of functional status. The disease involves numerous organ systems, is highly multifactorial and, as such, does not exhibit homogenous presentation in all patients. Heart failure is a progressive disease which can originate from chronic or acute events. Aberrant neurohormonal regulation of cardiac function is now understood to play a prominent role in the formation of some cardiomyopathies. Specifically, the renin-angiontensin-aldosterone antagonist system (RAAS), which plays a prominent role in vasoconstriction and response to volume depletion and hypotension, is known to result in heart failure when imbalanced[68]. Additionally, chronic cardiac failure can be resultant to valvular disease and high blood pressure, and is known to be associated with a number of comorbidities including obesity, hypertension, arterial disease, and pulmonary disease. Chronic heart failure is often characterized by ventricular dilation, a compensatory mechanism for reduced ejection fraction. Cardiac decompensation can occur as disease severity progresses. Often a life threatening condition, acute decompensated cardiac failure is characterized by development of dyspnea, pulmonary edema, and acutely elevated cardiac filling pressures[81]. Heart failure can also be of ischemic origin in which oxygen and nutrient deprivation can cause irreparable damage

to the myocardium.

The major classifications of myocardial diseases result in impaired generation cardiac output. Systolic dysfunction is characterized by reduction in myocardial contractility whereas diastolic dysfunction refers to abnormal ventricular filling and elevated filling pressures. Systolic dysfunction is most often a result of coronary heart disease, idiopathic dilated cardiomyopathy, hypertension, and valvular disease but also can include peripartum cardiomyopathy, viral myocarditis, and drug induced cardiomyopathies[77, 17]. Diastolic dysfunction, defined as heart failure with an ejection fraction of greater than 50%, is caused by many of the same conditions that cause systolic dysfunction including hypertension and ischemic heart disease.

Though there are no clinical tests for heart failure, several symptoms including dyspnea, fatigue, and fluid retention are present in nearly all patients with advanced stage disease. Diagnosis is often based on patient history and extensive physical exam. Additionally, presence of jugular venous distention and/or leg and ankle edema is common in heart failure[83, 55]. Electrocardiogram, chest radiograph, and echocardiography can be used to gather more information about the electrophysiology, cardiopulmonary structure, and cardiac dimensions, respectively. Additionally, a number of blood tests are utilized to gain better insight into organ function. Complete blood counts indicate anemia or signs of infection, hyponatremia is often associated with severe heart failure and is caused by fluid retention, indicators of liver function are used to estimate severity of right heart congestion, and creatinine is used to evaluate renal function[77, 81, 83].

1.2 Epidemiology of Heart Failure

Over the past centuries, as the United States has transitioned from a rural to an industrial country, the major causes of mortality and morbidity have shifted from infectious disease and nutritional deficiencies to chronic and degenerative diseases like cancer, diabetes, and cardiovascular ailments[4]. The prevalence of heart failure tripled in the years between 1979 and 2004, and continues to increase today[15]. In a population of 304 million Americans, approximately 5.7 million of those over the age of 20 years are living with heart failure- with the addition of 670,000 new cases in adults over the age of 45 years annually[65]. Heart failure, the most costly chronic illness in the United States and other developed countries including the UK and Sweden, costs Americans $23 billion annually[41]. This cost will continue to grow as the number of Americans

over the age of 65 years more than doubles by 2050[19]. It is expected this will drive an increased incidence of heart failure admissions by 1.5 million cases annually. Associated healthcare costs are expected to increase exponentially[19, 47].

1.3 Survival and Treatment for Heart Failure

Though survival with heart failure has been closely monitored in the past 6 decades, great heterogeneity in disease type and severity results in broad survival estimates ranging from 5 to 75% annual mortality[43]. With advances in drugs and devices for treatment of heart failure, survival rates after disease onset have improved over time[42]. Several risk models have been developed to improve prediction of survival in heart failure patients including the Seattle Heart Failure Risk Model and the MAGGIC Heart Failure Risk Model. Both were developed by tracking survival in large groups of heart failure patients and by using multivariate regression analysis to build multi-input models based on commonly available clinical diagnostics[43, 62]. These models aid clinicians in estimating survival and in tracking disease progression as heart failure advances.

Figure 1.1: Temporal Trends in Mortality After Diagnosis of Heart Failure for the Four Decades Between 1950 and 1990

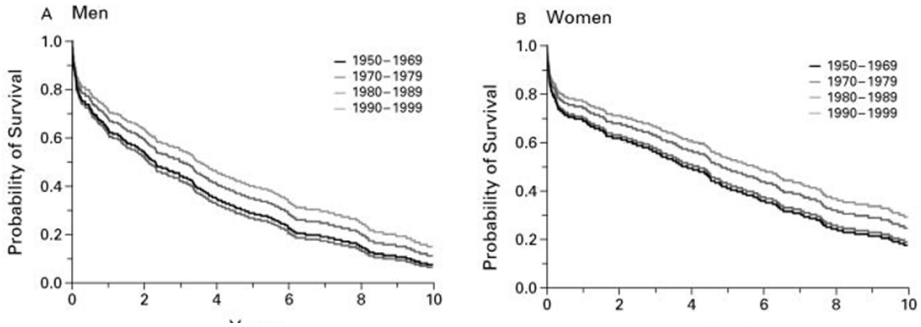

[42]Reproduced with permission from Levy, D, "Temporal Trends in mortality after diagnosis of heart failure for the four decades between 1950 and 1990", N. Engl. J. Med. 347 (2002), pp. 1397-1402, Copyright Massachusetts Medical Society

Heart failure is a progressive and, frequently, terminal disease. As such, pharmacotherapy is intended to reduce symptoms, slow degradation of the myocardial tissue, and minimize mortality. Lower extremity edema is a result of the failing heart's inability to move fluid adequately and causes fluid overload, further straining

the cardiovascular system. Consequently, use of oral diuretics can help return patients to euvolemia and reduce cardiac strain and dyspnea. Angiotensin converting enzyme (ACE) inhibitors are frequently used in patients with heart failure and systolic dysfunction[32]. Though the complete mechanism of ACE inhibitors is not known, it is thought that use of the drug is beneficial in a number of ways, including modulation of response to the RAAS, reduced sympathetic activity, and improvement of enthothelial function, including release of nitric oxide[14, 39, 32, 60, 30]. Following adminstration of ACE inhibitors, beta blockers are used to improve inotropy, chronotropy, dromotropy, and lusitropy in the heart. Beta-blockers act by binding ß1 and ß2 adrenoreceptors in the cardiac nodal tissue, conducting system, and cardiomyocytes, and are used in the vast majority of patients with advanced heart failure[6]. Additionally, inotropic agents, which improve the contractility of the heart, may be helpful in patients with severe ventricular dysfunction. Inotropic agents are used to relieve symptoms and improve end-organ perfusion; however long term use should be avoided due to adverse effects including increased heart rate, myocardial oxygen consumption, and increased risk for atrial arrythmia[57].

While these medical therapies, paired with electrical therapies like implantable pacemakers and intracardiac defibrillators, have improved outcomes in heart failure enormously, most patients progress to advanced heart failure and death. Intravenous inotropic therapy, which has been shown to improve short-term clinical status, still only results in a 1 year survival of 10-30%[70].

Chapter 2

Surgical Treatment for Advanced Heart Failure

When heart failure progresses to a stage in which pharmaceutical and electrical therapy are no longer adequate, there is often indication for surgical intervention. By definition, cardiac surgery is invasive, and the patient must be able to withstand the trauma, blood loss, significant anesthetic dose, and, in most cases, use of cardiopulmonary bypass, requisite to the procedure. Consequently, not all patients are candidates for surgical intervention for heart failure as postoperative outcomes are worsened by preoperative complications including aberrant cardiac pressures, renal, pulmonary, or hepatic failure, non-optimized coagulopathy, cognitive dysfunction, and others. Typical recipients of cardiac surgery have failed medical therapy and are worsening with current treatment, but are not in profound multi-organ system failure. There are many other contraindications to cardiac surgery including obesity, advanced age, poor social support, and non-compliance. However, patient selection is multifactorial and influenced by a team of specialists, who may deem an individual an appropriate candidate despite the presence of one or more apparent contraindications[44]. At this time there are numerous modes of surgical treatment for heart failure including coronary artery bypass grafting, valve reconstruction and replacement, partial mechanical support, total artificial heart implantation, and extracorporeal mechanical circulatory support with or without extracorpo-

real membrane oxygenation. However, heart transplantation and left ventricular assist device implantation are used in patients with severe ventricular dysfunction and are considered the most advanced therapies available[10].

2.1 Cardiac Transplantation

Cardiac transplantation, considered the gold standard in therapy for advanced heart failure, is the surgical replacement of a patient's failing heart with a properly functioning donor heart, typically harvested from a brain-dead donor. The first orthotopic heart transplantation was performed by Dr. Christian Bernard in 1967. At the time, immunosuppression was inadequate to prevent allograft rejection by leukocyte infiltration into the myocardium. Patient survival was limited. However, the advent of transvenous endomyocardial biopsy, which allowed cardiologists to monitor allograft rejection, and the development of cyclosporine, the first effective immunosuppressant for heart transplantation, improved outcomes considerably. The surgery became increasingly common in the late 1970s. Today cardiac transplantation is a widely accepted therapeutic option for patients with advanced heart failure[10].

The vast majority (90%) of patients undergoing heart transplantation have cardiomyopathy of ischemic or nonischemic etiology[79]. These patients typically have low ejection fraction (less than 20%), arrythmias, high pulmonary capillary wedge pressures (greater than 25 mmHg), reduced plasma sodium levels (less than 130 mEq/dL), and elevated b-type natriuretic peptide (greater than 5000 pg/mL), and, without surgical therapy, have an estimated 1 year survival of less than 50%[53, 20].

To perform the surgery, the recipient undergoes median sternotomy, is heparinized, and is prepared for cardiopulmonary bypass. Any form of mechanical circulatory support is removed. With bypass initiated, caval snares are tightened, the ascending aorta is cross-clamped, and the atria are incised along the atrioventricular grooves. The recipient heart is removed and the donor heart is sewn to the atrial cuffs. Following atrial anastamosis, the pulmonary artery and aorta are sewn together, end-to-end. The recipient is weaned off cardiopulmonary bypass and transferred to hemodynamic support generated by the implanted organ[10]. Following transplantation, the patient is moved to an intensive care unit for recovery. All transplant patients maintain strict immunosuppression regimens and periodically undergo invasive venous catheter endomyocar-

dial biopsy to assess graft rejection.

Survival following cardiac transplantation is about 50% at 10 years. Recent advances in postoperative management including treatment of rejection, arrythmias, hypertension, and infection have resulted in improved survivals in recent years, compared to previous eras (Figure 2.1).

Figure 2.1: Kaplan-Meier Survival Plot for Heart Transplant Recipients by Era

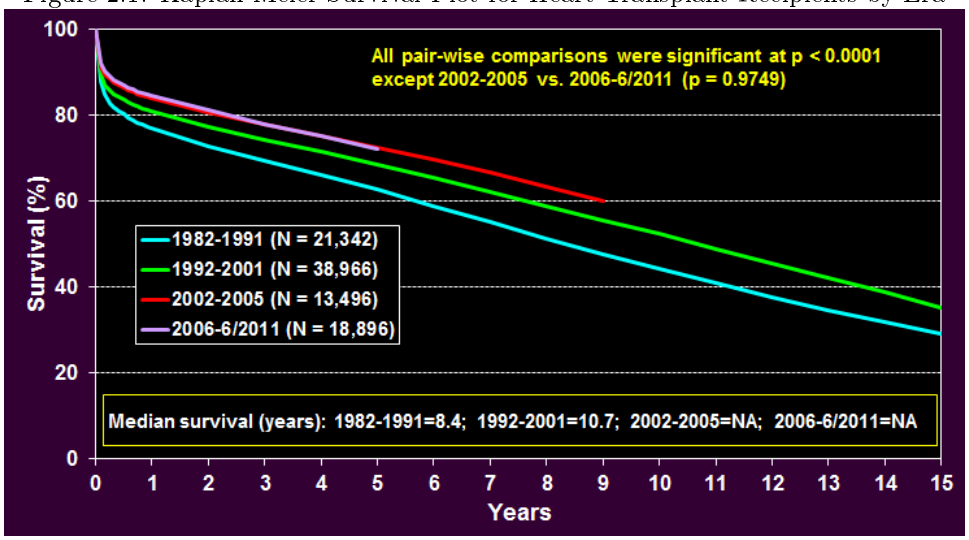

There is significant improvement in survival in the modern era compared to previous results[29].

Despite the favorable outcomes known to be associated with heart transplantation for treatment of advanced heart failure, the number of patients receiving heart transplantation has remained relatively constant for 2 decades. This is due to limited availability of donor organs. Though there are over 5.1 million Americans with heart failure, fewer than 2500 transplantations are performed in the whole of North America each year (Figure 2.2).

The relative paucity of donor hearts available for transplantation has several implications. One is that there are long waiting lists for transplantation and that patients must be optimal candidates to be deemed eligible for the surgery. Second is that there is great need for cardiac support for individuals with advanced heart failure who are not undergoing immediate heart transplantation. This need has driven the development of mechanical circulatory support: the use of artificial pumps to supplement cardiac output in patients with failing hearts.

Figure 2.2: Frequency of Heart Transplant By Year for North America, Europe, and All Others

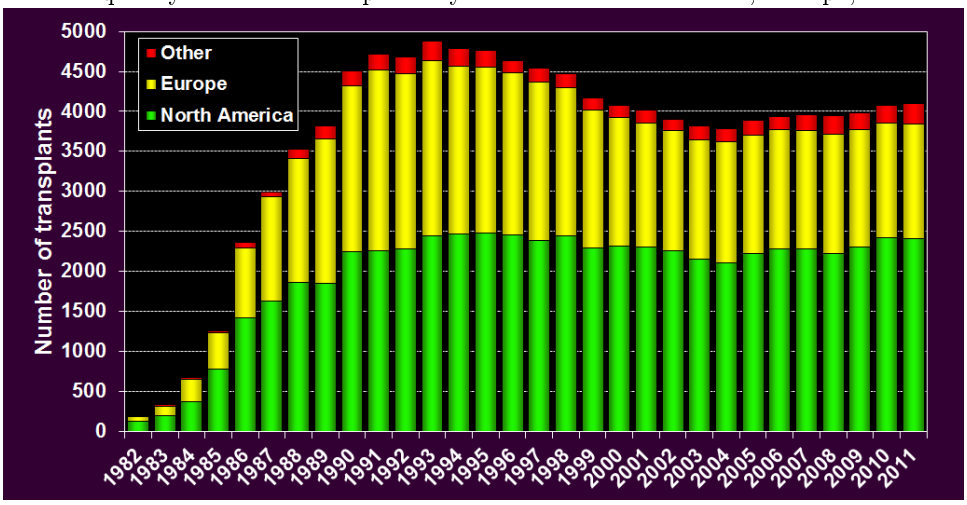

This therapy is severely donor limited and cannot be used for all patients with advanced heart failure[29].

2.2 Left Ventricular Assist Devices

Left ventricular assist devices (LVADs) are surgically implanted blood pumps used to supplement cardiac output in patients with advanced, refractory heart failure[59]. Though medical and electrical therapies for heart failure have advanced significantly in recent years, heart failure often progresses and requires surgical intervention[3, 9]. Inotropic support can improve symptoms and quality of life in the short term, but is associated with a 1-year mortality of 10-30%, and cardiac transplantation is severely limited by a paucity of donors[37, 26]. Newly designed continuous flow LVADs improve hemodynamics, the function of end organs (including the kidneys, pancreas, and liver), quality of life, and functional capability of patients with advanced heart failure. These pumps pull blood from the left ventricle and deliver it to the ascending aorta (in very rare cases, to the descending aorta) using an electrically powered motor[50, 56]. Usage of LVADs as an FDA approved therapy for advanced heart failure increased more than 10-fold between January 2009 and January 2014. This increase is due to the remarkable improvement in patient survival in the modern, continuous-flow generation of LVADs over medical management of heart failure (Figure 2.3). The most recent generation of LVADs has indicated greater than 70% survival at 24 months post randomization, compared to approximately 10% survival in patients with medical management alone (Figure 2.4)[15].

Figure 2.3: Actuarial Survival for all LVAD Patients

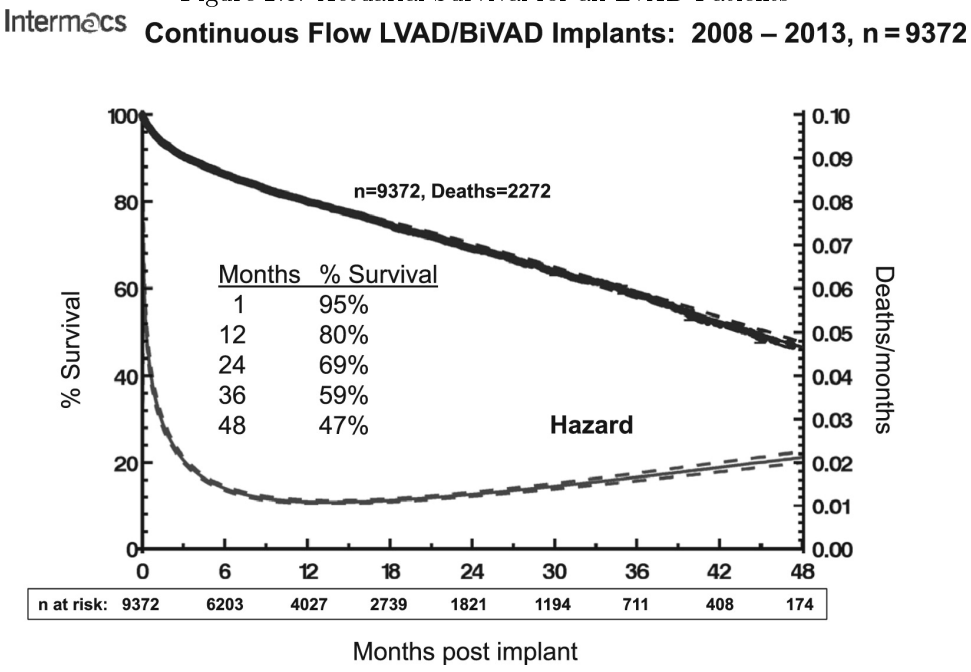

[37]

Figure 2.4: Patient Survival In All LVAD Generations

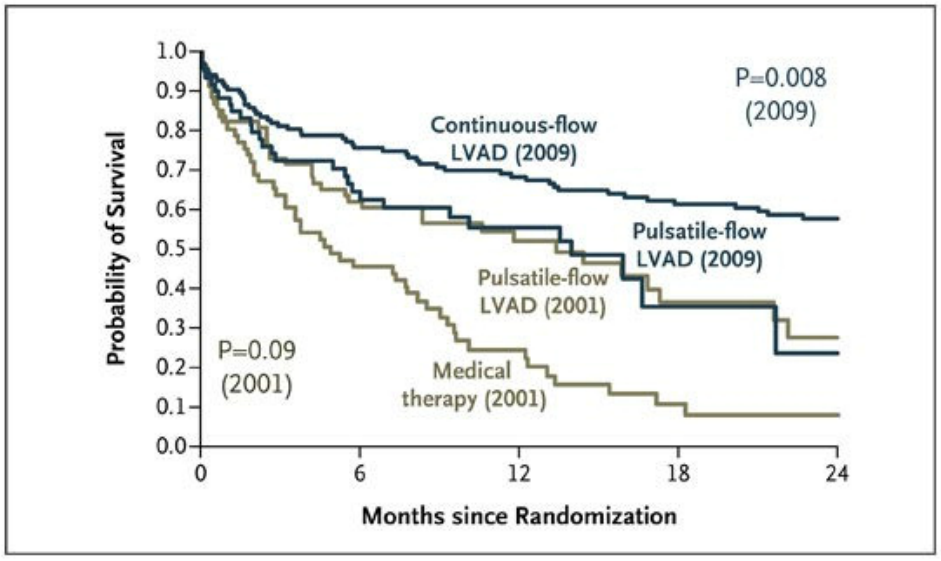

A significant improvement in survival is seen in continuous flow devices compared to both pulsatile devices and medical therapy[16].

LVADs are surgically implanted, typically via a full median sternotomy, with the use of full anesthesia and cardiopulmonary bypass. The surgery requires cardiotomy, the coring of a small hole in the left ventricular myocardial tissue, and sewing of the LVAD inflow tract to to the heart. Blood is moved through the pump by an electric motor and returns to the circulatory system via an outflow graft which is typically sewn to the ascending aorta. Though there are several different pump designs, each uses a percutaneous driveline which powers the pump via external batteries. The driveline exits the abdomen at a bandaged site and connects directly to a pump controller with onboard software for management of pump operation. Patients are free to move around with the use of portable batteries. Typically, wall chargers are used at night[10].

Chapter 3

Left Ventricular Assist Device Design and Operation

Left ventricular assist devices, implanted within the cardiovascular system, represent a major foreign body, and can elicit negative hematologic responses during normal operation. Design of the these pumps is largely focused on minimizing disruption to blood flow while generating enough output to effectively treat heart failure. The physiologic pumping mechanism of the heart generates highly pulsatile flow with aortic valve opening during systole and closure during diastole. Cyclic alteration in blood velocity results in appropriate washing of the circulatory system[52]. When washing is not sufficient and areas of stasis form, either within the LVAD or in other areas of the vasculature, clotting can occur. Modern LVADs are continuous flow, in contrast to the previous generation of pusher plate pulsatile pumps. These pulsatile pumps used pneumatically driven plates with one-way inflow and outflow valves to pull blood into the pumping chamber from the left ventricle and push it out into the aorta. These pumps were known to be effective in treating heart failure, however, due to the large number of moving parts and the friction generated by normal operation, their utility was limited by relative short lifetime. Industry responded to this issue by developing the current generation of pumps, known as continuous flow LVADs. These pumps utilize a spinning impeller which moves blood continuously through the cardiac cycle from the left ventricle to the systemic circulation. No valves

are required for the operation of continuous flow LVADs, and the impellers are driven by electromagnets imbedded within the pump housing. Sequential charging of these fixed magnets exerts a radial torque on the impeller, causing it to spin in place. This relieves the need for a driveshaft, minimizing contact between moving parts and reducing potential locations for fibrin deposition and thrombus formation[72]. The impellers are held in place by several different bearing mechanisms, discussed below. In each system, however, pump operation is wholly controlled via alteration of impeller speed. Besides increasing flow through the device, the speed of the impeller also effects intraventricular and intraaortic pressures, the frequency of aortic valve opening, pulsatility, cardiac dimensions, and power consumption. Current devices lack direct measurements of flow generated by the device. Instead, an estimation incorporating impeller speed, power consumption, and in the HeartWare HVAD, the patient's blood viscosity (or hematocrit), which must be manually inputted into the device controller, is used. Intraoperative comparison of the flow estimation generated by the HeartMate II pump against flow measured by an ultrasonic probe placed on the pump's outflow graft demonstrated a R^2value of only 0.56, indicating an inaccuracy ranging from 15-20%[71].

Though ventricular contraction is severely impaired in advanced heart failure, increased pressure is generated within the left ventricle during systole. Depending on the strength of the contraction, the speed of the pump, and the volume status of the patient, variation in cardiac ejection occurs with the cardiac cycle. This is quantified in the HeartMate II using the pulsatility index or P.I. which is calculated via equation 3.1.

$$PI = \left(\frac{MaxFlow_{15} - MinFlow_{15s}}{AvgFlow_{1min}} \right) \times 10 \tag{3.1}$$

Where PI is HeartMate II pulsatility index, $AvgFlow_{1\text{min}}$is the average flow over the previous minute of operation, $MaxFlow_{15\text{s}}$ is the 15 second maximum flow, and $MinFlow_{15\text{s}}$ is the 15 second minimum flow.

The HeartWare device does not use calculated PI, but rather displays a graphical waveform of flow over time which allows clinicians to assess pulsatility. Physicians integrate these parameters as well as numerous other clinical signs and symptoms to determine optimal long term treatment of the LVAD patient[51].

3.1 The HeartMate II: An Axial Flow Pump

The HeartMate II is the most prevalent rotary LVAD currently used for treatment of advanced heart failure[27]. The pump utilizes an axial flow design with left ventricular and ascending aortic cannulation. The device itself is cradled in a surgical pump pocket below the cardiac margin and between inflow and outflow elbow connectors. Blood first enters the HeartMate II through a titanium cannula which sits within the left ventricle[7]. A flexible woven Dacron graft protected by silicone sheathing carries blood from the intraventricular cannula to a titanium inflow elbow which is directly attached to the pump body. The pump body, displacing 124 mL and weighing 290 g, is primarily constructed of titanium and houses the motor assembly. Consecutive charging of magnets fixed radially around the pump bore generates a spinning magnetic field and imparts rotational torque on the impeller, causing it to spin. As blood enters the 12 mm diameter pump bore it first encounters a three-vaned inflow stator[27]. The neutral, airfoil shaped vanes on the stator remove pre-rotation of the blood and suspend the impeller via one of two ball-and-cup bearings. Distal to the inflow stator, the spinning three-bladed impeller imparts radial and axial velocity to the blood flow field. The impeller is suspended by a second mechanical bearing at the outflow stator. Unlike the inflow stator, the vanes of the outflow stator are curved to convert radial blood rotation to axial velocity at the pump outflow, generating net increase in blood pressure across the pump. Blood exits the pump through a second woven Dacron graft which typically is sewn, end-to-side, to the ascending aorta.

The pump housing and the impeller surfaces are smooth titanium, however, sintering of the stators and intraventricular cannula improves biocompatibility[7, 27, 51]. Blood flow in the HeartMate II can be thought of as fluid moving through a pipe. The impeller behaves like an Archimedes screw, advancing fluid towards the outflow conduit. This design results in a relatively little change in blood flow with change in pressure differential between inflow and outflow conduits (known as head pressure). This can be represented as a steep negative slope in the HQ curve shown in Figure 3.2 for an axial flow pump. The HQ curve demonstrates that the HeartMate II operates over a relatively small range of flows for large changes in head pressure. As a result, flow through the HeartMate II is less affected by contractions of the left ventricle than other pump designs which respond more acutely to changes in head pressure (Figure 3.2). However, blood flow is largely dependent on patient fluid status and impeller rotational speed. Pump speed is set for each patient in the

Figure 3.1: HeartMate II Design and Placement

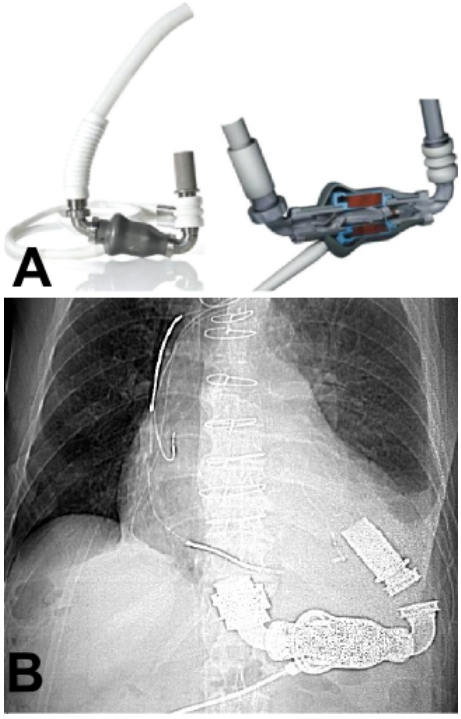

A: design of the HeartMate II LVAD showing the sintered titanium inflow cannula, cross section with impeller and stators, and woven dacron outflow graft. B: Surgical placement of the HeartMate II in the preperitoneal pocket below the heart. Some dissection may be required to create a space for the pump to sit without disturbing blood flow through the outflow graft.

clinic and typically ranges between 8600 and 9800 RPM with the pump achieving flows of 3-7 L/min[51].

Figure 3.2: HQ Curves- Centrifugal and Axial Flow Pumps

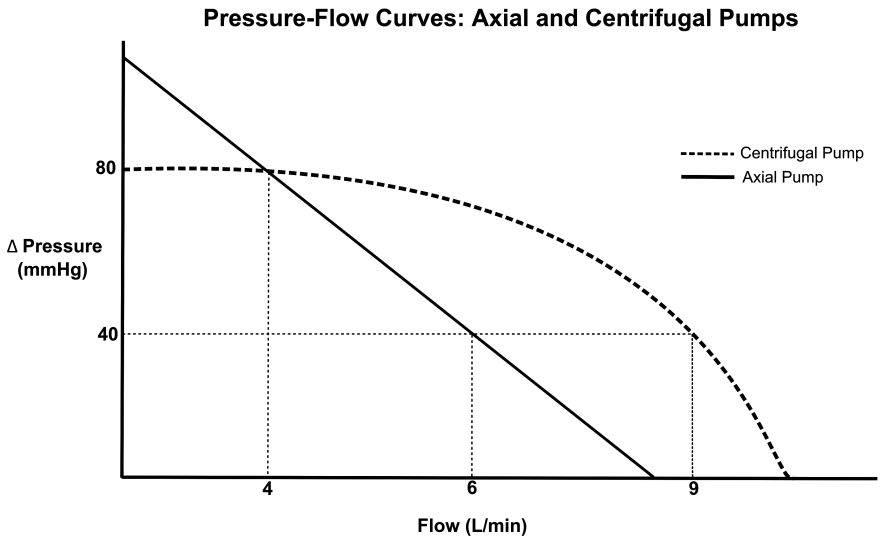

HQ Curve for the HeartMate II axial flow pump versus the HeartWare HVAD centrifugal pump. The axial flow pump generates a narrow range of flows over a range of pressures while the centrifugal pump generates a wide range of flows over a range of pressures.

3.2 The HeartWare HVAD: A Centrifugal Flow Pump

The HVAD is a small centrifugal pump with an integrated pump housing and inflow cannula that permits surgical placement within the pericardial space. Blood enters this 50 ml, 145 g pump through a sintered titanium inflow cannula and is accelerated by a wide-bladed, disk shaped impeller before exiting through a 10 mm tangential outflow conduit[40]. The impeller utilizes electromagnetic and hydrodynamic thrust bearing levitation systems, allowing for operation without mechanical bearings. The impeller contains rare earth magnets which permit magnetic alignment and levitation within the pump housing as well as magnetic coupling to the two motors contained within the front and rear housing assemblies.

This device does not incorporate blood diffusing or straightening stator vanes like the HeartMate II and Jarvik 2000 pumps do. Rather, blood moving through the HVAD contacts only the pump housing and the spinning impeller[73, 56]. The HVAD is designed to operate at speeds of 1,800 to 4,000 RPM with a maximum

Figure 3.3: Design and Placement of the HeartWare HVAD

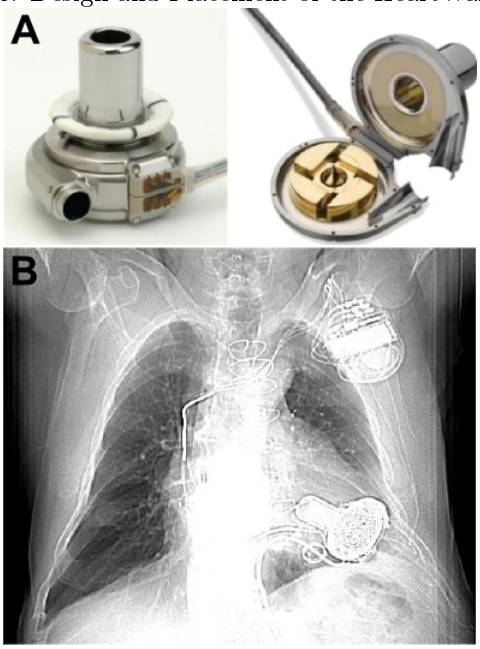

A: Surgical Placement of the HVAD within the pericardial space, and B: cross section of the device showing the grooved, disk-like impeller (gold), pump housing (silver), and driveline (cord structure).

output of 10 L/min. The HVAD, unlike the axial flow pumps, has a relatively flat HQ curve, operating across a wide range of flows for small changes in pressure across the pump (Figure 3.2). Consequently, as shown in Figure 3.3, the flow response of the HVAD to pressure change results in significant flow pulsatility during the cardiac cycle[54]. Normal operation of the HVAD reveals cyclic pulsatility of blood flow and wattage across time in response to left ventricular contraction (Figure 3.4)[51, 40, 56].

Figure 3.4: Flow Waveforms- Centrifugal and Axial Flow Pumps

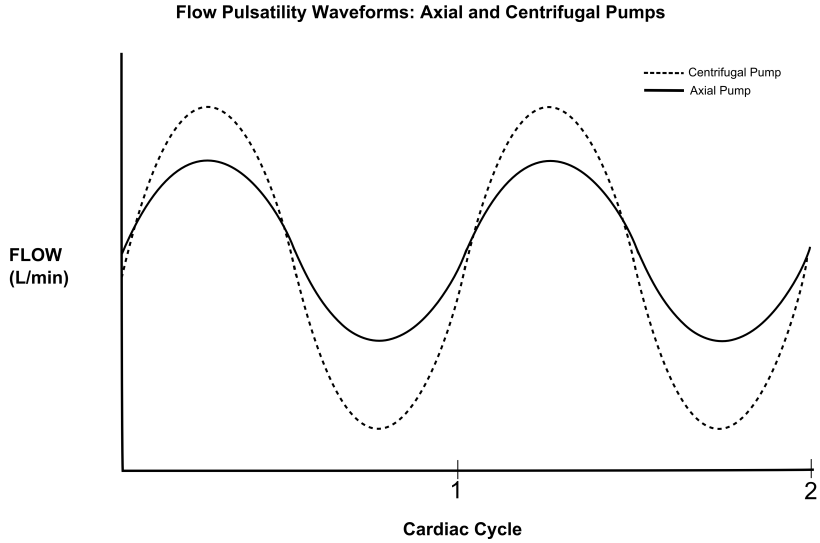

Flow variation in the HeartWare HVAD centrifugal pump is greater than that of the HeartMate II axial flow pump.

3.3 The Jarvik 2000: An Axial Flow Pump

Like the HeartMate II, the Jarvik 2000 is an axial flow pump which makes use of a screw-like impeller suspended within a pump housing between two fixed bearings. This 90 g, 2.5 cm diameter pump is approximately the size of C-cell battery and displaces 25 mL[23, 21]. Unlike the HeartMate II, the pump housing of the Jarvik 2000 is implanted within the left ventricle, meaning blood does not need to pass through an inflow conduit or elbow connector before reaching the pump motor[82]. The two-bladed impeller is driven by fixed electromagnetic motors in the same manner as the HeartMate II, and is suspended, via ceramic

bearings between an inflow cage and a three-vaned outflow stator. All blood contacting surfaces are made of smooth titanium[69, 22]. While the 16 mm Hemashield outflow graft in the patient investigated in this study was sewn to the ascending aorta, the Jarvik 2000 design allows for anastomosis to either the ascending or descending aorta. The Jarvik 2000 is designed to provide up to 7 L/min of support at a maximum speed of 12,000 RPM[75].

Figure 3.5: Design and Placement of the Jarvik 2000

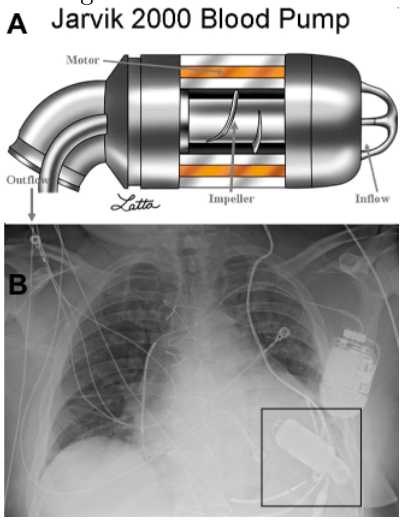

A: Design of the Jarvik 2000 showing the two-bladed impeller, inflow, and outflow track, B: Surgical placement of the device within the left ventricle.[33]

3.4 Pertinent Design Considerations: Differences in Pump Function

Bearings are used within all pumps to support the impeller as it turns within the stationary pump housing. Of note, the axial flow and centrifugal flow LVADs utilize distinct bearing design. The HeartMate II impeller is suspended between the stationary inflow and outflow stators via two mechanical bearings. Though these bearings provide excellent stability in respect to the 6 degrees of freedom, mechanical contact between the rapidly turning impeller and stationary support generates friction and can lead to fibrin deposition and formation of thrombus. Theoretically, friction at these bearing surfaces makes them life-limiting in the long

term operation of LVADs. The HVAD centrifugal flow system makes use of a dual non-contact bearing system. The impeller surface is grooved such that hydrodynamic lift is generated as the impeller turns. The lift separates the impeller from the posterior and anterior surfaces of the pump housing, generating a load-bearing fluid film to support the impeller. The impeller is also balanced by an electromagnetic bearing, which generates a repulsive force between the impeller and the middle column of the pump housing when the pump is powered on. Importantly, both the hydrodynamic and magnetic bearing systems rely on proper pump function and electronic control to maintain impeller position[40, 56]. In the event of a software error, power supply inadequacy, or physical obstruction, it is possible for the impeller to become imbalanced. Departure from the prescribed impeller position will result in non-ideal blood flow path formation, potentially increasing residence time within the hydrodynamic bearing. This, or other forms of aberrant flow through the pump may cause increased stress on blood and blood components[35]. In contrast, the mechanical bearings used in the HeartMate II do not allow for abnormal impeller movement unless physically damaged or altered.

As indicated in Figures 3.2 and 3.4, the hydrodynamic response of the axial and centrifugal pumps to changes in pressure are different. The slope of the HQ curve shown in Figure 3.2 indicates the wide range of flows over which the centrifugal pump operates across the pressures ranges relevant to physiologic systole and diastole. This means that during a single cardiac cycle, the velocity of the flow varies greatly, and the pump generates highly pulsatile flow. In contrast, the axial flow pump operates within a narrow flow range for all physiologic pressures, and as such, evidences relatively little pulsatility during a cardiac cycle.

Most patients with LVADs sustain low grade hemolysis, breakdown of blood components, for the duration of their support. Device manufacturers strive to minimize hemolysis with minimally destructive design, but rapid rotation of the impeller is associated with shear stress in the blood field, which can cause hemolysis. Axial flow design is associated with higher rotational velocities at the impeller blade tips as well as minimal clearance between impeller and device housing, both contributors to hemolysis[28, 11]. The design utilized by the HVAD can result in high residence time in the fluid film that comprises the hydrodynamic bearing[54]. However, proper pump architecture ensures that blood moves swiftly through the fluid film, mitigating hydrodynamic bearing hemolysis. These design features may be relevant, also, to the formation of pump thrombus. The mechanical bearings used in the HeartMate II, where heat and particle generation can occur, represent potential sites for fibrin deposition and thrombosis. Sufficient washing of these bearing surfaces

should prevent blood component deposition. However, the stator vanes at the inflow and outflow of the pump, which are intended to remove blood rotation, are optimized for a single pump condition corresponding to approximately 5 liters per minute of flow at 10,000 RPM. When these conditions are not met, it is possible that areas of stasis or impeded blood flow form within the pump, resulting in suboptimal washing of the bearings[76]. This is a potential contributor to increases in thrombus formation observed in the HeartMate II.

Chapter 4

Clinical Complications Associated with LVAD Support

As discussed in Chapter 1, mechanical circulatory support is associated with significant improvements in survival, functional capacity, and quality of life when compared to medical management. Presumably this is due to improved perfusion of end organs and tissues. Unfortunately, long term support with LVADs is associated with a large number of complications which can be inconvenient, frustrating, and/or lethal. A significant portion of patient morbidity and mortality while on LVAD support is due to complications associated with device operation[37].

4.1 Driveline Infections, and Effects of Systemic Blood Flow Alteration

The presence of the LVAD generates numerous complications, most of which are associated with perturbation of hematologic and hemodynamic systems. However, driveline infections are also common and notoriously difficult to control. Each LVAD is powered by a driveline, or power supply cord, which exits the body through the muscle wall of the abdomen. The exit site is a permanent wound which must be cared for painstakingly

to minimize the chance of infection. The wound should be clean and bandaged at all times, but mechanical tugging of the driveline, lack of proper sanitation, and inadequate healing can lead, nonetheless, to infection. Bacterial colonization often spreads from the epidermal wound site, up the driveline where it can cause life-threatening LVAD-pocket infections and sepsis. Future designs will incorporate transcutaneous charging using induction coils, relieving the necessity for a percutaneous driveline[61].

Continuous flow LVADs, unlike their pulsatile predecessors, generate no cyclical changes in blood velocity or pressure during normal operation. Though some pulsatility generated by the contraction of the left ventricle is preserved, it is significantly less than typical of the native heart. The degree of pulsatility produced in a continuous flow LVAD depends on cardiac dimension, LVAD speed, blood pressure, hydration status, and other variables. The aortic valve does not open during each cardiac cycle in most patients with mechanical circulatory support. This results in lack of detectable pulse in the systemic arterial vasculature. It is currently thought that this lack of pulsatile flow may result in inadequate washing of some vascular sinuses, and may also cause increased stress on the vascular endothelium. LVAD patients often suffer from recurrent epistaxis, gastro-intestinal bleeding, and both ischemic and hemorrhagic stroke, potentially resulting from this lack of pulsatile flow[1, 2]. Further, patients with continuous flow LVADs often present acquired Von Willebrand's disease which is marked by lack of Von Willebrand multimers- blood components required for appropriate clotting[49].

4.2 LVAD Hemolysis and Thrombosis

Of eminent concern in the use of LVADs is the formation of thrombus within any portion of the device. Device thrombosis, essentially the formation of clot within the inflow tract, pump housing, or outflow tract, impedes proper blood flow and can cause device malfunction. Typically, clot formation is precipitated by fibrin deposition on one or more device surfaces. Fibrin provides a matrix for the recruitment of denatured protein and other blood components to the site of the thrombus, resulting in expansion[48]. Clot formation appears to occur, commonly, at the inflow and outflow bearings of the HeartMate II where there is friction between moving parts. The pump relies on fluid for lubrication and dissipation of heat at these bearing locations, and in the absence of adequate flow through the device, it is possible that thrombus formation

begins at the bearing surfaces[74]. Further, human blood has been shown to be sensitive to shear-stress induced platelet activation, a prominent concern in LVAD operation[46, 34, 80]. Blood passage across the inflow and outflow stators causes a minor level of shear, but the movement of the impeller blade tips and bearing surfaces through the blood is associated with a clinically relevant degree of shear stress. This can result in both platelet aggregation and the disruption of the von Willebrand clotting factor. The von Willebrand factor, a high molecular weight multimer, attaches to endothelial surfaces, forming fibrous deposits which platelets adhere to. Platelet aggregation is promoted via interaction of the glycoprotein alpha subunit within the platelet with the A1 domain of the von Willebrand factor. Increased stress on the von Willebrand factor facilitates multimer degradation, resulting in clotting abnormalities[12, 45].

Formation of even minor thrombus within an LVAD threatens proper flow of blood through the device. A perturbation of laminar flow may be sufficient to precipitate further development of a clot, especially where the flow path of blood through the pump is altered. In fact, the presence of thrombus likely generates increased shear stress at the thrombus-blood interface, triggering further fibrin deposition and thrombus formation. Thus, three stages of thrombus formation in the LVAD patient have been suggested: the initial phase in which there is thrombus deposition with hemolysis but no hemodynamic compromise, the second phase in which thrombus formation causes frank hemolysis and abnormal pump function, and finally, complete thrombosis and pump stoppage. Improper pump function is of great concern in the LVAD patient who relies on pump output for adequate systemic perfusion. Consequently, LVAD failure may be associated with acute cardiac and respiratory failure as the patient is unable to appropriately oxygenate in the setting of decreased cardiac output. Lack of perfusion is eventually lethal to the end organs, including the brain. Advanced hemolysis generates increased plasma-free hemoglobin concentrations in the blood. This is known to cause acute kidney injury via renal iron compound deposition and nitric oxide sequestration with subsequent loss of renal microcirculation and ischemia[64]. Further, mobilization of clot formed within the left ventricular assist device threatens stroke or small vessel blockage, a potentially lethal complication. Device thrombosis frequently requires re-operation and pump replacement, an expensive, lengthy, and complex procedure. Re-operation requires accessing the thoracic cavity of a patient who has already undergone at least one prior sternotomy under full anesthesia with the use of cardiopulmonary bypass. Scar-tissue adhesion to the heart, arteries, and rib cage is common in re-operative patients and can make dissection difficult and

time consuming for the surgeon and exposes the patient to longer operative length. Recovery can be painful, lengthy, and frustrating for patients who had been accustomed to independent living with the support of their previous device.

The potential for stroke in the setting of treatment of advanced heart failure with continuous flow left ventricular assist devices has been long recognized, and indeed, usage of chronic anticoagulation in the LVAD patient has been a critical aspect of pharmaceutical care since the development of these devices. Prior to the usage of continuous flow LVADs, the need for anticoagulation in patients with artificial heart valves was well established, largely due to turbulent blood flow through non-native valve architecture[63]. Despite general recognition of the risk for LVAD thrombus, it remains largely unclear at this time what the precise causes of device failure are in most patients. In fact, a recent study of three of the largest LVAD implanting centers in the United States determined that the rate of thrombus has been increasing dramatically[74]. It was found that rates of thrombus at 3 months post-LVAD implantation increased from 2.2% in March 2011 to 8.4% in January 2013 in these three institutions. Further, the median time to pump thrombosis decreased from 18.6 months prior to March 2011 to 2.7 months after March 2011. This same pattern has been observed anecdotally at Advocate Christ Medical Center, where the research reported herein was conducted. Given the potential for patient morbidity and mortality in the event of LVAD thrombosis as well as its increasing prevalence, the need for early detection and, when possible, treatment of thrombus is pertinent.

4.3 Current Methods for Detection and Imaging of Thrombus

Detection of LVAD thrombosis is necessary for diagnosis and subsequent treatment of the issue. Clinically relevant thrombi are typically visible to the naked eye and produce significant alterations within the blood flow field, suggesting that imaging studies may be used for detection. However, the pump housings of the HeartMate II, HeartWare HVAD, and Jarvik 2000 are built from titanium, which is hematologically compatible but opaque to electromagnetic radiation in the wavelengths used for both planar X-Ray and computerized tomography with X-Ray (CT). Though CT cannot be used to image within the pump housing, high resolution images of the polymer inflow and outflow grafts, with the use of a contrast agent, may reveal either thrombus in the grafts, or flow suggestive of thrombus within the device. However, the use of contrast

agents in patients with renal failure or history of acute kidney injury is contraindicated, precluding this modality in many LVAD patients[36, 38]. Magnetic resonance imaging (MRI), likewise is contraindicated in the LVAD patient as many of the device components are magnetic and may shift position in large magnetic fields. Echocardiography is a safe and non-invasive means of intracardiac imaging with the use of ultrasonic imaging. This technique is used frequently, with great effect, in heart failure and advanced heart failure for the measurement of cardiac dimensions, ejection fractions, valve competencies, and blood velocities[25]. Ultrasound waves, like radio waves, are not able to penetrate and image within the device housing however, and often are limited by physical constraints. However, echocardiography does allow for Doppler imaging of blood flow into the LVAD inflow cannula, which has been shown to be aberrant in patients with suspected device thrombus. Specifically, reduced cannula diastolic flow velocity and increased systolic to diastolic flow velocity ratios were shown to be significantly different in patients with suspected thrombus compared to controls[18]. There are no direct laboratory markers for the presence of thrombus, however, because hemolysis occurs in nearly all cases of LVAD thrombosis, it is used as an indirect marker. Hemolysis can be detected via spikes in markers associated with red blood cell disintegration – often a result of increased shear stress at the thrombus-blood interface. The mostly commonly utilized markers are lactate dehydrogenase (LDH) and plasma free hemoglobin, both of which are released from the red blood cell during apoptosis. Clinical signs like hemoglobinura or jaundice can also lead to the diagnosis of hemolysis in the context of LVAD support. LDH has recently been shown to be a better marker than plasma free hemoglobin for hemolysis and thrombus in the HeartMate II axial flow LVAD, but it remains indirect and non-specific, and may be elevated due to other physiologic processes including liver injury [11]. Currently, the only consistently successful treatment for LVAD thrombosis is surgical exchange, which is resource intensive and associated with a large number of potential complications[52]. Alternative therapy is intended to minimize the necessity for surgical exchange and includes treatment of hemolysis with sodium bicarbonate and fluids to reduce risk for heme pigment-induced kidney injury and treatment of the thrombus itself with thrombolytic drugs.

Part II

Experimental Methods for Acoustic Characterization of LVAD Function

Left ventricular assist devices, by nature, operate in a complex environment. The human circulatory system is influenced by a vast number of biological mediators including neurohormonal, biochemical, and structural inputs, all of which can effect the operation of the LVAD. In the context of characterization of device function, quantification of each of these factors is impossible. Consequently, our approach was two tiered, incorporating both laboratory and human-subject measurements. Laboratory investigation required simulation of the human circulatory system, with allowance for variation of fluid pressures, flow rates, viscosities, and LVAD speed. Device acoustics were also measured in human subjects supported with LVADs.

Recording of device acoustics required a non-invasive microphone apparatus which would be easy to use, sensitive in the frequency ranges relevant to LVAD operation, and inexpensive. In fact, such microphones have been used for hundreds of years by physicians, and a recent development rendered them perfectly suited for our purpose. The stethoscope is designed to transmit the sounds of the body (primarily heart, lung, and gastrointestinal sounds) to the ear of the clinician. The device typically employs a diaphragm of 1-4 square inches which may be placed directly on the human skin and permits transmission of pressure fluctuations through tubing to an earpiece. Recently, several device manufacturers have developed digital stethoscopes which are capable of amplifying, filtering, and recording the sounds of the human body. Largely, the design of older, non-digital stethoscopes is preserved, allowing for smoother integration of the device into the clinical arena. For the purposes of this study we used the Littmann 3200 electronic stethoscope. The Littmann records sounds in the frequency range 0-2000 Hz, is capable of applying 3 filters, amplifying sound, recording up to twelve 30-second audio clips, and transmitting acoustic data to a personal computer via a bluetooth connection.

Several modes of computer aided acoustic analysis were performed. The Cornell Lab of Ornithology BioAcoustics Laboratory Raven Pro 1.5 software (build 11) was used to generate spectrograms, spectrogram slices, and make acoustic measurements. Spectrographic analysis was performed for each recording. A Hann Window function at 256 samples with 3 dB bandwidth and 22.5 Hz was used. The hop size was 128 and the overlap was 50 percent. The frequency grid used a direct Fourier transform grid (DFT) of 256 samples and a grid spacing of 15.6 Hz. A spectrogram slice function was used to generate frequency vs. amplitude plots for time periods ranging from 0.1 seconds to 30s. A tool within the program permits automated detection of peak frequency, and amplitude within a selected range. This was used to determine peak frequency and

amplitude for individual harmonics visualized in the spectrogram slice. Amplitude and frequency data was manually extracted from spectrogram slices and collected in Microsoft Excel. When appropriate, Student's T-Tests were used to determine if differences in mean frequency, bandwidth, and amplitude were statistically significant.

Differences between measured and expected experimental values were analyzed using Bland-Altman analysis, a means for comparing experimentally and theoretically derived continuously-scaled variables. The Bland-Altman chart is a scatter-plot of the difference of the two samples (measured versus expected values, in this case) on the y-axis and the mean of the two samples on the x-axis[5]. A One-Sample T-Test was conducted to determine the mean, standard deviation, standard error of the mean, 95% confidence intervals for the mean, and significance level for the difference of the measurements. All statistical operations were performed using SPSS version 20 (SPSS Inc., Chicago, Ill)

Additionally, custom software was written in Matlab to further analyze the behavior of the spectrogram slice. The Matlab software implemented the following steps:

i) Return sample rate of data and encode data in file;

ii) Determine the two-sided power spectral density with 50% overlap and Hanning windowing;

iii) Generate spectral slices with respect to frequency and harmonic order; and

iv) Calculate the area under the spectral slices in 50 Hz increments.

Other data were collected from clinical instrumentation and records. This includes hemodynamics, laboratory measurements, blood work, echocardiography results, imaging studies including planar and computerized tomography (CT) X-ray studies, non-invasive blood pressure measurements, subjective clinical assessments, and subjective patient feedback. These results were tabulated in Microsoft Excel and were timestamped to correspond as closely as possible to acoustic measurements.

Chapter 5

In Vitro Model Using the HeartMate II

5.1 Materials and Methodologies

A mock-circulation *in vitro* model was developed and built (Figure 1). A HeartMate II LVAD (Thoratec, Pleasanton, CA, USA) was embedded in EcoFlex (Smooth-On Inc, Easton, PA, USA), a gel with acoustic and viscoelastic properties similar to that of soft biological tissue. The LVAD was suspended within a polypropylene reservoir with volume 1800 mL. EcoFlex is a polyorganosiloxane epoxy with density 1.03 g/mL and Young's modulus of elasticity 57 kPa. The gel was prepared by mixing parts 1A and 1B in a 1:1 ratio by volume and was poured into the reservoir, filling it[67, 84]. The gel was de-aired in a vacuum chamber (5305-1212, Thermo Scientific Nalgene, Rochester, NY) for 5 minutes, then was allowed to cure at room temperature. The polypropylene reservoir was removed once the gel had cured. The LVAD was positioned such that the entirety of the pump housing was contained within the gel and the driveline, inflow cannula, and outflow cannula remained unobstructed and accessible. To the outflow cannula was attached 1.27 cm inner diameter flexible vinyl tubing with length 157 cm. Suspended above the pump and counterbalanced with a 2.27 kg weight to allow for rapid height adjustment, this tubing drained into a PVC funnel to relieve downward negative pressure. The funnel emptied into a 2.84 L reservoir independently suspended and counterbalanced in an identical manner to the outflow tubing. Finally, flexible vinyl tubing drained the reservoir into the inflow cannula of the HeartMate II. The downward gravitational force created

by the column of water in the outflow tubing provided simulation of arterial resistance against which the LVAD worked. Similarly, the column of water above the inflow cannula provided simulation of pressures generated by the left ventricle at the inflow cannula of the pump *in vivo*. The system was leak-free and was operated using both pure water and varying concentrations of a water/glycerin solution. The pump driveline was connected to a pocket controller, which, in turn, was connected to the Thoratec pump driver and monitor apparatus. Using markings on the gel to ensure consistent stethoscope placement, auscultation was conducted at the surface of the EcoFlex. Acoustics, flow, revolutions per minute (RPM), pulsatility, and power consumption data were recorded across a range of inflow pressures, outflow pressures, viscosities, pump speeds, and artificial stenoses. Pressures at the inflow cannula were altered by changing the height of the "left ventricular" reservoir, and consequently the height of the column of water flowing into the pump. The pressure at the outflow cannula, intended to simulate arterial resistance pressures against which the device must pump, was altered in an identical manner.

A number of experiments were undertaken with the purpose of determining how device acoustics were affected by the alteration of inflow pressures, outflow pressures, fluid viscosity, and the presence of artificial stenoses or narrowing of the system tubing.

Figure 5.1: In vitro *apparatus with HeartMate II and circulatory resistance*

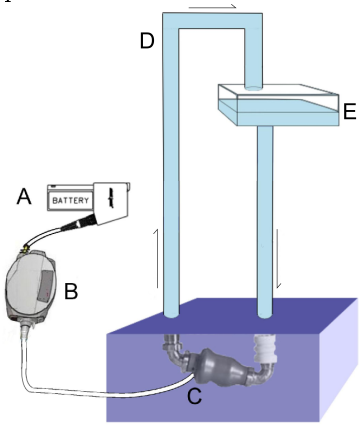

A: Battery energy supply to pump, B: controller unit, C: HeartMate II LVAD unit, D: outflow tubing, E: inflow reservoir. Not pictured: funnel to empty outflow tubing into inflow reservoir.

5.1.1 Mechanical Indentation Test with EcoFlex Gel to determine Young's Modulus

A quasistatic mechanical indentation test was performed to determine the modulus of elasticity at a single point of the surface of the gel where the stethoscope would be placed in the subsequent experiments. A steel cylindrical indenter was used to depress the surface of the gel. The increment of displacement (d) was 0.25 mm and the maximum displacement was 2.0 mm. Displacement was measured using a micrometer and the applied force F was measured using a digital force gauge (DS2-1, Imada, Northbrook, IL). The applied force F is related to the displacement d by

$$F = 2ERd \tag{5.1}$$

where $1/E = (1 - v_1^2)/E_1 + (1 - v_2^2)/E_2$, and $E_1$and $E_2$are the Young's moduli and $v_1$and $v_2$are the Poisson ratios associated with the gel and the steel indenter, respectively. In equation 5.1, R is the radius of the cylindrical indenter. Since the steel indenter is much stiffer than the Ecoflex gel, $E_2 \gg E_1$ and the gel relaxed shear modulus $\mu_0$is related to its relaxed Young's modulus, by $\mu_0 = (E/2(1 + v_1))$ the applied force and displacement ratios may be expressed as

$$F = 2\frac{2\mu_0}{1 - v_1}Rd \tag{5.2}$$

where $2\mu_0/(10v_1)$ can be evaluated from F by the slope of d. With assumed v_1=0.42 μ_0 was calculated under quasistatic conditions using equation 5.2[13].

5.1.2 Stethoscope Placement

The electronic stethoscope was used to auscultate at the surface of the EcoFlex gel. However, it was hypothesized that the location of auscultation may affect the quality or character of sound. Consequently, recordings were made at 6 locations on the surface of the gel so that the signal to noise ratio (SNR) of each might be recorded. During these recordings the inflow pressure was set to 60 mmHg, the outflow pressure was set to 140 mmHg, the device was operated at 9200 RPM, and pure water was used as a fluid. Figure 5.1 shows each of the 6 auscultative locations. A 15 second recording was made at each location. The pump

body, where the majority of vibrations were hypothesized to originate was located longitudinally between sectors two and five (Figure 5.1). Samples were uploaded to a personal computer via the protocol stated in section 5.1.

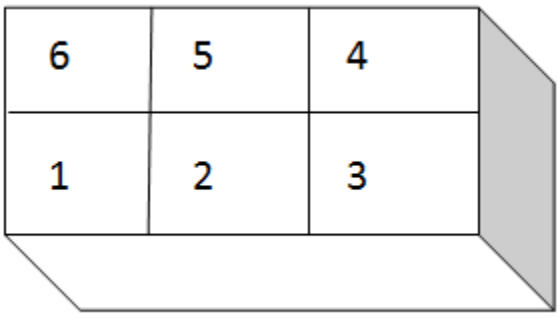

Figure 5.2: 6 Locations on Surface of Gel Tested for Optimal Signal to Noise Ratio

SNR was evaluated for each sample by comparison of amplitudes measured in frequency ranges associated with harmonics generated by normal pump function. It was determined that sector 2 generated the most optimal acoustic measurements. The surface of the gel was subsequently marked to ensure consistency in stethoscope placement in ensuing measurements.

The stethoscope diaphragm was placed lightly on the surface of the gel and held in place by hand for the duration of the measurement. The stethoscope proved sensitive to any movement of the diaphragm across the surface of the gel or any contact with the stethoscope head or tubing. At times aberrant movement introduced unwanted noise into samples intended to only include acoustics of LVAD origin.

5.1.3 Speed Trials "LVAD Ramp Study"

In the clinical arena, LVAD speed is adjusted based on a number of indications including hemodynamic requirements, aortic valve closure, hydration levels, and complications like gastrointestinal bleed and device thrombosis. Consequently, recordings were made in the laboratory which included a range of speeds used clinically, as well as speeds often considered too high and too low to be appropriate *in vivo*. Speed is controlled by the HeartMate II pocket controller at all times and is set by a clinician. Speed does not

change during normal operation. The Thoratec clinical screen and control apparatus displays instantaneous flow, RPM, pulsatility index, and power consumption data. Additionally, the monitor's touchscreen permits clinicians to silence alarms, set low flow limits, browse operational history, and change pump speed. The HeartMate II speed adjusts in 200 RPM increments between 7,000 and 14,000 RPM. Recordings were made at each speed increment between 7,000 and 13,000 RPM using pure water. Flow, power consumption in watts, and pulsatility index were recorded at each increment.

5.1.4 Viscosity Alterations

Viscosity, the measure of fluid resistance to flow, is an important consideration in the usage of artificial blood pumps and can vary during continuous support. Even small changes in viscosity may affect the LVAD's ability to move blood from the left ventricle into the circulatory system. It was presumed that higher viscosities would increase the work required to move fluid through the LVAD, and ,consequently, affect device acoustics. Viscosity was altered using varying concentrations of pure vegetable glycerin (viscosity=934 cP) in distilled water (viscosity=0.89 cP). Blood viscosity, though variable, averages approximately 3.3 cP; the following experiments were conducted at the range of viscosities listed in Table 5.1. 2500 mL of pure water was added to the *in vitro* system, the pump was connected to a pocket controller, in turn connected to the clinical screen apparatus. The pump speed was set to 9400 RPM, room temperature was 24.5 °C, and recordings were made at the following concentrations of glycerin:

Table 5.1: Variable Viscosity with Glycerin Additions

Recording	Glycerin Vol. (mL)	% Weight Glycerin	Soln. Visc. (cP)	Dens. Soln (kg/m^3)
1	0	0	1.005	998.02
2	50	0.024	1.067	1004.6
3	100	0.048	1.113	1010.8
4	150	0.070	1.119	1016.8
5	200	0.091	1.269	1022.5
6	250	0.111	1.342	1027.9
7	300	0.130	1.419	1033.1
8	350	0.149	1.498	1038.1
9	400	0.167	1.580	1042.8
10	450	0.184	1.665	1047.4
11	500	0.200	1.76	1051.8

Abbreviations: Vol. (Volume), Soln (Solution), Visc (Viscosity), Dens (Density)[8]

The viscosity of the glycerin-water mixture was calculated using the parameterization established by NS Cheng in which the dynamic viscosity of the glycerin-water solution, μ, is given by

$$\mu = \mu_w^{\alpha} \mu_g^{1-\alpha} \tag{5.3}$$

where w represents water, g represents glycerin, and α represents the weighting factor of glycerin in the solution varying from 0 to 1. With some derivation, α may be determined by

$$\alpha = 1 - C_m + \frac{abC_m(1 - C_m)}{aC_m + b(1 - C_{m)}} \tag{5.4}$$

where $C_m$is the glycerin concentration by mass, and a and b may be determined by

$$a = 0.705 - 0.0017T \tag{5.5}$$

$$b = (4.9 + 0.036T)a^{2.5} \tag{5.6}$$

where T is the temperature in centigrade and where μ_w and μ_g may be determined, respectively, by

$$\mu_w = 1.790 \exp\left(\frac{(-1230 - T)T}{36100 + 360T}\right) \tag{5.7}$$

$$\mu_g = 12100 \exp\left(\frac{(-1233 + T)T}{9900 + 70T}\right) \tag{5.8}$$

This method is reproduces measured viscosities with 5% error in glycerin-water solutions ranging from 0-100 percent mass in the range of 0-100 °C[8].

5.1.5 Artificial Stenotic Narrowing & Pressure Tests

LVAD thrombosis may manifest as clot adhered to the device impeller, stator vanes, and/or inflow and outflow tracts. Each has the potential to cause significant compromise to pump function. In these experiments, the presence of thrombus in the inflow and outflow tracts was simulated by partial occlusion of the pliable grafts

and vinyl tubing with artery clamps. The clamps were placed at varying locations along the inflow and outflow tract. Occlusion was estimated at 70%. Recordings were made under the following conditions:

Distance from outflow cannula: no clamp, clamp at 30cm, 120cm, 160cm, 200cm, 220cm, 260cm, 300cm.

Distance from inflow cannula: no clamp, clamp at 30cm, 120cm, 160cm, 200cm, 220cm, 260cm, 300cm.

All recordings were made at the surface of the EcoFlex gel at the location noted in section 5.1.2, using pure water as a pumping liquid, with the LVAD set to 10,000 RPM, inflow pressure of 80 mmHg, and outflow pressure of 100 mmHg.

Subsequent tests were undertaken to investigate the effects of changing pressures at the inflow and outflow cannulae of the HeartMate II on device acoustics. Pressure was altered by raising and lowering the the height of the outflow tubing (arterial resistance) and inflow reservoir (inflow pressure). Water pressure generated was assumed to be static, via

$$P_{static} = \rho h g \tag{5.9}$$

where P_{static} is the downward pressure felt at the inflow and outflow cannulae, ρ is the density of the solution, h is the height of the tubing or reservoir for the arterial resistance and inflow pressure, respectively, and g is the force of gravity (9.81 m/s^2). LVAD pumping function is independent of the respective pressures at the inflow and outflow tracts; instead pressure differential (or pressure head) determines instantaneous loading conditions[51]. Consequently, pressure was varied by keeping either the outflow resistance or inflow pressures constant while the other was varied. The following heights and pressure were utilized:

With inflow pressure set at 68.6 cm, 40.5 mmHg, acoustic samples were gathered at outflow pressures:

Table 5.2: Outflow Height and Resistance

Height (cm)	Outflow Pressure (mmHg)	Pressure Differential (mmHg)
101.6	64.8	24.3
114.1	74	33.5
127.0	83.5	43.0
144.8	96.6	56.1
154.9	104.0	63.5

With outflow resistance set at 132.1 cm, 87.2 mmHg, acoustic samples were gathered at inflow pressures:

Table 5.3: Inflow Height and Resistance

Height (cm)	Inflow Pressure (mmHg)	Pressure Differential (mmHg)
35.6	16.2	71.0
61.0	34.9	52.3
81.3	49.9	37.3
91.4	57.3	29.9
104.1	86.6	0.6

Testing parameters were based on physiological pressures experienced during normal LVAD operation. It should be noted that outflow pressures in our model do not reach the pressures generated during systole in healthy adults. There are two reasons for this. First, as discussed in sections 3.1-3.4, arterial pulsatility in the LVAD patient is significantly altered by mechanical circulatory support. Because the aortic valve may be closed in the LVAD patient, systolic blood pressure is shifted towards the mean arterial pressure (MAP). Consequently, a time average of the resistance against which the LVAD must pump is best approximated by the MAP, which averages approximately 90 mmHg in LVAD patients at Advocate Christ Medical Center. Further, systolic and diastolic pressures are an effect of the cyclic process of contraction and relaxation in the native heart and are absent from flow produced by continuous flow devices. Since our model contained only the continuous flow device without a pulsatile pumping chamber, the most relevant arterial resistance pressures were those approximating clinical MAPs. Likewise, the pressures used at the inflow conduit were meant to approximate mean intraventricular pressures in the heart failure patient.

5.1.6 Modal Analysis

Modal analysis was performed on a HeartMate II LVAD using a PCB Piezotronics ceramic piezoelectric accelerometer (model #352A10, sensitivity 10.40 mV/g, mass 0.7 g), a PCB Piezotronics model 086C01 modally tuned impulse hammer with force transducer (PCB Piezotronics, Depew, NY, USA), and an Agilent 35670A Dynamic Signal Analyzer (Agilent Technologies, Santa Clara, CA, USA). With the LVAD suspended by its driveline, the accelerometer was glued to a fixed point in the center of the LVAD using cyanoacrylate. Acceleration was generated radially at 10 points distributed circumferentially around the LVAD, with 3 hammer taps per point to ensure repeatability, which was assessed by confirming near unity coherence between measurements in the frequency range of interest[24, 66]. Data was transferred to a personal computer

and analyzed using custom Matlab software.

Chapter 6

Methods for *In Vivo* Acoustic Measurements

6.1 Devices and Data

A Littmann 3200 electronic stethoscope was used for all measurements. This is the same device used in the *in vitro* studies. Measurements were made for approximately 30 seconds and data were uploaded to a personal computer over a bluetooth connection. Methodology for analysis of the acoustic data was identical to that outlined in Part II with utilization of the Cornell Ornithology Laboratory Raven software and custom software developed in Matlab.

6.2 Patients

All individuals involved in this study were patients of the advanced heart failure service at Advocate Christ Medical Center. This includes patients supported by both the HeartMate II and HeartWare HVAD LVADs. The clinical progression of heart failure is complex, but typically follows a progression of outpatient and inpatient visits for care of advancing heart failure proceeding prolonged admission for assessment of LVAD candidacy, surgical implantation, and recovery and rehabilitation. Following discharge from index admission

for LVAD implantation, patients visit the outpatient clinic at Advocate Christ Hospital for regular follow up visits. Initially, patients will return every 2-3 weeks. Following stabilization, follow-up visits may only be scheduled once per 6 or 8 weeks. However, complications associated with LVAD support, as described in Chapter 4, are frequent and often require unscheduled outpatient visits and/or admission to the hospital. This study included patients at the following time points:

1) Advanced heart failure patients: this includes patients with advanced heart failure who had indication for LVAD implantation, but had not yet received their device. These patients are considered a control against which the noise recorded in a patient with an operational LVAD may be compared. In many cases, recordings were made in patients both before implantation (without LVAD) and following implantation (with LVAD).

2) Post-operative LVAD patients: Immediately following surgical LVAD implantation, patients are intubated, sedated, often have trans-thoracic drainage tubes, and are recovering from sternal division and multiple venous and arterial access. These patients, therefore, were ausculatated no less than 36 hours post-operation.

3) LVAD patients in post-operative rehabilitation: Postoperative recovery is a complex process which typically requires approximately 21 days of recovery for reversal of surgical trauma, nutritional derangements, weaknesses, any iatrogenic or nosocomial complications, and education for device management. Patients are typically awake and ambulatory during this time. Auscultation was performed when clinically appropriate.

4) LVAD patients during scheduled outpatient visits. As mentioned previously, long term LVAD support requires regular follow up in our outpatient clinic. Patients were auscultated at this time.

5) LVAD patients during unscheduled outpatient and inpatient visits: Patients admitted for complications associated with LVAD support were auscultated when the clinical scenario was thought to potentially impact LVAD function, as in the case of emergent device thrombosis. When surgical intervention was required (as for device thrombosis), auscultation was performed both prior to and following the surgery to allow for comparison of acoustics with and without the presence of the complication.

6.3 Method of Auscultation and Clinical Data Collection

The Littmann 3200 electronic stethoscope is similar to other stethoscopes used clinically. It has a small diaphragm, which can be placed anywhere on a patient's body, and amplifies and transmits sounds to attached earpieces.

An initial pilot study was conducted to determine whether there were significant differences in LVAD acoustics at several locations on the patient body. All patients were measured in the supine or upright sitting positions. Acoustics were measured at the mitral, tricuspid, pulmonic, and aortic positions over the heart as well as over the right breast. Samples were transmitted to a personal computer and analyzed using spectral analysis, which allowed for a basic assessment of signal to noise ratio by comparison of amplitude within spectral bands, to background noise. Peak frequencies at each harmonic were compared. It was determined, that, in the HeartMate II LVAD, the most optimum signal was obtained slightly medial to the mitral position. This is the closest exterior location to the HeartMate II implantation site within the diaphramatic pump pocket. Likewise, the strongest signals obtained from the HeartWare were obtained slightly lateral to the mitral site, or approximately exterior to the implantation site within the left ventricular pericardium. These sites would be used for all subsequent recordings.

Standard procedure for recording:

1) Patient asked to recline in chair if upright, or lie on back if supine.

2) If possible, clothing was removed to allow for auscultation at the surface of the skin.

3) Patient asked to breathe normally.

4) Several locations (over the heart) were quickly tested to determine where the highest amplitude signal could be obtained.

4) 1-4 recordings, each 30 seconds in length, were made.

At the time of auscultation the following data were collected: LVAD flow, LVAD speed, LVAD pulsatility (for the HeartMate II only), LVAD power consumption, blood pressure, heart rate, and weight. LVAD parameters were read either from the clinical screen or pocket controller, blood pressure was read from a Terumo Doppler cuff, heart rate from a pulse-oximeter, and weight from a standard scale.

The following data were collected from the electronic medical records as near to the time of auscultation

as possible:

Laboratory parameters including: B-type natriuretic peptide, creatinine, white blood cell count, lactate dehydrogenase, plasma free hemoglobin, sodium, hemoglobin, and international normalized ratio.

Echocardiographic parameters including: ejection fraction, left ventricular end diastolic diameter, right ventricular end diastolic diameter, mitral valve regurgitation, aortic valve regurgitation, and pulmonary artery pressure.

Hemodynamic parameters including: right atrial systolic and diastolic pressures, central venous pressures, pulmonary artery pressures.

Clinical course including: postoperative complications, readmissions, and mortality. Sections 4.2 and 4.3 discuss the formation of LVAD thrombosis as well as its clinical presentation and detection. However, surgical removal of the LVAD accompanied by visual inspection of the pump is the only means by which thrombosis can be confirmed. Consequently, in the 3 patients who underwent LVAD exchange with auscultation, a video bronchoscope was used to visualize thrombus within the device housing. This was done perioperatively, immediately upon removal from the sterile field within the operating room. The bronchoscope's articulating camera was fed into the inflow and outflow sections of the HeartMate II and HeartWare LVADs so that clot could be visualized and photographed.

Part III

Results: *In Vitro* and *In Vivo* Studies with the HeartMate II

Chapter 7

Results from *In Vitro* studies in the HMII

The results presented in this section pertain only to the axial flow HeartMate II (HMII) LVAD. *In vitro* experimentation was primarily conducted prior to the studies *in vivo*. The results of these experiments informed the methodology and analysis of data collected in the hospital as the interaction of pressure, viscosity, speed, and stenoses with LVAD acoustics became increasingly clear. Consequently, though these methods and results are presented in a sequential format, indeed the approach to this project evolved with our understanding of our results.

7.1 Spectrographic Analysis of *In Vitro* HMII Acoustics

A spectrogram generated from an *in vitro* recording with pump speed 8000 RPM, inflow pressure 50 mmHg, outflow pressure 83.5 mmHg is presented in Figure 7.1. The graph may be interpreted as such: the horizontal axis plots the time course of the sample, while the horizontal axis plots the frequency components of that sample. Amplitude is expressed as heat (color), with darker colors representing higher amplitudes. The repeating harmonic structure is immediately evident as harmonic "bands," which occupy frequency ranges of progressively higher amplitude. It is also evident that the lowest harmonic bands, occurring between the

frequency ranges of 150-600 Hz, are the highest in amplitude and that amplitude attenuates as frequency increases.

Figure 7.1: Spectrogram For *In Vitro* Operation of a HeartMate II LVAD at 8,000 RPM

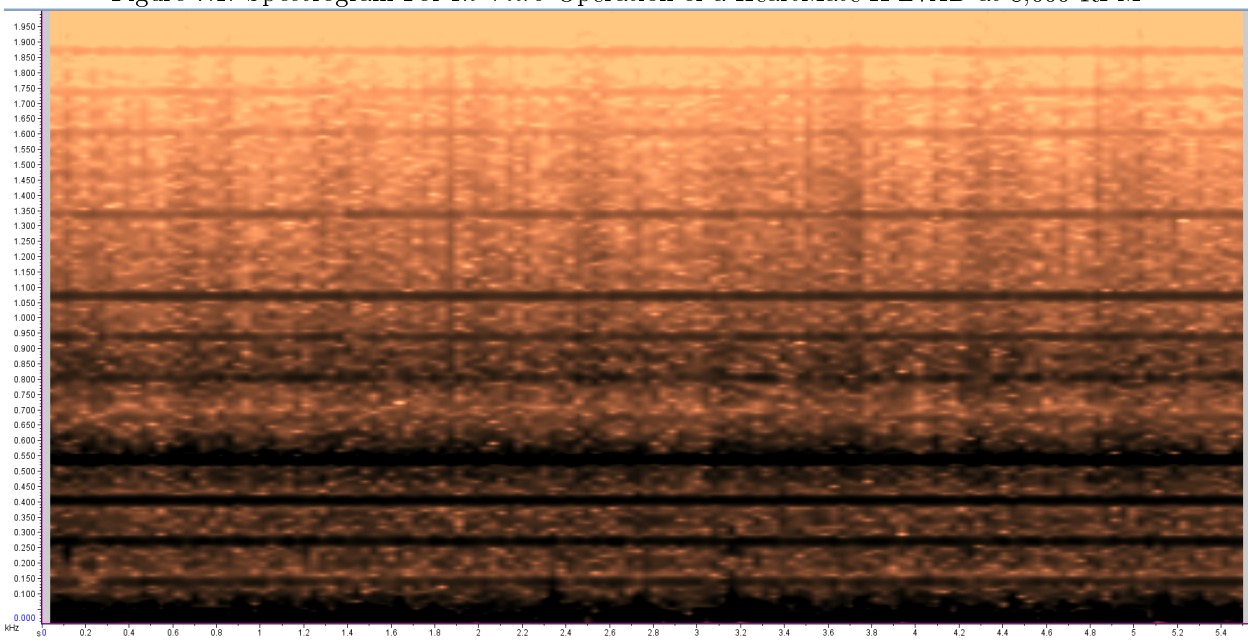

A spectrogram slice, a plot of amplitude (vertical axis) versus frequency (horizontal axis), allows for more nuanced analysis of an acoustic sample's frequency components. The spectrogram slice for the acoustic sample plotted in Figure 7.1 is provided in Figure 7.2. Peaks in the spectrogram slice correspond to harmonic bands in the spectrogram, and accordingly, are repeated in a regular manner. The spectrogram slice allows improved analysis of frequency ranges between harmonics. As described in Part II, Raven Pro software allows for automated detection of the frequency with maximum amplitude within a selected range. This tool was found to be exemplary for determining the precise frequency peak location in the spectrogram slice, as well as its corresponding amplitude value. Automated peak detection was used to record peak frequencies and amplitudes for all harmonics. It appeared that the frequencies of the harmonics expressed in the spectrogram and spectrogram slice were related to device speed. A series of speed trials, in which the HeartMate II speed was increased regularly in 200 RPM increments, were undertaken to investigate this hypothesis.

Figure 7.2: Spectrogram Slice For *In Vitro* Operation of a HeartMate II at 8,000 RPM

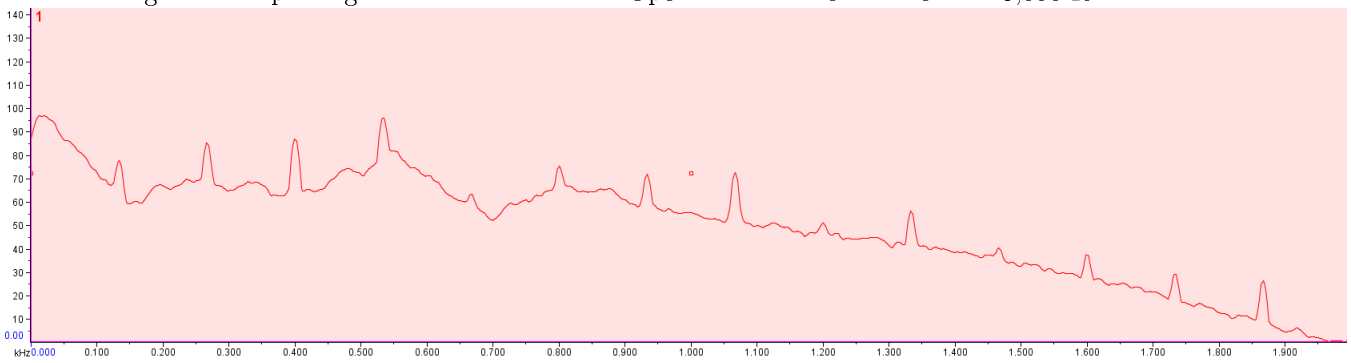

7.2 Speed Trials - "LVAD Ramp Study"

Speed is increased in the HeartMate II using the clinical screen apparatus, as mentioned previously. Higher speeds are achieved by increasing the frequency with which the fixed magnets in the pump housing are charged, a change that demands increased power supply. Consequently, with constant pump loading conditions, power increases with speed. Accordingly, as the impeller turns more rapidly, flow through the device also increases. This was observed in all cases during *in vitro* testing.

Recordings were made at each of the incremental speeds listed in Table 7.1. Flow was recorded when available.

Measures of flow were not calculated for recordings 1-9. The HeartMate II calculates and estimation of flow using device speed and wattage. This is based on the nearly linear relationship between power consumption and impeller rotational speeds at speeds typically used clinically; 8,800-10,000 RPM. However, outside of this range, the accuracy of the flow estimation decreases considerably. Consequently, when flows are too low or too high, the device will display (—) or (+++), respectively, to indicate that flow estimations are not currently accurate. Additionally, pulsatility, unlike power and flow, showed no trend with increasing speed. Pulsatility, measured as the pulsatility index is calculated via

$$PI = \left(\frac{MaxFlow_{15} - MinFlow_{15s}}{AvgFlow_{1min}} \right) \times 10 \tag{7.1}$$

Where PI is HeartMate II pulsatility index, $AvgFlow_{1\text{min}}$is the average flow over the previous minute

Table 7.1: *In Vitro* Ramp Study with the HeartMate II

Recording	Speed (RPM)	Power (Watts)	Pulsatility	Flow (LPM)
1	7,000	1.6	2.3	—
2	7,200	1.9	2.2	—
3	7,400	2.3	2.2	—
4	7,600	2.6	2.7	—
5	7,800	2.8	2.6	—
6	8,000	3.1	1.9	—
7	8,200	3.5	1.8	—
8	8,400	3.8	2.6	—
9	8,600	4.1	2.5	—
10	8,800	4.5	2.4	3.2
11	9,000	4.9	2.7	3.4
12	9,200	5.2	2.4	3.5
13	9,400	5.5	2.7	3.8
14	9,600	5.9	2.2	3.9
15	9,800	6.4	2.2	4.4
16	10,000	6.7	2.1	4.4
17	10,200	7.0	2.4	4.7
18	10,400	7.4	2.6	4.8
19	10,600	7.9	2.3	4.8
20	10,800	8.2	2.3	5.2
21	11,000	8.5	2.2	5.4
22	11,200	8.6	2.0	5.5
23	11,400	9.0	1.9	6.0
24	11,600	9.5	1.8	6.2
25	11,800	10.1	1.8	6.4
26	12,000	10.6	1.8	6.7

Figure 7.3: *In Vitro* Ramp study with the HeartMate II

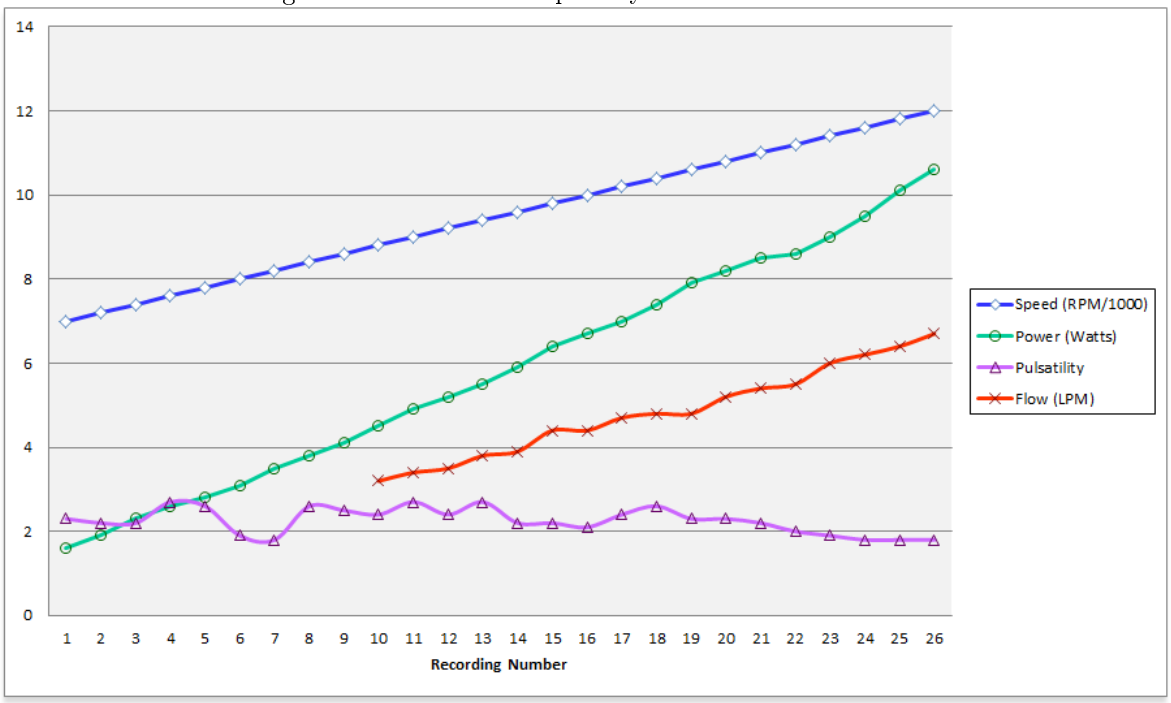

of operation, $MaxFlow_{15s}$ is the 15 second maximum flow, and $MinFlow_{15s}$ is the 15 second minimum flow. When the device is implanted in the native heart, residual contractility of the left ventricle creates maximum and minimum flows during the cardiac cycle, and pulsatility can be calculated. However, because the system used in these laboratory experiments lacks a pulsatile pump in line with the LVAD, pulsatility is meaningless.

Auscultation was performed for each of the 26 speeds listed in Table 7.1. Peak harmonic frequency increased linearly with speed for all harmonics and all speeds. Figure 7.2 plots peak frequency (vertical axis) for each harmonic 1-12 (horizontal axis) for speeds between 7,000 and 12,000 RPM.

Figure 7.4: Acoustic Analysis: *In Vitro* Ramp Study

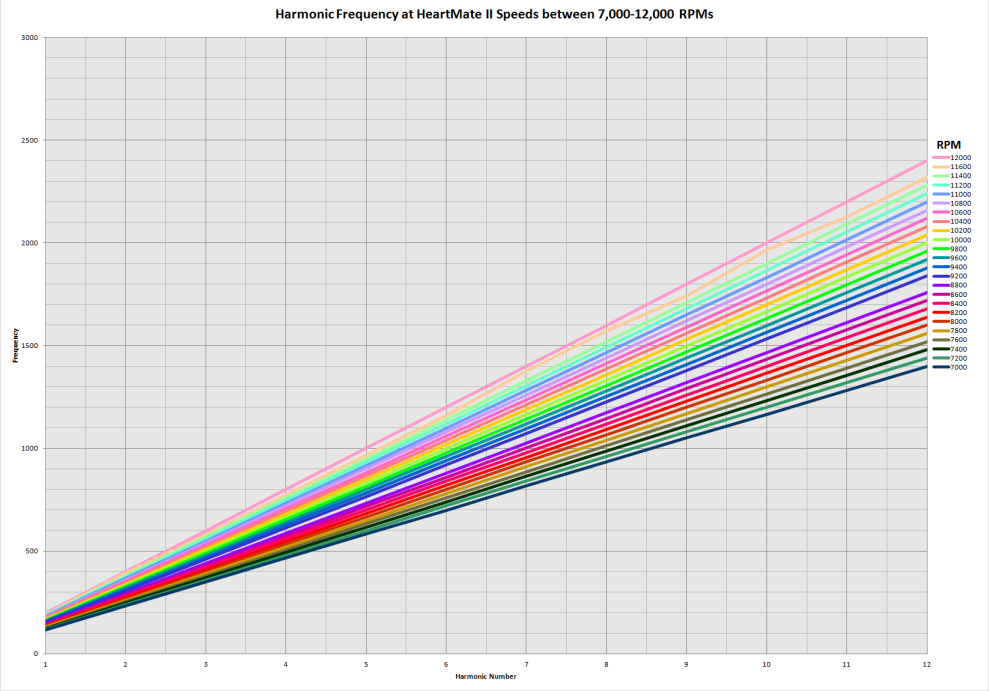

The relationship between device speed and peak harmonic frequency is linear, and can be described using

$$\lambda_{h(HMII)} = \frac{(n \times RPM)}{60} \tag{7.2}$$

Where $\lambda_{h(HMII)}$is the expected harmonic frequency in the HeartMate II, n is the harmonic number, and RPM is the device rotational speed at the time of auscultation. λ_h was calculated for harmonics 1-12 for

each speed measured during this ramp test. Figure 7.3, a Bland-Altman graph, indicates the agreement between predicted and measured peak harmonic frequency at all speeds.

Figure 7.5: Bland-Altman Comparison of Predicted vs. Measured Peak Harmonic Frequency

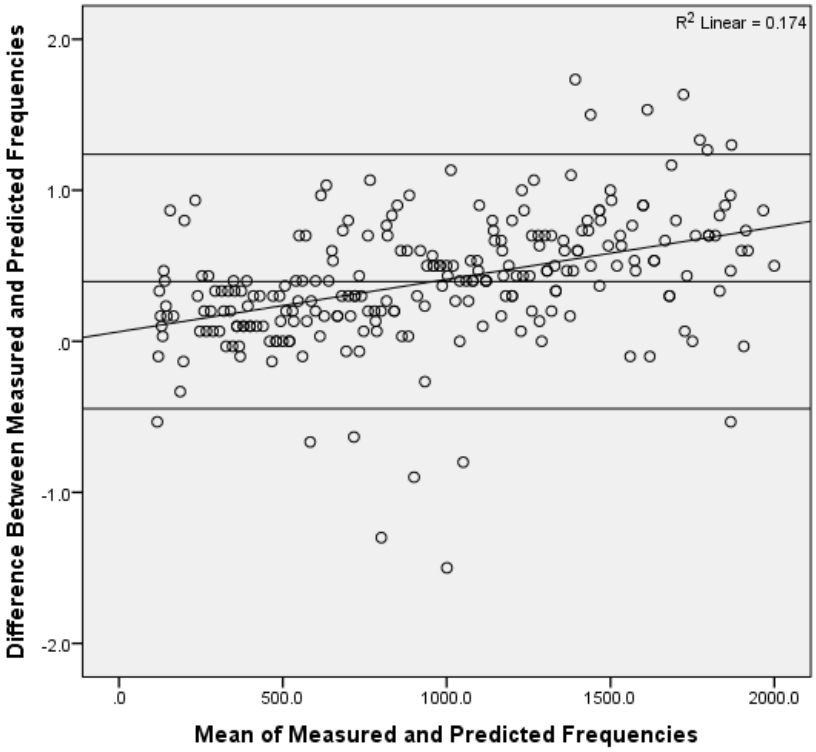

The reference lines in this chart are equal to (mean of the difference between the measured and the predicted frequencies) +/- (1.96 * the standard deviation of the difference between the measured and predicted frequencies). A One-Way T-Test for the difference in measurements (n=244) generated a mean = 0.396, standard deviation = 0.423, standard deviation of the mean = 0.027, 95% CI = 0.342-0.450, $p < 0.001$. The Bland-Altman Chart indicates high consistency between measured and predicted frequencies across the range of experimental frequencies (0-2 kHz).

Agreement between measured and predicted peak harmonic values was further assessed using correlations. Frequency and device speed arrays were compared individually:

Correlations were strong between measured and predicted values in all cases, with average correlation

Table 7.2: Correlations Between Predicted and Measured Frequency Values For Device Speeds 7,000-12,000 RPM

Speed	r-Value, All Harmonics
7000	0.999999041
7200	0.999999942
7400	0.999999802
7600	0.999998549
7800	0.999999925
8000	0.999999999
8200	0.999999935
8400	0.999999907
8600	0.999999777
8800	0.999999854
9200	0.999999776
9400	0.999999551
9600	0.999999387
9800	0.999999895
10000	0.999999877
10200	0.999999924
10400	0.999999913
10600	0.999999835
10800	0.999999527
11000	0.999999906
11200	0.999999923
11400	0.999999943
11600	0.999999948
11800	0.999999965
12000	0.999999227
Average	0.999999733

Table 7.3: Correlations Between Predicted and Measured Frequency Values For Harmonics 1-12

Harmonic Number	r-Value All Speeds
1	0.999908926
2	0.999706479
3	0.999996427
4	0.999661106
5	0.999979228
6	0.999998894
7	0.999689565
8	0.999696503
9	0.999993907
10	0.999698217
11	0.999996395
12	0.999994497
Average	0.999860012

between all measurements r=0.99993. The strength of the correlation did not vary as device speed was increased in 200 RPM increments from 7000 to 12,000 RPM (Table 7.2), nor did it vary with increasing harmonic number from 1 to 12 (Table 7.3).

7.3 Viscosity Alterations

Viscosity tests were undertaken with consecutive additions of glycerol. System volumes as well as LVAD speeds, flows, pulsatilities, and wattages were recorded for each glycerol addition and are displayed in Table 7.4. Power, flow, and pulsatility were left unchanged as viscosity was increased.

When peak harmonic frequency was analyzed for harmonics 1-11 for all viscosities, there was no observable effect of viscosity on peak frequency or amplitude (Figure 7.4, Table 7.5).

Two tailed, paired T-Tests assessing differences in peak frequency arrays across all harmonics between solution viscosities, indicated no trend towards significant inter-sample differences. Table 7.5 displays p-values calculated by analysis with independent samples T-Tests of each sample against all other samples. The arrays assessed in each test are composed of the peak harmonic frequency at each harmonic 1-11. Using a cutoff value of $p<0.05$, only arrays 2 and 5 (highlighted green in Table 7.5) showed significant difference. It is likely this is the result of chance alone. All other tests indicated non-significant differences in arrays.

Table 7.4: *In Vitro* Viscosity Alteration Tests

Recording	Vol. Glycerol (ml)	Visc. Solution (cP)	RPM	Flow (LPM)	Pulsatility	Power (Watts)
1	0	1.005	9400	5.3	1.8	6.6
2	50	1.067	9400	5.3	1.8	6.6
3	100	1.113	9400	5.3	1.9	6.6
4	150	1.119	9400	5.3	2.0	6.6
5	200	1.269	9400	5.4	2.1	6.7
6	250	1.342	9400	5.5	2.1	6.8
7	300	1.419	9400	5.6	2.2	6.8
8	350	1.498	9400	5.3	1.9	6.6
9	400	1.580	9400	5.3	1.9	6.6
10	450	1.665	9400	5.3	2.0	6.6
11	494	1.76	9400	5.4	2.0	6.6

Figure 7.6: *In Vitro* Comparison of Peak Harmonic Frequency with Increased Viscosity

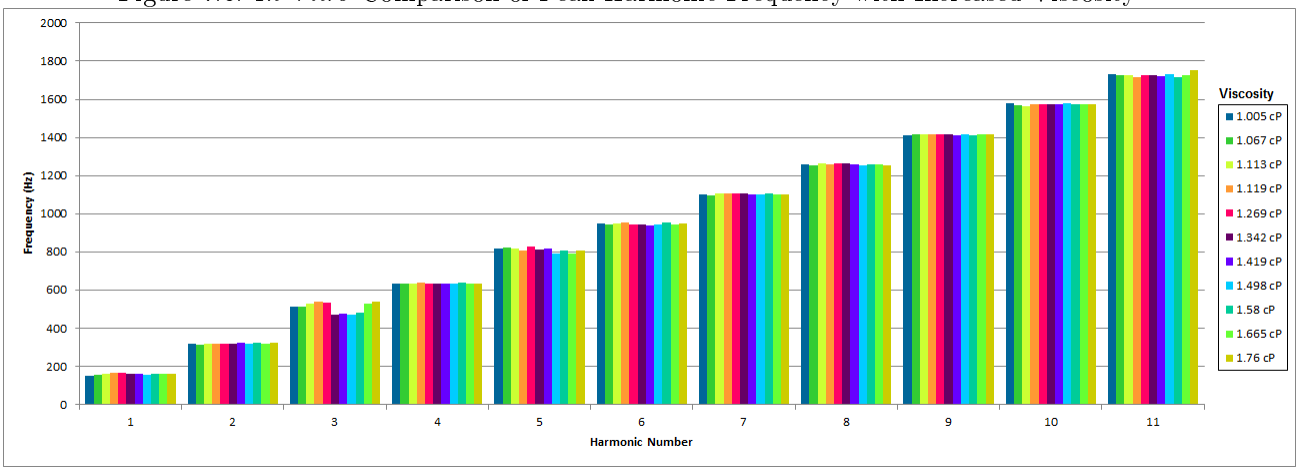

Table 7.5: Assessment of Statistical Difference in Peak Harmonic Frequency Arrays Between Viscosities

	Sample	**1**	**2**	**3**	**4**	**5**	**6**	**7**	**8**	**9**	**10**
Sample	**Viscosity**	**1.005**	**1.067**	**1.113**	**1.119**	**1.269**	**1.342**	**1.419**	**1.498**	**1.58**	**1.665**
1	**1.005**										
2	**1.067**	0.2707									
3	**1.113**	0.4815	0.0763								
4	**1.119**	0.4690	0.1967	0.8000							
5	**1.269**	0.1030	**0.0066**	0.1736	0.4253						
6	**1.342**	0.5448	0.8710	0.4113	0.4334	0.2488					
7	**1.419**	0.3622	0.6806	0.2639	0.3024	0.1376	0.4543				
8	**1.498**	0.2422	0.5014	0.2139	0.2145	0.1335	0.2788	0.5212			
9	**1.58**	0.5355	0.9012	0.3678	0.3678	0.2214	0.9017	0.5350	0.2392		
10	**1.665**	0.8671	0.6818	0.3723	0.1239	0.1220	0.7151	0.5742	0.3597	0.7031	
11	**1.76**	0.1823	0.0764	0.4222	0.5274	0.9058	0.2927	0.2099	0.1183	0.0834	0.2735

Identical analysis was performed to assess trends in peak amplitude at each harmonic. Figure 7.7 displays amplitude at each harmonic for all viscosities. No trend is visibly evident, and T-Tests indicated no significant differences in amplitude arrays between viscosities (Table 7.6). Though many of the p-values achieve significance, there is no trend towards higher or lower amplitude as viscosity increases.

Figure 7.7: *In Vitro* Comparison of Peak Harmonic Amplitude with Increased Viscosity

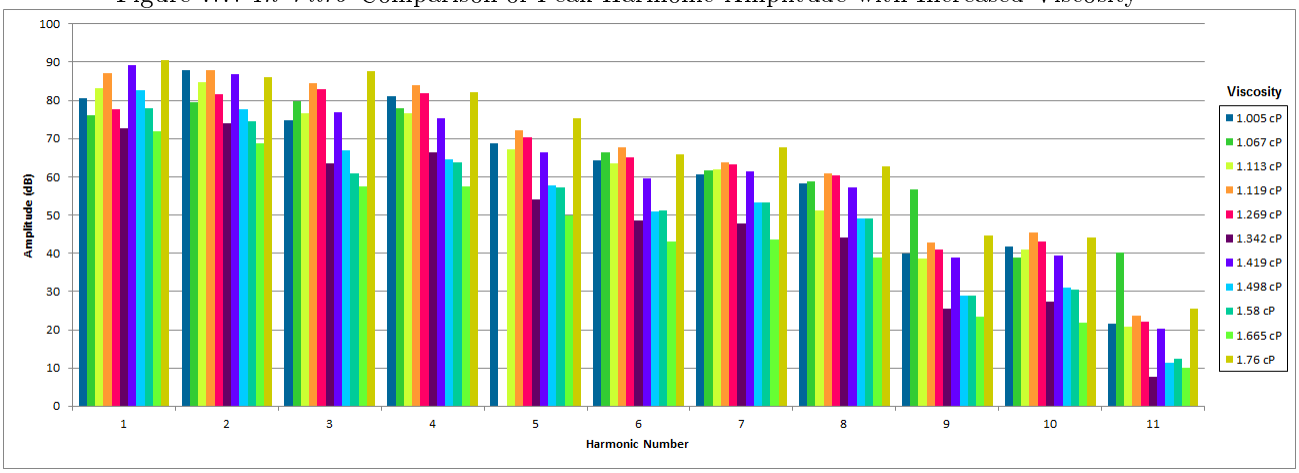

Table 7.6: Assessment of Statistical Difference in Peak Harmonic Amplitude Arrays Between Viscosities

	Sample	1	2	3	4	5	6	7	8	9	10
Sample	**Viscosity**	**1.005**	**1.067**	**1.113**	**1.119**	**1.269**	**1.342**	**1.419**	**1.498**	**1.58**	**1.665**
1	**1.005**										
2	**1.067**	**0.3943**									
3	**1.113**	**0.1707**	**0.2197**								
4	**1.119**	**0.0007**	**0.6965**	**0.0000**							
5	**1.269**	**0.3856**	**0.5494**	**0.1001**	**0.0069**						
6	**1.342**	**0.0000**	**0.0006**	**0.0000**	**0.0000**	**0.0000**					
7	**1.419**	**0.5403**	**0.3571**	**0.5753**	**0.0012**	**0.3232**	**0.0000**				
8	**1.498**	**0.0000**	**0.0066**	**0.0000**	**0.0000**	**0.0002**	**0.0010**	**0.0000**			
9	**1.58**	**0.0000**	**0.0017**	**0.0000**	**0.0000**	**0.0000**	**0.0182**	**0.0000**	**0.0761**		
10	**1.665**	**0.0000**	**0.0000**	**0.0000**	**0.0000**	**0.0000**	**0.0009**	**0.0000**	**0.0000**	**0.0000**	
11	**1.76**	**0.0034**	**0.4856**	**0.0001**	**0.1463**	**0.0040**	**0.0000**	**0.0002**	**0.0000**	**0.0000**	**5.6E-09**

7.4 Pressure Variations and Artificial Stenotic Narrowing

Pressure was first varied by changing the height of the outflow resistance tubing, as discussed in section 5.1.5. When peak harmonic frequency was compared at all harmonics for the five different outflow pressures, no differences were observed. Figure 7.8 indicates peak harmonic frequency across all harmonics for the range of outflow pressures, and shows no trend as pressure increases. Table 7.7 indicates p-values calculated by two-tailed paired T-Tests. No differences are significant.

Table 7.7: Assessment of Statistical Difference in Peak Harmonic Frequency Arrays As Outflow Pressure is Increased

Sample	1	2	3	4	5
	Pressure	**64.8 mmHg**	**74 mmHg**	**83.5 mmHg**	**96.6 mmHg**
1	**64.8 mmHg**				
2	**74 mmHg**	0.0809			
3	**83.5 mmHg**	0.7370	0.2222		
4	**96.6 mmHg**	0.2209	0.6622	0.1818	
5	**104.0 mmHg**	0.7027	0.3887	0.3887	0.6210

Corresponding analysis was performed for amplitude at peak harmonic frequency. Significant differences were observed, however, there does not appear to be a trend in amplitude associated with increased outflow pressures in Figure 7.9 (Table 7.8).

Next, pressure was varied by changing the height of the inflow reservoir, as discussed in section 5.1.5.

Figure 7.8: *In Vitro* Comparison of Peak Harmonic Frequency with Increased Outflow Pressure

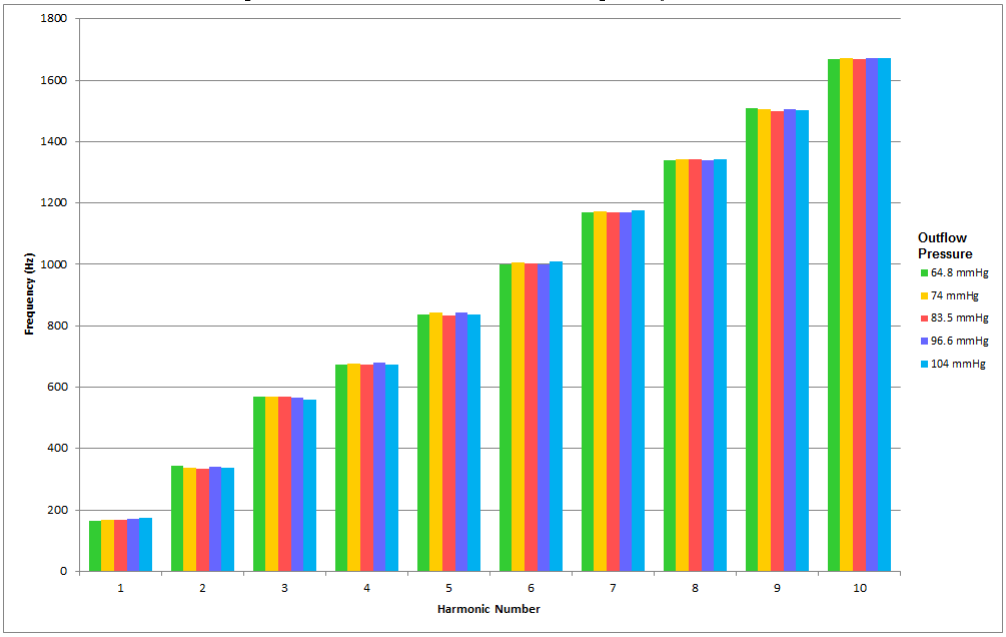

Figure 7.9: *In Vitro* Comparison of Peak Harmonic Amplitude with Increased Outflow Pressure

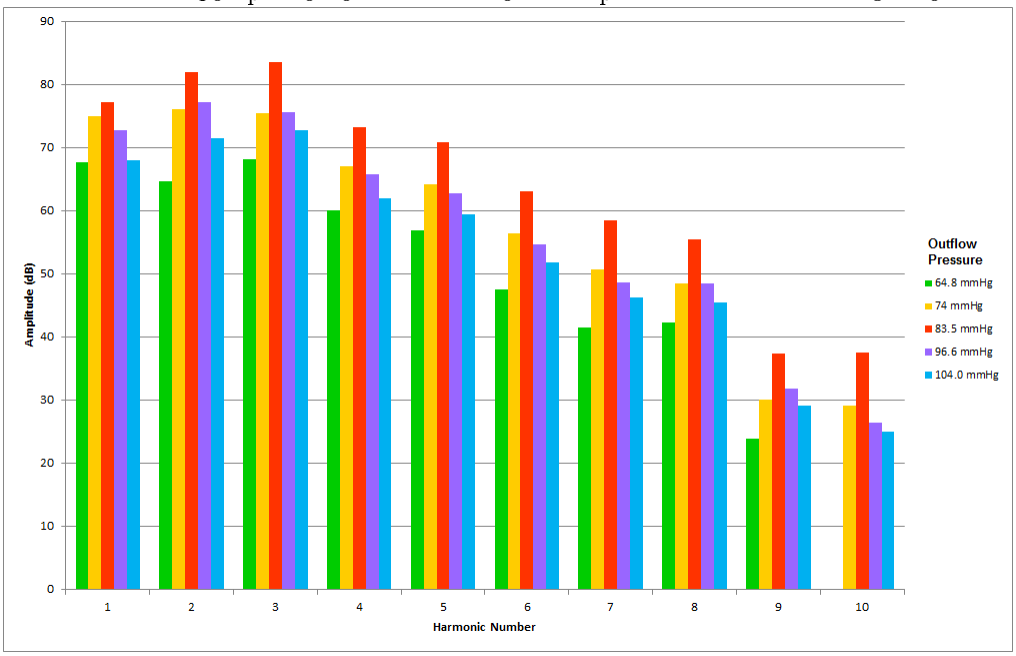

Table 7.8: Assessment of Statistical Difference in Peak Harmonic Amplitude Arrays As Outflow Pressure is Increased

Sample	**1**	**2**	**3**	**4**	**5**
	Pressure	**64.8 mmHg**	**74 mmHg**	**83.5 mmHg**	**96.6 mmHg**
1	**64.8 mmHg**				
2	**74 mmHg**	7.57561E-08			
3	**83.5 mmHg**	1.06796E-08	7.94922E-07		
4	**96.6 mmHg**	2.26339E-06	1.31977E-06	0.10006263	
5	**104.0 mmHg**	0.000119954	2.07293E-05	8.42824E-10	1.1928E-05

When peak harmonic frequency was compared at all harmonics for the five different inflow pressures, no differences were observed. Figure 7.9 indicates peak harmonic frequency across all harmonics for the range of inflow pressures, and shows no trend as pressure increases. Table 7.9 indicates p-values calculated by two-tailed paired T-Tests. No differences are significant.

Figure 7.10: *In Vitro* Comparison of Peak Harmonic Frequency with Increased Inflow Pressure

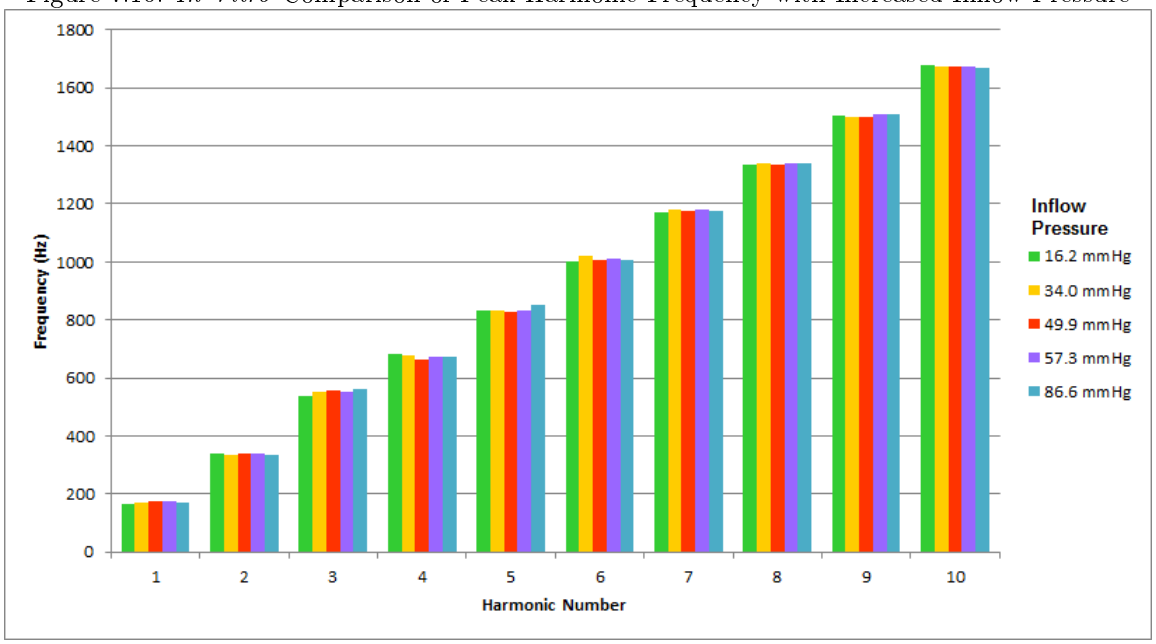

Corresponding analysis was performed for amplitude at peak harmonic frequency. Significant differences were observed, however, there does not appear to be a trend in amplitude associated with increased inflow pressures in Figure 7.11 (Table 7.10).

Table 7.9: Assessment of Statistical Difference in Peak Harmonic Frequency Arrays As Inflow Pressure is Increased

Sample	**1**	**2**	**3**	**4**	**5**
	Pressure	**64.8 mmHg**	**74 mmHg**	**83.5 mmHg**	**96.6 mmHg**
1	**64.8 mmHg**				
2	**74 mmHg**	0.3093			
3	**83.5 mmHg**	0.9686	0.2938		
4	**96.6 mmHg**	0.1187	0.5744	0.0223	
5	**104.0 mmHg**	0.2904	0.7414	0.9949	0.1830

Figure 7.11: *In Vitro* Comparison of Peak Harmonic Amplitude with Increased Inflow Pressure

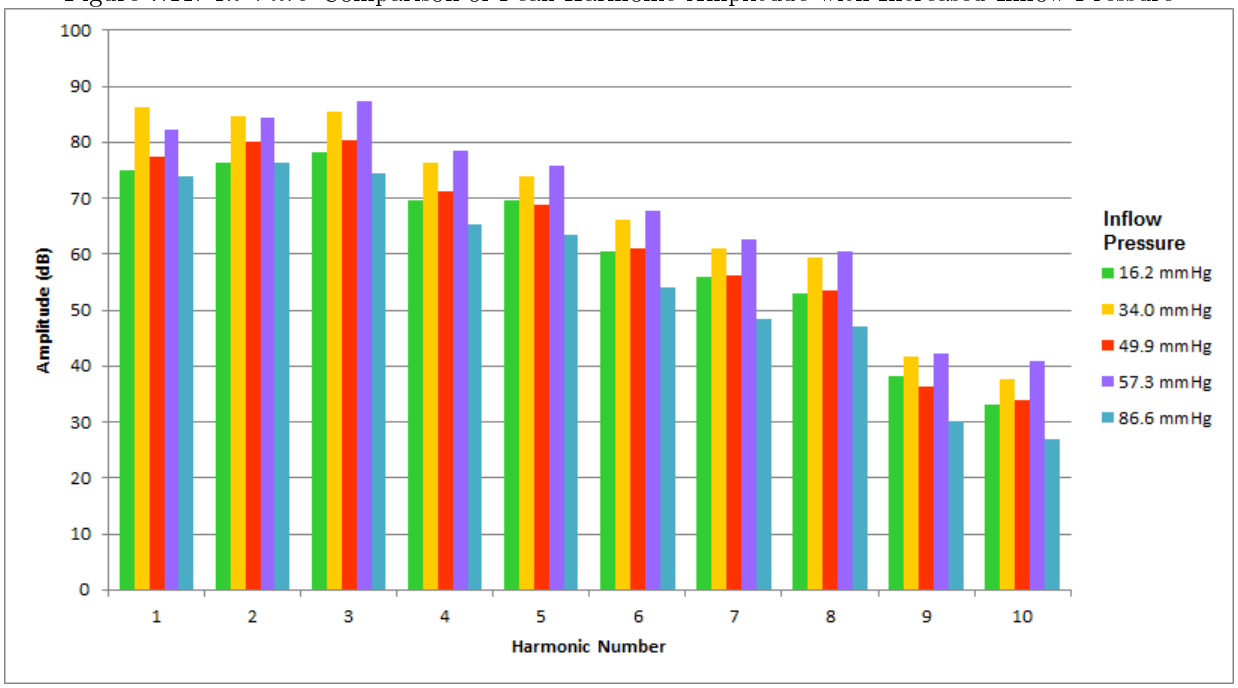

Table 7.10: Assessment of Statistical Difference in Peak Harmonic Frequency Arrays As Inflow Pressure is Increased

Sample	**1**	**2**	**3**	**4**	**5**
	Pressure	**64.8 mmHg**	**74 mmHg**	**83.5 mmHg**	**96.6 mmHg**
1	**64.8 mmHg**				
2	**74 mmHg**	1.3E-05			
3	**83.5 mmHg**	9.8E-02	4.8E-07		
4	**96.6 mmHg**	1.1E-07	1.6E-01	1.5E-08	
5	**104.0 mmHg**	2.5E-04	5.9E-10	2.1E-07	3.6E-08

Device thrombosis was simulated under laboratory conditions by partially occluding the outflow graft using arterial clamps. This was done under controlled conditions at RPM = 10,000, using pure water, inflow pressure = 50 mmHg, outflow pressure = 90 mmHg. A baseline recording, without the arterial clamps, was compared to a recording at approximately 70% occlusion. Flow disruption was noted at the site of occlusion. We have found comparison of spectral components between 2-4 samples most meaningful when plotted as 50 Hz area under the curve (AUC) segments (See Part II, Introduction). This allows for comparison of spectral behavior at all frequencies and at higher resolution.

Figure 7.12: Spectral Component Comparison: *In Vitro* Occlusion vs. Baseline

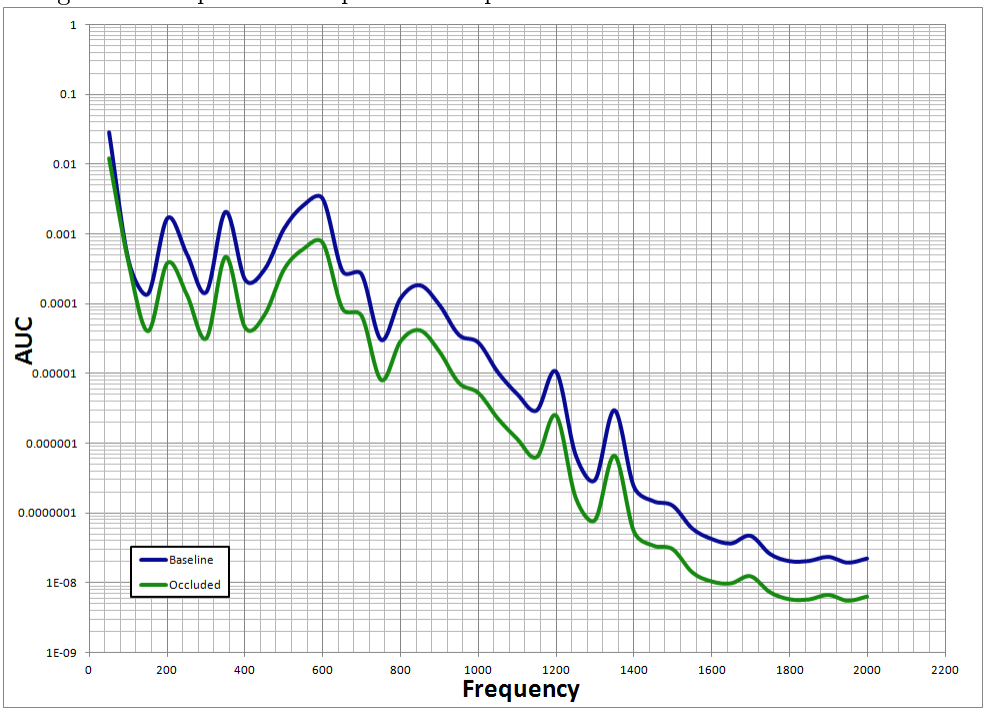

Figure 7.12 notably indicates a reduction in amplitude in the spectral tracing associated with the occluded outflow graft. Of additional note is the mirroring of the curves- much of the baseline sample's curve morphology is preserved in the occluded sample's morphology.

7.5 Modal Analysis

As indicated by Figure 7.13 and 7.14, the lowest frequency flexural mode of resonant vibration of the LVAD occurred at 8.5 kHz, approximately 4.25 times the highest LVAD frequencies we recorded. It is unlikely this structural resonance impacted acoustics in the ranges used in this investigation (0-2kHz).

Figure 7.13: Frequency Response Functions for Points 1-5

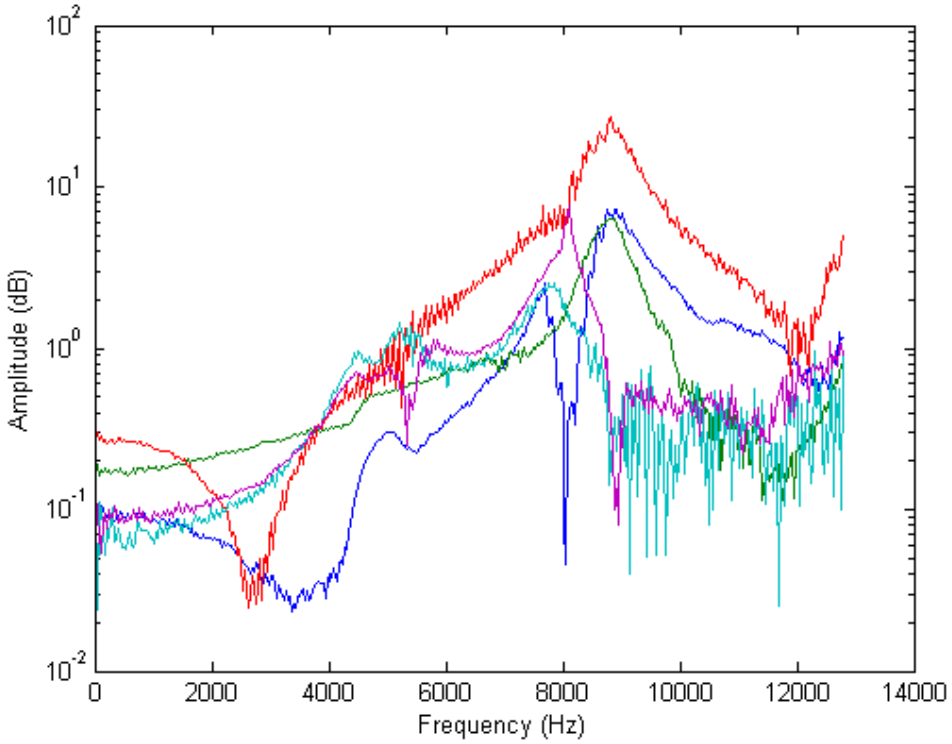

Figures 7.15 and 7.16 show the operating deflection shape at 8.5 kHz at two different phases (90 degrees separated). The shapes suggest the mode shape pattern depicted in Figure 7.17, which would be the expected mode shape for the lowest frequency flexural resonance.

Figure 7.14: Frequency Response Functions for Points 6-10

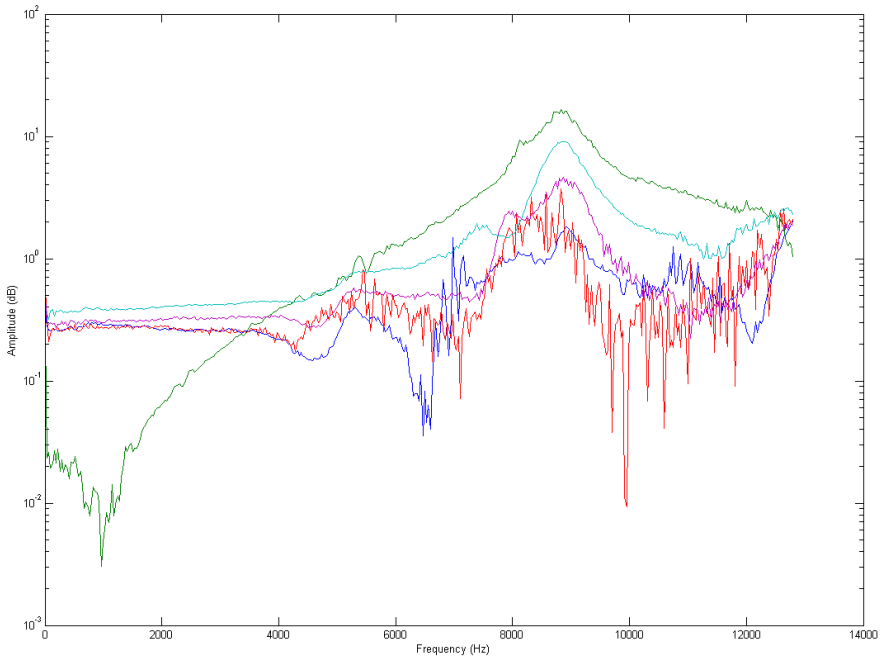

Figure 7.15: Radial Plot Points 1-5

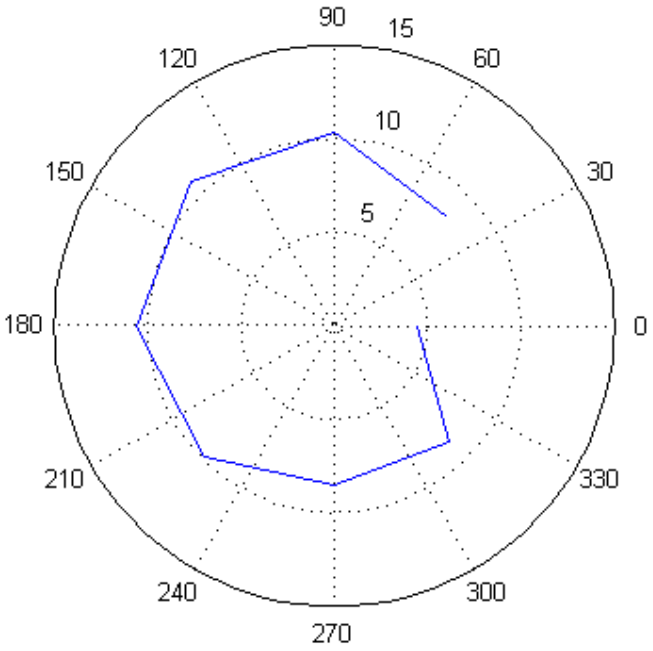

Figure 7.16: Radial Plot Points 6-10

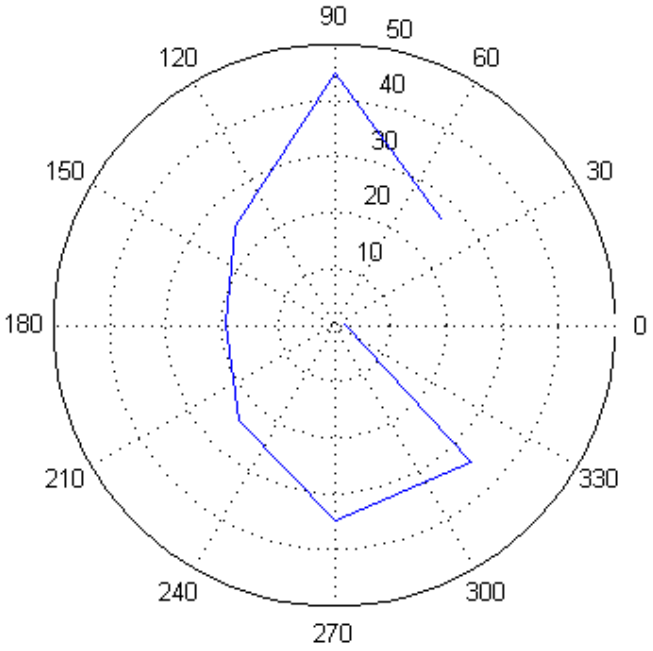

Figure 7.17: Modal Analysis Ring Mode with 2 Nodal Diameters

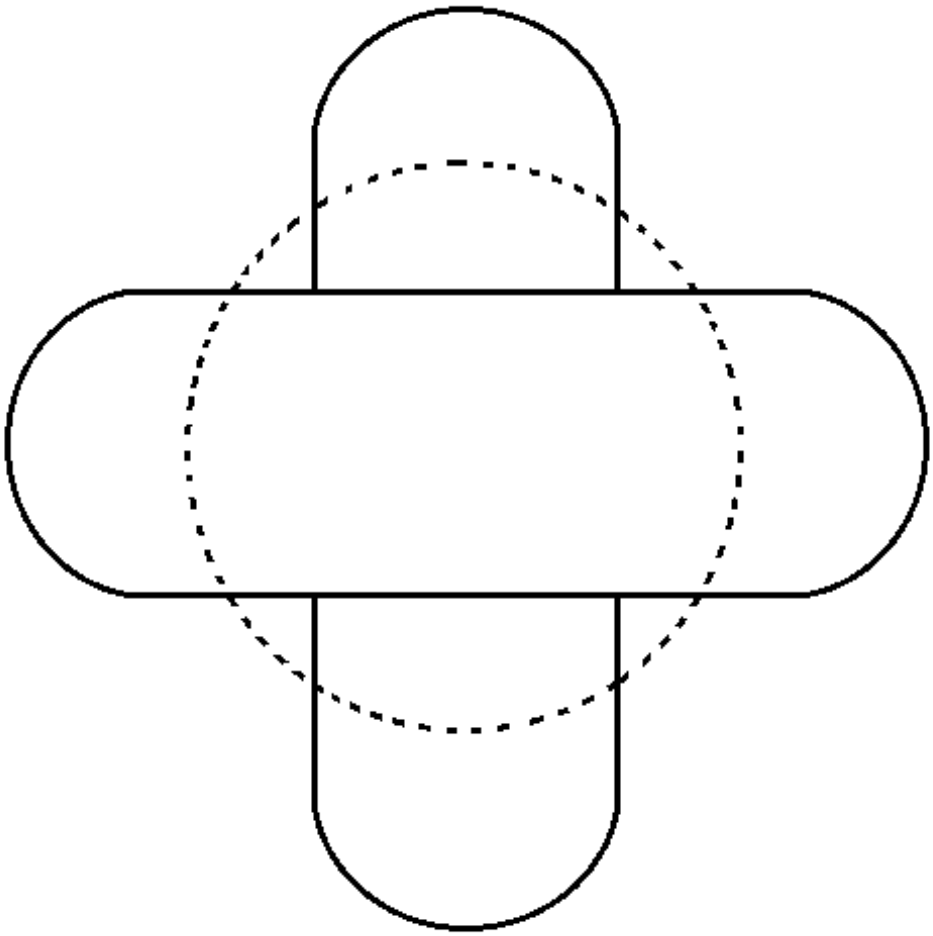

Chapter 8

Results From *In Vivo* Studies

Data reported in this section were collected from patients of the Advocate Christ Medical Center LVAD service. Heart failure is a non-homogenous syndrome; it presents differently in nearly every patient and may be caused by a wide number of inciting factors including chronic cardiovascular disease, viral infection, acute ischemic insult, a period of atypical cardiovascular loading, and others. Further, the patient response to hemodynamic support is varied. Some patients thrive, regain quality of life, and experience remediation of their heart failure related symptoms. Some experience continual complications such as those detailed in chapter 4, while still others remain inadequately supported- in chronic heart failure. All types of patients were auscultated for this study, however, only those who were known by hospital staff to be stable on LVAD support were included in the preliminary study detailed in section 8.1. Before discussing these results, however, a comment on the logistics of recording bodily sounds in a hospital environment. The *in vivo* "laboratory" is, by definition, of increased complexity compared to the *in vitro* laboratory. Many factors notably affected not only the ability for recordings to be made, but also the quality of those recordings. For instance, recording was precluded in patients who were in pain, had open chest lesions, active infection, and in patients who refused to participate in a research study. Likewise, it was noted that signal quality was often decreased in obese patients, when breast tissue prevented access to the skin directly over the LVAD, and when the hospital environment was noisy.

8.1 Acoustic Model in 10 Stable LVAD Patients

A total of ten HeartMate II supported patients with mean age of 69 ± 7.2 years and BMI 24.2 ± 2.4 were auscultated in our outpatient clinic. These patients were known to be in stable condition and relatively free of complications at the time of auscultation. The average duration on LVAD was 573.6 ± 162.5 days and LVAD, lung, and kidney function were noted to be normal. Echocardiography revealed 2 patients (20%) with mild mitral regurgitation, 1 patient (10%) with mild aortic insufficiency, 5 patients (50%) with mild tricuspid regurgitation, 3 patients (30%) with mild pulmonic insufficiency, 1 patient (10%) with mitral valve replacement, and 1 patient (10%) with tricuspid valve replacement (Table 8.1). Additionally, hemodynamic and laboratory values did not suggest the presence of hemolysis or thrombus in any of the pumps.

Acoustic samples from each of these patients were plotted together in Figure 8.1. With normalization of frequency to device speed, preservation of peak harmonic structure is evident. Yet, despite consistency of harmonic peaks, there is notable inter-sample heterogeneity in peak amplitude as well as curve shape between peaks.

Figure 8.1: Spectrogram Slices for Patients 1-10 Plotted With Normalization of Frequency to Harmonic Order

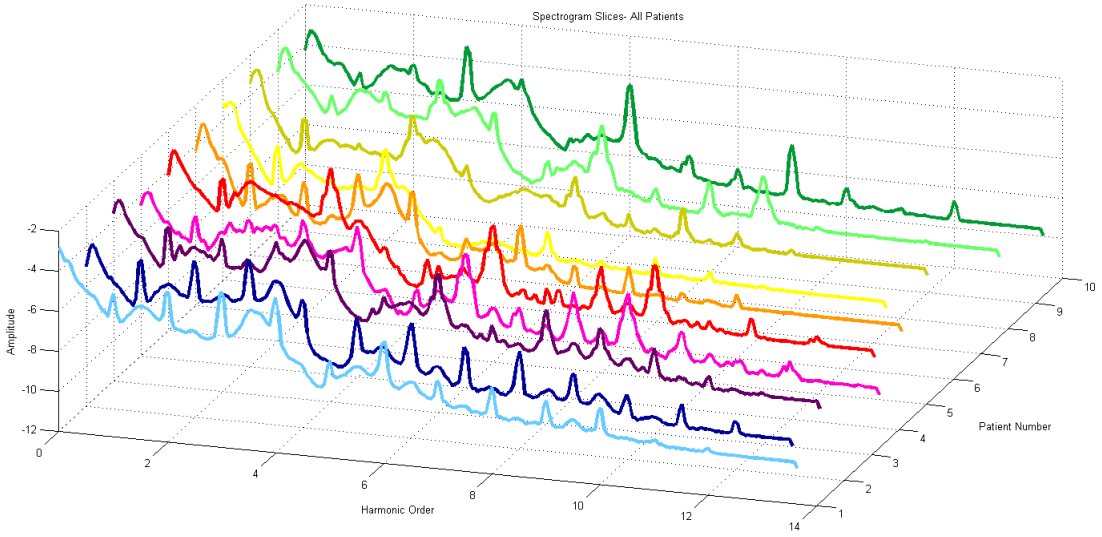

Spectrographic analysis revealed that pump acoustics in vivo are very similar to pump acoustics in vitro.

Table 8.1: Baseline Demographics in 10 Stable LVAD Patients

	Patient Number									
	1	2	3	4	5	6	7	8	9	10
Days to Ausc	948	496	738	1129	195	333	446	371	83	756
Age (years)	74	68	52	54	34	43	66	65	51	57
BMI (kg/m^2)	24.6	28.4	25	21.1	37.3	34.9	30	27.5	27.1	27
Race	AA	AA	Caucasian	Caucasian	Caucasian	AA	Caucasian	Caucasian	Hispanic	Caucasian
Indication	ICM	NICM	IDCM	ICM	NIDCM	NICM	NIDCM	IDCM	NICM	ICM
RPM	9200	9000	9200	8800	9600	9800	9200	8800	9200	9200
Flow (L/min)	4.8	4	4.7	4.1	5.4	6.2	6.3	5.9	5.2	6.4
PI	6	7.6	4.7	8.3	4.9	5	5.2	6.4	5.1	5.6
Power (Watts)	5.1	4.8	5	4.4	5.9	7.1	5.8	5.2	5.5	6.8
Sys BP (mmHg)	119	103	94	98	98	102	89	106	87	106
Dia BP (mmHg)	79	79	71	68	84	68	70	76	62	75
Pulse Rate	77	66	67	92	79	75	63	70	82	70
RVDd (cm)	3.1	3.7	3.1	3.1	3.1	2.6	3.7	2.7	3.2	3.1
LVDd (cm)	6.1	6.5	6.4	6.2	6.5	6.2	8.6	3.2	5.7	6.8
Ejection Fraction (%)	0.3	0.224	0.14	0.24	0.21	0.2	0.1	0.213	0.154	0.12
Pulm. Sys. BP (mmHg)	29	35	34	16	22	24	35	27	23.6	39
Creatinine (mg/dL)	1.99	1.77	1.14	1.7	0.93	1.69	1.48	1.79	0.95	1.21
Hemoglobin (g/dL)	10.6	12.4	14	11	15.3	12.4	15.3	13.3	9.2	14.9
Plasma Free Hb (mg/dL)	9.1	11	3.7	3	7.5	13.4	9.5	1	5	10.6
LDH (Units/L)	360	310	363	264	325	411	420	214	328	339
INR	3.1	1.7	2.3	1.9	3	2.2	2.3	2.5	1.8	4.2

Abbreviations: Days to Ausc. (number of days between implant and auscultation), RPM (device revolutions per minute at time of auscultation), PI (device pulsatility index at time of auscultation), Sys BP (systolic blood pressure), Dia BP (diastolic blood pressure), RVDd (right ventricular dimension in diastole), LVDd (left ventricular dimension in diastole), Pulm. Sys. Pressure (pulmonary systolic blood pressure), Plasma free Hb (plasma free hemoglobin), LDH (lactate dehydrogenase), INR (International normalized ratio), ICM (ischemic cardiomyopathy), NICM (non-ischemic cardiomyopathy), NIDCM (non-ischemic dilated cardiomyopathy), AA (African American).

Typically these acoustic samples generated excellent spectrograms, like the ones shown in Figure 8.1, with defined harmonic bands, comparable to recordings made *in vitro*. Occasionally, short frequency ranges and individual harmonics exhibited lower signal to noise ratio (SNR) and obfuscated peaks *in vivo* recordings compared to *in vitro* recordings. Despite signal artifacts, which may be a result of a considerably more complex acoustic environment *in vivo*, peak harmonic frequencies occurred within a very small range of the expected values calculated by Equation 11. The location of the pump harmonics in these ten patients again correlated well with expected values and with measured *in vitro* values for equivalent speeds (r>0.999 for all). In six of the ten patients average amplitudes across all twelve recorded harmonics were significantly less than those measured *in vitro* at equivalent pump speeds. Using custom Matlab software, areas under the spectral curve (AUC) were measured for each patient's spectrogram slice in 50 Hz segments over the 2000 Hz spectrum. Comparison of *in vivo* AUC segments and *in vitro* AUC segments at each patient's corresponding speed showed strong correlations in all incidences (r>0.966) (Table 8.2, Figure 8.3).

Figure 8.2: Example of an *In Vivo* Spectrogram (top) and Spectrogram Slice (bottom)

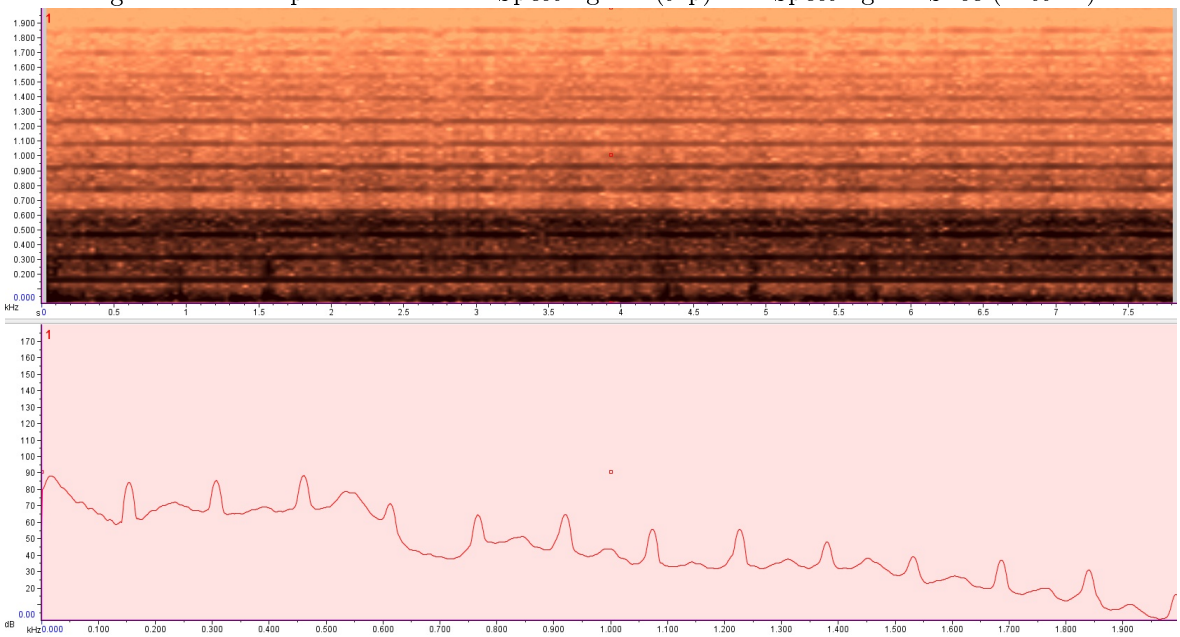

Table 8.2 is a comparison of acoustic data derived from each patient (1-10), against predicted peak frequency values, and against AUC arrays generated from recordings made *in vitro*. The r-values, used to

Table 8.2: Comparison of Acoustics *In Vitro* Acoustics From 10 Stable HMII Patients to Expected Values

Patient #	Speed (RPM)	Predicted H_0 (λ)	*r*-value Measured λ Vs. Predicted λ	*r*-value *in vivo* λ Vs. *in vitro* λ
1	9200	153.3	>0.999	>0.999
2	9000	149.5	>0.999	>0.999
3	9200	153.3	>0.999	>0.999
4	9200	153.3	>0.999	>0.999
5	9600	160.0	>0.999	>0.999
6	9800	163.3	>0.999	>0.999
7	9200	153.3	>0.999	>0.999
8	8800	146.7	>0.999	>0.999
9	9200	153.3	>0.999	>0.999
10	9200	153.3	>0.999	>0.999

Abbreviation: H_0(fundamental frequency)

compare predicted versus measured frequencies, are calculated using Spearman's Rank Correlation Tests across peak frequency at each harmonic. All values are greater than 0.999, indicating strong correlation between measured and predicted frequencies at all harmonics. The *r*-values used to compare *in vitro* and *in vivo* frequencies are calculated using Spearman's Rank Correlation Tests across 50 Hz AUC segments calculated from using the Matlab procedure described in Part II, introduction. This method of comparison also generated very strong correlations. This means of comparison indicates similarity in peak frequency values, but does not necessarily indicate similarity or difference in amplitude. Figure 8.2 plots 50 Hz AUC segments from patient 4, whose LVAD speed was set at 9,200 RPM, alongside an *in vitro* measurement made at 9,200 RPM. This graphical comparison, like that shown in Figure 7.12, evidences a similar curve morphology between the two samples, with areas of curve mirroring.

8.2 Thrombosis in Two Patients with HeartMate II LVADs

Two poignant examples of device thrombosis in patients (separate from the 10 stable patients described previously) who were supported by the HeartMate II LVAD are discussed here. Each patient was admitted with clinical indications of severe hemolysis suggesting device malfunction and the presence of thrombus including hematuria, hemoglobinuria, and lactate dehydrogenase (LDH) values at least twice their normal values.

Figure 8.3: Spectral Plot of Patient 4 Sample vs 9200 RPM *In Vitro*

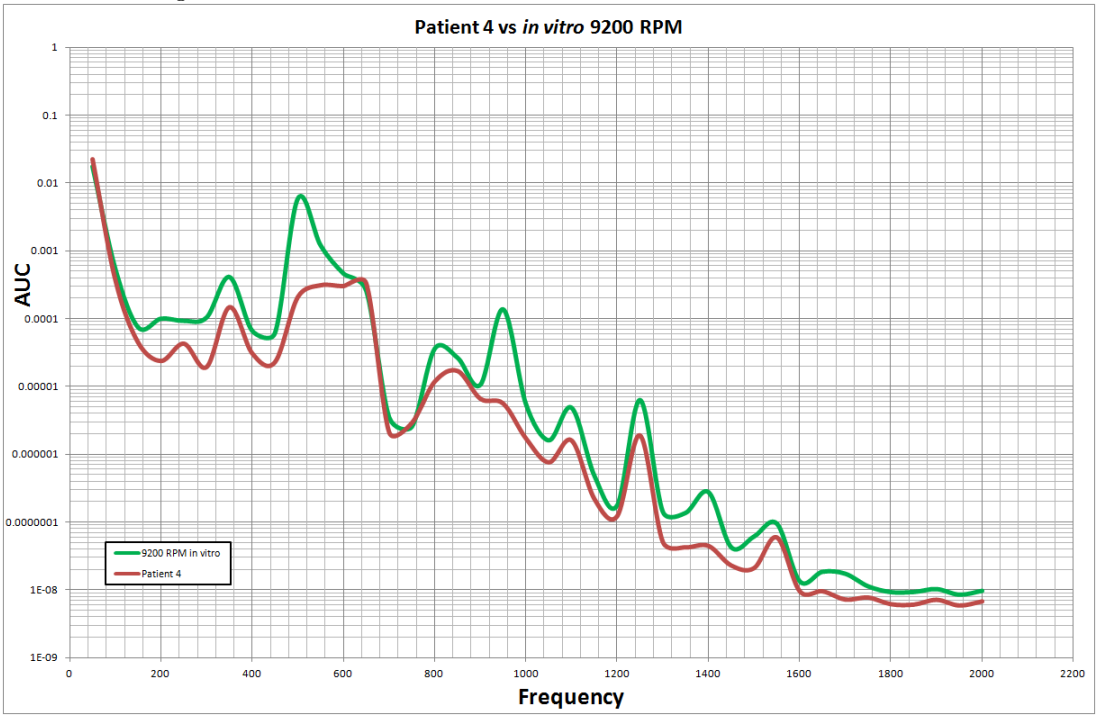

8.2.1 Clinical Events- Patient 1

In August of 2013 a 44-year-old man was admitted to our Heart and Vascular Institute for exacerbation of congestive heart failure. His past medical history was significant for non-ischemic cardiomyopathy, non-sustained ventricular tachycardia, atrial fibrillation, chronic kidney disease, obstructive sleep apnea, and pulmonary hypertension. At this time workup for LVAD placement as bridge to cardiac transplantation was initiated. Echocardiography revealed a dysfunctional right ventricle (RV), a globally dilated, dysfunctional left ventricle (LV) with a left ventricular diastolic diameter of 8.3 cm, ejection fraction (EF) of 25% and moderate mitral regurgitation (MR). The patient required inotropic support with milrinone and dobutamine prior to surgical intervention. The decision was made to implant the patient with a HeartMate II LVAD. Initial LVAD placement was free of complications. Routine post-operative echo demonstrated well-placed intra-ventricular inflow cannula, resolution of mitral insufficiency, and no aortic insufficiency. Other than the requirement of prolonged post-operative inotropic support due to RV failure, the patient's post-operative recovery was unremarkable, and he was discharged with stable LVAD function 16 days after pump implantation. Despite stable outpatient pump function and hemodynamics over the three weeks following discharge from index hospitalization, he was admitted for possible pump hemolysis when laboratory tests indicated a lactate dehydrogenase (LDH) level of 1525 U/L. During the next 10 days the patient's LDH values continued to increase before stabilizing at approximately 2500 U/L. Sodium bicarbonate and heparin drips were initiated upon admission. An integrellin drip was also initiated, without any improvement in the patient's LDH. Additionally, admission echocardiography revealed marked right heart enlargement and RV hypocontractility. The patient remained short of breath at rest with apparently stable LVAD function. Despite return to therapeutic INRs, and the use of hydration and alkalanization therapy, LDH values remained elevated, and surgical re-intervention with LVAD device exchange was considered. With a creatinine stable at 1.53 mg/dL the patient underwent surgical exchange of his LVAD for a second HeartMate II pump 69 days after initial implantation and 26 days after admission for hemolysis. During this second surgery his intraventricular inflow cannula, titanium outflow elbow, and Dacron outflow graft remained in place. The HeartMate II pump body alone was replaced. Immediate intraoperative bronchoscopic exploration of the explanted pump revealed the presence of a circumferential clot located at the inflow stator (Figure 8.4).

Figure 8.4: Thombus Formation - Patient 1

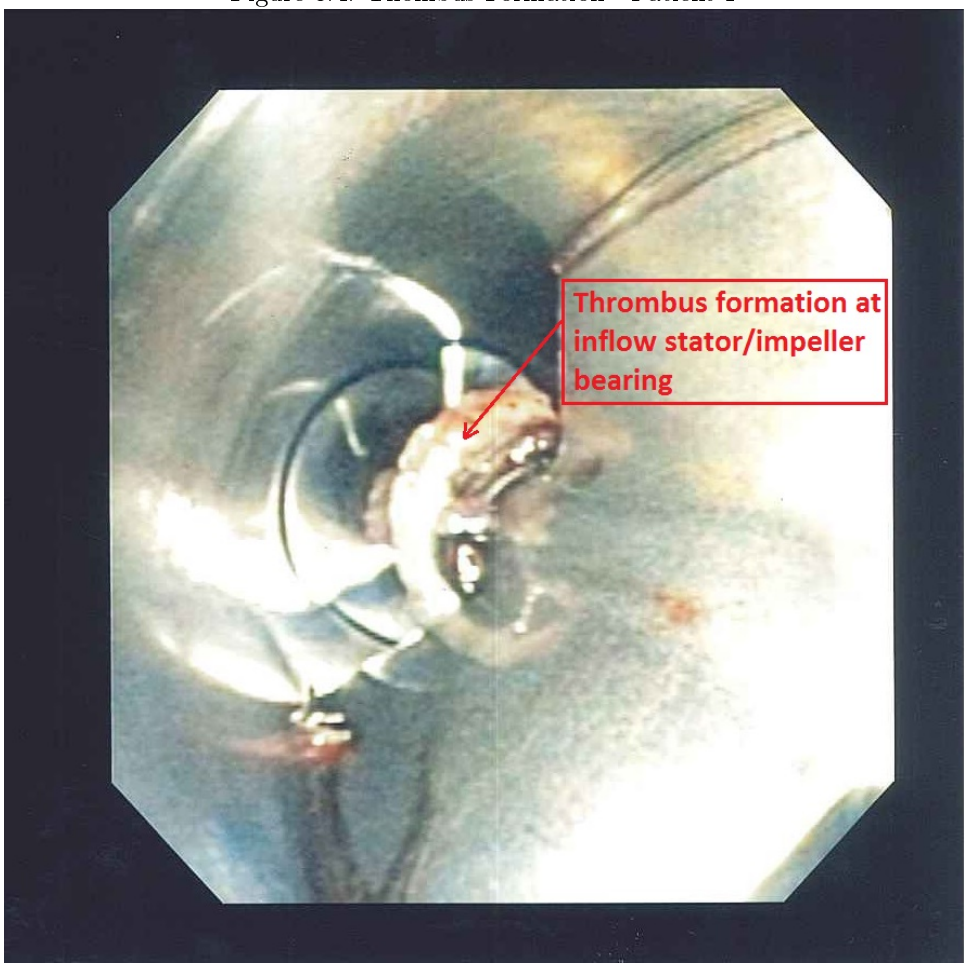

Image taken inside the patient's HeartMate II using a video-bronchoscope. Inflow of the device is shown with the inflow stator on the right side of the image and the impeller and clot at center. Clot has formed circumferentially around the bearing between the inflow stator and the impeller.

Due to persistent intra-operative LV dysfunction, a temporary right ventricular assist device (RVAD) was implanted with cannulation at the femoral vein and pulmonary artery. Following a period of prolonged detention due to profound coagulopathy, the patient was transferred to intensive care with adequate hemostasis. Despite surgical complications, post-operative recovery was relatively expeditious. INR reached therapeutic levels within 10 days, RVAD weaning was begun at post-operative day 6, and the RVAD was explanted on post-operative day 16 with demonstration of hemodynamic stability. The patient was discharged with LDH levels stable in the low 400's U/L. The patient was again admitted 36 days later with dyspnea on exertion and an elevated LDH of 1272 U/L. With initiation of sodium bicarbonate at 6.52 mEq/hr, dipyridamole at 75 mg TID, and pentoxifylline at 400 mg TID, LDH values began to downtrend, reaching a nadir of 883 U/L 13 days after admission (Figure 8.5).

Figure 8.5: Lactate Dehydrogenase Levels - Patient 1

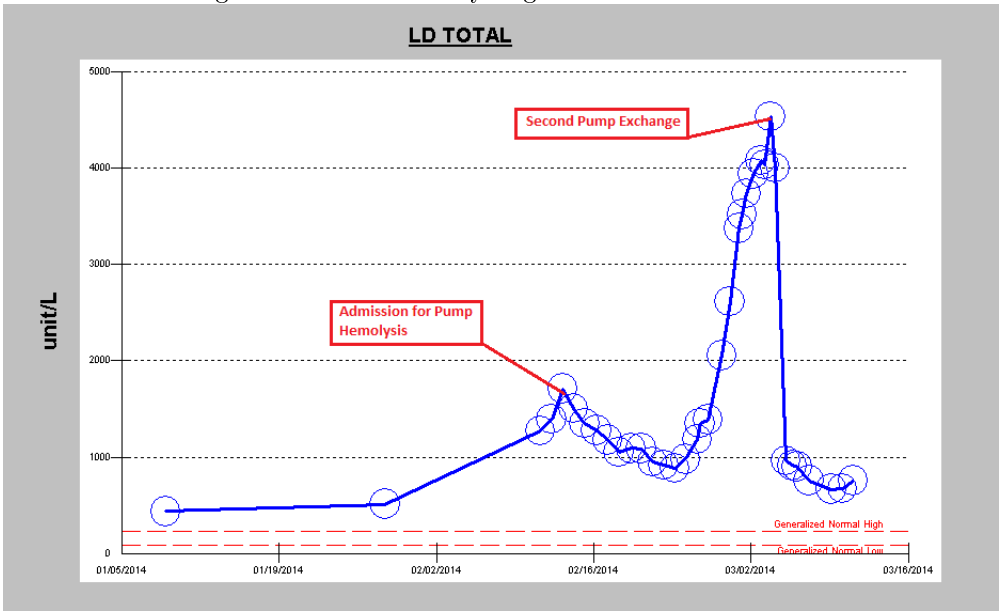

In the third week of admission, echocardiography revealed increased mitral regurgitation and cardiac catheter measurements indicated a cardiac index by thermodilution of 1.96 L/min/m^2 and a mixed venous oxygenation of 41%, suggesting poor left heart function. These indications, in addition to continually elevated LDH values and the necessity for increased pump speeds to maintain adequate LVAD flows, led the

team to move towards a second pump exchange. Thus, with a peak LDH of 4,530 U/L, the patient underwent surgical implantation of a third LVAD. However, since he had demonstrated propensity for thrombus formation, it was decided to use a HeartWare HVAD instead of a third HeartMate II. The HVAD is thought to generate lower shear stress than the HeartMate II during normal operation and does not require mechanical contact between parts. It is thought that thrombogenesis may be reduced in long term use of this pump. Although this third operation was complicated by dense mediastinal adhesions, with appropriate dissection, the HVAD was implanted with adequate flows, improved left ventricular dysfunction, and lessened mitral insufficiency. Intraoperative inspection of the explanted HeartMate II again revealed presence of substantial thrombus formation at the inflow stator-impeller bearing. With sustained post-operative respirator dependence, marginal LVAD flows, and mixed venous saturations in the 50's, the patient again required temporary right ventricular support. Attempts were made at RVAD weaning over the next 60 days, however removal of the system was complicated by sustained bleeding and the presence of clot at the pulmonic valve. Finally, following an increase in LDH levels to 1982 U/L, the RVAD was surgically removed with demonstration of stable post-operative hemodynamics. Inspection of the explanted RVAD pump revealed evidence of extensive fibrous debris. The patient has remained stable on HVAD support for 61 days since discharge.

8.2.2 Spectral Analysis - Patient 1

The average correlation between predicted peak frequencies and measured peak frequencies in this patient was strong (r>0.998 at all time points). These results indicate that this method of acoustic detection of pump operation is sensitive and accurate and that the frequency of each harmonic peak of the HeartMate II acoustic signal are not significantly altered in the presence of pump thrombosis. Additionally, comparison of *in vivo* and *in vitro* acoustic samples from the HeartMate II in section 8.1 demonstrated that transmission of LVAD acoustics through the thoracic or abdominal tissues does not result in significant frequency modulation. Despite the relationship between measured and expected harmonic peak frequency location, the amplitude of the peaks and the behavior of the spectrogram slice between peaks evidence degrees of non-linearity and heterogeneity, hypothesized to be related to pump function. Investigation of these heterogeneities was achieved by measuring AUC for each spectrographic slice. Measurement of AUC allowed for quantification of spectrogram slice morphology across the range of frequencies sampled. AUC were calculated and compared

for all acoustic measurements taken during the patient's course of therapy. The patient was auscultated the day prior to his first pump exchange surgery with LDH 1,726 U/L and significant clot formation, and again following post-operative stabilization, at which time the LVAD was presumably free of clot. Though differences in AUC were not statistically significant (p=0.079), Figures 8.6 and 8.7 indicate a clear delineation between the thrombosed and patent pumps.

Figure 8.6: Exchange # 1: Spectral Comparison from Clotted and Patent Pumps

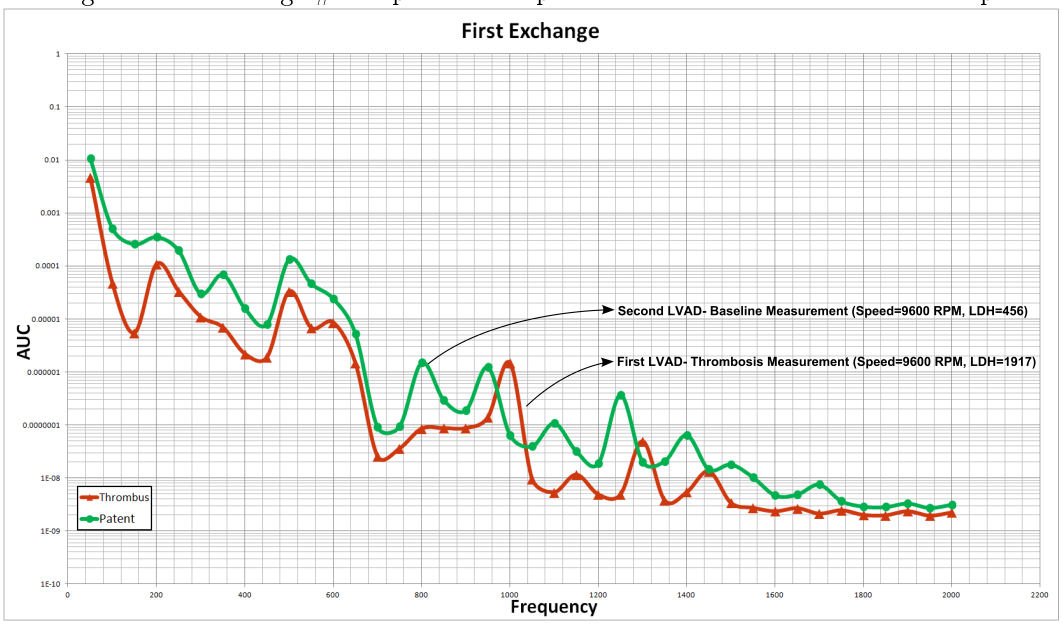

Figure 8.6 shows the difference in AUC for this patient's first (clotted) and his second (patent) LVADs. Though these curves represent the acoustic signatures generated by two separate pumps, the engineering standards for the production of these LVADs are exacting and it is unlikely individual pumps produce unique acoustic profiles. The curves in Figure 8.7 represent the acoustic signatures for the patient's second pump exchange and exhibit a similar trend to those in Figure 8.6. These curves suggest that a reduction of amplitude with mirroring of predominant curve morphology may be indicative of a departure from a baseline acoustic signature caused by the presence of a thrombus. Acoustic data were collected during the patient's second admission for hemolysis as well. Each sample collected at this time shows higher amplitude than the sample from the clotted pump. However these data are difficult to compare accurately due to periodic

Figure 8.7: Exchange #2: Spectral Comparison From Clotted and Patent Pumps

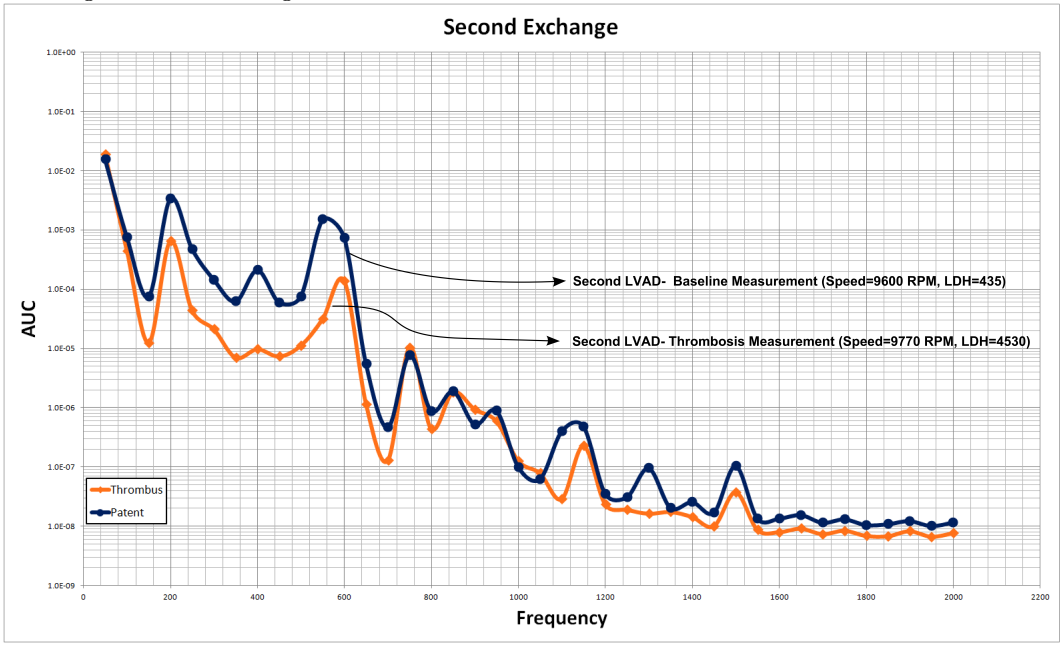

changes in LVAD speed during this admission. Increases in LVAD speed result in increases in harmonic frequency, making intersample comparison difficult when speeds have been altered for clinical purposes. Consequently, Figures 8.6 and 8.7 compare acoustic measurements taken at equivalent speeds: 9,400 RPM and 10,200, respectively. Additionally, despite continually elevated LDH levels during his second course of hemolysis, it is unclear at what point thrombus began to form and at what point it became significant enough to affect pump acoustics. Consequently, we compared the AUC from a sample taken the day before his second pump exchange (with LDH values of 4530 U/L) with AUC from a measurement taken shortly after his first exchange (Figure 8.7). We presume that these represent clotted and patent pumps. The curves shown in Figure 8.7 demonstrate a similar relationship to those shown in Figure 8.6. We suggest that this mirroring of the AUC curves, with reduction in amplitude in the clotted pump is indicative of thrombus formation in the HeartMate II.

8.2.3 Clinical Events - Patient 2

In June of 2012 a 24 year old Caucasian male weighing 138 kg was admitted to our Heart and Vascular Institute following a syncopal episode. At that time the patient was diagnosed with non-ischemic dilated cardiomyopathy with worsening systolic heart failure. The patient had a history of obesity, obstructive sleep apnea, recurrent syncope, and severe migraine headaches. Evaluation for LVAD placement revealed a profoundly hypokinetic LV with an end-diastolic diameter of 3.5 cm and ejection fraction of 17%. The decision was made to implant the patient with a HeartMate II LVAD as a bridge to transplantation. The surgery was unremarkable and the patient made an expeditious recovery with stable laboratory values, rapid weaning from inotropes, stable pump function, and discharge on postoperative day 11. The patient remained stable on LVAD therapy with minor rehospitalizations for diarrhea, headache, and syncope for 24 months. Approximately 2 years after initial LVAD implantation the patient was readmitted for increasing shortness of breath, severe pain in the left upper quadrant overlying the device location, and device controller alarms. No significant fluid collection was observed in the area around the LVAD in either CT or X-Ray imaging studies and no infectious agents were cultured. In the context of an elevated LDH to 1201 U/L and continued LVAD alarms, the patient was taken into the operating room for surgical exchange of his LVAD. Upon explantation, extensive thrombus was found within the inflow cannula, device housing, and outflow cannula. The thrombus had completely obstructed flow through the LVAD, rendering it totally ineffective.

It is possible that the diffuse chest pain the patient felt over the area of the LVAD was resultant to heat generated within the stagnant pumping chamber. Without blood flow to wash impeller bearings and cool the device motor, it is conceivable the device reached a temperature sufficient to cause significant discomfort. The patient was implanted with a new device and proceeded through a relatively uncomplicated recovery, with discharge on postoperative day 15. Despite feeling well at an outpatient visit ten days after discharge, the patient was airlifted to our center 14 days after discharge with diaphoresis, shortness of breath, tachypnea, and an international normalized ratio (INR) of 12.5. Shortly after arrival, the patient had an acute subarachnoid hemorrhage with acute hydrocephalus and was found to be brain dead. There was no indication of a linkage between this cerebral bleed and the previous LVAD thrombosis.

Figure 8.8: LVAD Thrombus - Patient 2

Top: explanted HeartMate II showing clot at the outflow. Bottom: complete occlusion of the inflow.

8.2.4 Spectral Analysis - Patient 2

Acoustic data were collected for this patient prior to and following his exchange for thrombosis. The samples were compared in the same manner used for Patient 1, and it was noted that peak harmonic amplitude again occurred at intervals associated with device speed. It was noted that the AUC curves for the clotted and patent data again evidenced strikingly similar morphology, with most peaks occurring at equivalent frequencies. Likewise, the curve representing the thrombosed sample was considerable lower in amplitude than that of the patent sample, the same trend noted in Patient 1. Unlike Patient 1, however, there was no overlap between the curves (Figure 8.9). This may be due to the complete occlusion of Patient 2's LVAD which was entirely prohibitive to flow through the device (Figure 8.8). The difference in AUC, therefore, may represent difference in noise generated by flow. Interestingly, the separation in curves was minimal at approximately 1000 Hz, the same location where the curves overlapped in Patient 1. This trend appears to be driven by an increase in spectral energy in the fifth and sixth harmonics in each of the clotted pumps.

Figure 8.9: Patient 2 Exchange: Spectral Comparison From Clotted and Patent Pumps

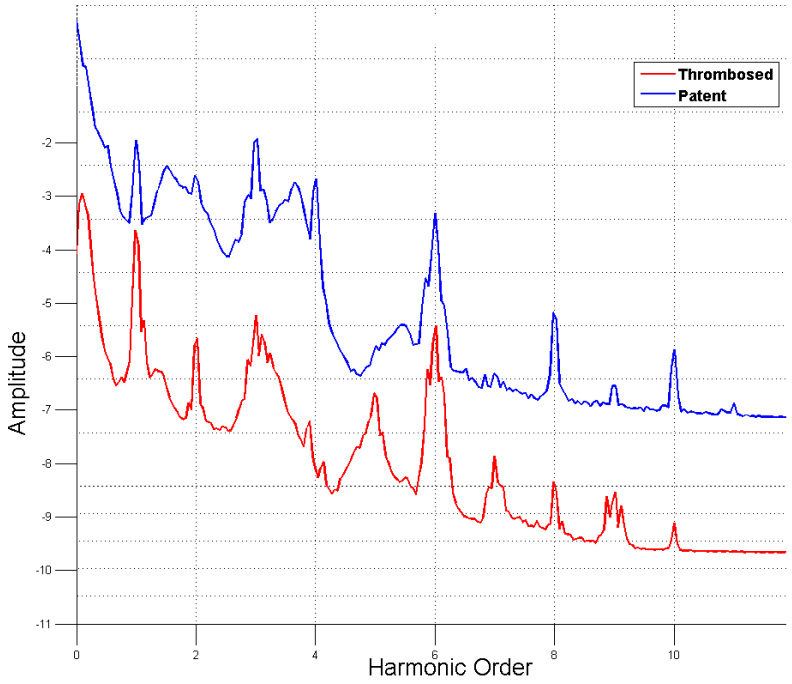

Part IV

Results: Studies in the HeartWare HVAD and Jarvik 2000

Chapter 9

Results from In Vivo Studies in the HVAD

The HeartWare HVAD, discussed at length in section 3.2, is currently an investigational device. At the time of writing it is approved only for implantation as a bridge to transplant, not as destination therapy. Its market-share remains limited in the United States, and it is used only occasionally at Advocate Christ Medical Center. Consequently, we were not able to obtain an unused device for laboratory testing. The results presented herein are, therefore, limited to *in vivo* studies of the HeartWare HVAD.

9.1 Spectrographic Analysis of the HVAD

A spectrogram generated by HVAD acoustics is shown in Figure 9.1. The graph may be interpreted as such: the horizontal axis plots the time course of the sample, while the horizontal axis plots the frequency components of that sample. Amplitude is expressed as heat (color), with darker colors representing higher amplitudes. The repeating harmonic structure is immediately evident as harmonic "bands," frequency ranges of higher amplitude. It is also evident that the lowest harmonic bands, occurring between the frequency ranges of 30-70 Hz, are the highest in amplitude and that amplitude attenuates as frequency increases.

A spectrogram slice, a plot of amplitude (vertical axis) versus frequency (horizontal axis), allows for

Figure 9.1: Spectrogram of *In Vivo* Operation of the HVAD at 3,000 RPM

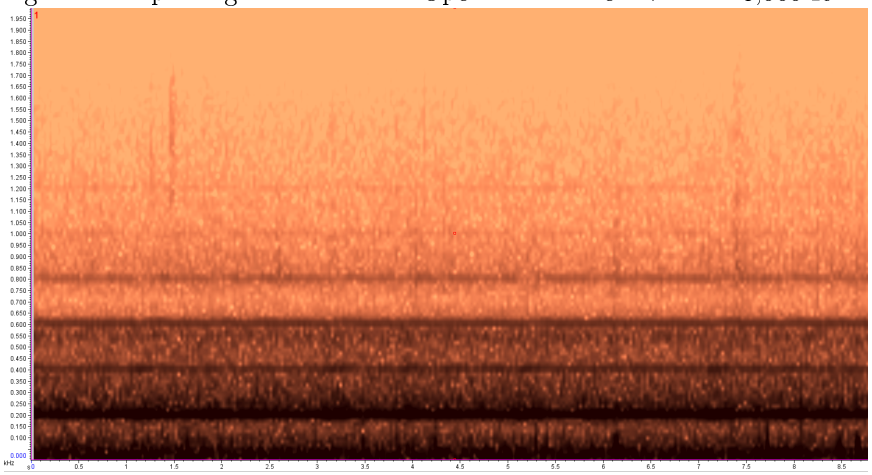

nuanced analysis of an acoustic sample's frequency components. The spectrogram slice for the acoustic sample plotted in Figure 9.1 is provided in Figure 9.2. Peaks in the spectrogram slice correspond to harmonic bands in the spectrogram, and accordingly, are repeated in a regular manner. The spectrogram slice allows improved analysis of frequency ranges between harmonics. As described in Part II, Raven Pro software allows for automated detection of the frequency with maximum amplitude within a selected range. This tool was found to be exemplary for determining the precise frequency peak location in the spectrogram slice, as well as its corresponding amplitude value. Automated peak detection was used to record peak frequencies and amplitudes for all harmonics. It appeared that the frequencies of the harmonics expressed in the spectrogram and spectrogram slice were related to device speed.

9.2 *In Vivo* Ramp Study with the HeartWare HVAD

A series of acoustic measurements were made during a clinical ramp study, in which HVAD speed was increased from 1,800 RPM to 2,800 RPM in a single patient with visualization using echocardiography. The clinical purpose of this test is to determine the optimal speed to enhance unloading of the left ventricle, reduction of mitral regurgitation, and cardiac support. Peak harmonic frequency was calculated for each harmonic band was plotted for 100 RPM increments between 1,800 RPM and 2,800 RPM (Figure 9.2). Speed

and peak harmonic frequency increased in a linear fashion, as in the HeartMate II.

Figure 9.2: Acoustic Analysis: *In Vivo* Ramp Study

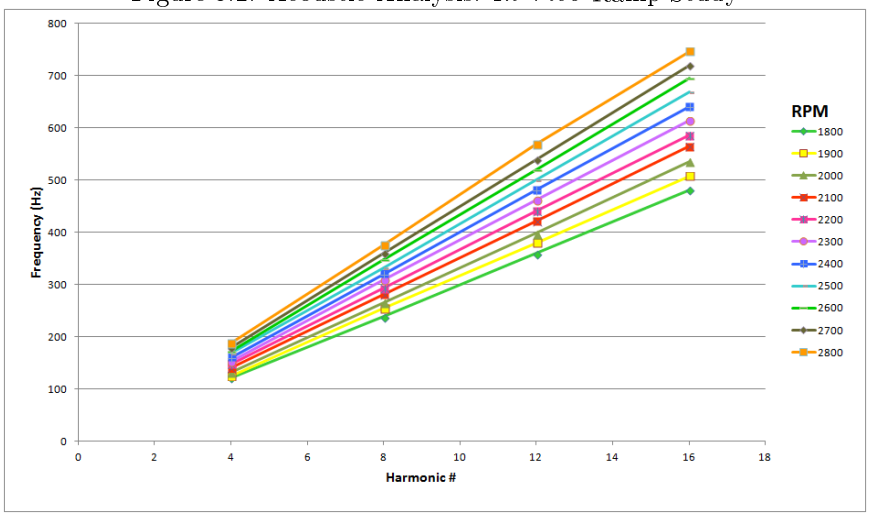

The HVAD operating speeds, between 1,800 and 4,000 RPM, are significantly lower than the speeds typical of HeartMate II operation. Accordingly, first harmonic frequencies occur between 30 and 66 Hz, a range also occupied by noise from heart valve closure, fluid flow in the heart and large vessels, and air flow in the lungs[58]. Analysis of HVAD spectrograms does not indicate the presence of a first harmonic, potentially due to the low signal-to-noise environment in which it is expected to occur. However, the second and third harmonics are also notably absent in all HVAD spectrograms, both *in vivo* and *in vitro*. In fact, only the fourth, eighth, and twelfth harmonics are consistently present, with less frequent occurrence of the 16th and 20th. Consequently, Equation 12, a slight modification of equation 11, predicts the presence of harmonic bands at 4th-integer multiples:

$$\lambda_{H(HVAD)} = \frac{(4n \times RPM)}{60} \tag{9.1}$$

9.3 Acoustic Model In 7 Stable HVAD Patients

Acoustics were sampled in 7 HVAD patients who were known by the clinical service to be relatively free of complications and stable at the time of auscultation (Table 9.1)

Table 9.1: Baseline Demographics for 7 Stable HVAD Patients

Patient #	**1**	**2**	**3**	**4**	**5**	**6**	**7**
Days to Ausc	1191	177	603	631	825	1112	1015
Age (years)	71	70	34	81	62	74	71
BMI (kg/m²)	31.1	28.3	33.2	30.9	31.8	30.6	30.6
Race	Caucasian	AA	Caucasian	Caucasian	Hispanic	Caucasian	Caucasian
Indication	IDCM	NICM	ICM	IDCM	IDCM	ICM	ICM
RPM	3000	2660	2600	2745	2760	2800	2700
Flow (L/min)	4.9	4.1	4.3	4.6	4.1	4.9	4.4
Power (Watts)	5.3	4	4	4.4	4.4	4.4	4.3
Sys BP (mmHg)	96	100	87	102	95	94	98
Dia BP (mmHg)	84	81	76	58	–	–	–
Pulse Rate	80	70	74	70	83	75	88
RVDd (cm)	3.5	3.0	2.6	3.9	3.0	3.5	4.4
LVDd (cm)	3.5	5.4	6.0	5.7	7.2	5.9	5.2
Ejection Fraction (%)	30	25.0	20.0	27.0	10.0	30.0	20.5
Pulm. Sys. BP (mmHg)	33.9	28.0	23.3	–	29.1	16.0	–
Creatinine (mg/dL)	1.8	1.4	1.2	1.2	1.6	0.9	1.2
Hemoglobin (g/dL)	9.0	8.6	12.7	11.8	13.1	12.7	9.7
LDH (Units/L)	319.0	325.0	194.0	251.0	234.0	271.0	287.0
INR	2.0	2.1	3.2	1.6	2.1	2.2	2.2

Abbreviations: Days to Ausc. (number of days between implant and auscultation), RPM (device revolutions per minute at time of auscultation), PI (device pulsatility index at time of auscultation), Sys BP (systolic blood pressure), Dia BP (diastolic blood pressure), RVDd (right ventricular dimension in diastole), LVDd (left ventricular dimension in diastole), Pulm. Sys. Pressure (pulmonary systolic blood pressure), Plasma free Hb (plasma free hemoglobin), LDH (lactate dehydrogenase), INR (International normalized ratio), ICM (ischemic cardiomyopathy), NICM (non-ischemic cardiomyopathy), NIDCM (non-ischemic dilated cardiomyopathy), AA (African American).

Acoustic samples from each of these patients were plotted together in Figure 9.2. With normalization of frequency to device speed, preservation of peak harmonic structure is evident. Yet, despite consistency of harmonic peaks, there is notable inter-sample heterogeneity in peak amplitude as well as curve shape between peaks. It should be noted that, in comparison to the HeartMate II, spectral peaks attenuate at a lower frequency in the HVAD (~1000 Hz in the HVAD vs. ~2000 Hz in the HMII).

Figure 9.3: Spectrogram for HVAD Patients 1-7 With Normalization to Harmonic Order

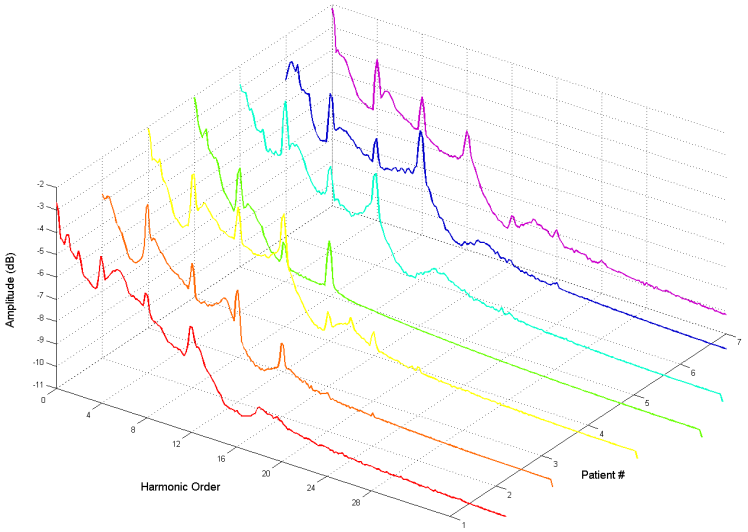

In each of these seven patients measured peak harmonic frequency was compared to predicted peak harmonic frequency (based on Equation 12) across all harmonics using two tailed paired T-Tests. The r-values for all frequency arrays were >0.999, indicating a very strong relationship between predicted and measured peak harmonic frequencies (Table 9.2).

Analysis of HVAD acoustics reveals another trend unique to this pump: the presence of pulsatility over the time sample of the spectrogram with respect to acoustic amplitude. This amplitude fluctuation is periodic with ventricular contraction, but does not occur in all patients or in the absence of pressure variations at the inflow conduit. Figures 9.4, 9.5, and 9.6 demonstrate spectrograms from HVAD patients with low, moderate, and high amplitude pulsatility, respectively.

Table 9.2: Comparison of Acoustic Values in 7 HVAD Patients Against Expected Values

Patient #	Speed (RPM)	Predicted H_0 (λ)	Predicted H_4 (λ)	r-Value Measured λ Versus Predicted λ
1	3000	50.0	200.0	>0.999
2	2660	44.33	177.33	>0.999
3	2600	43.33	173.33	>0.999
4	2745	45.75	183.0	>0.999
5	2760	46.0	184.0	>0.999
6	2800	46.66	186.66	>0.999
7	2700	45.0	180.0	>0.999

Abbreviations: H_0: fundamental frequency (base harmonic), H_4: fourth harmonic frequency

Figure 9.4: Low Amplitude Pulsatility HVAD Spectrogram

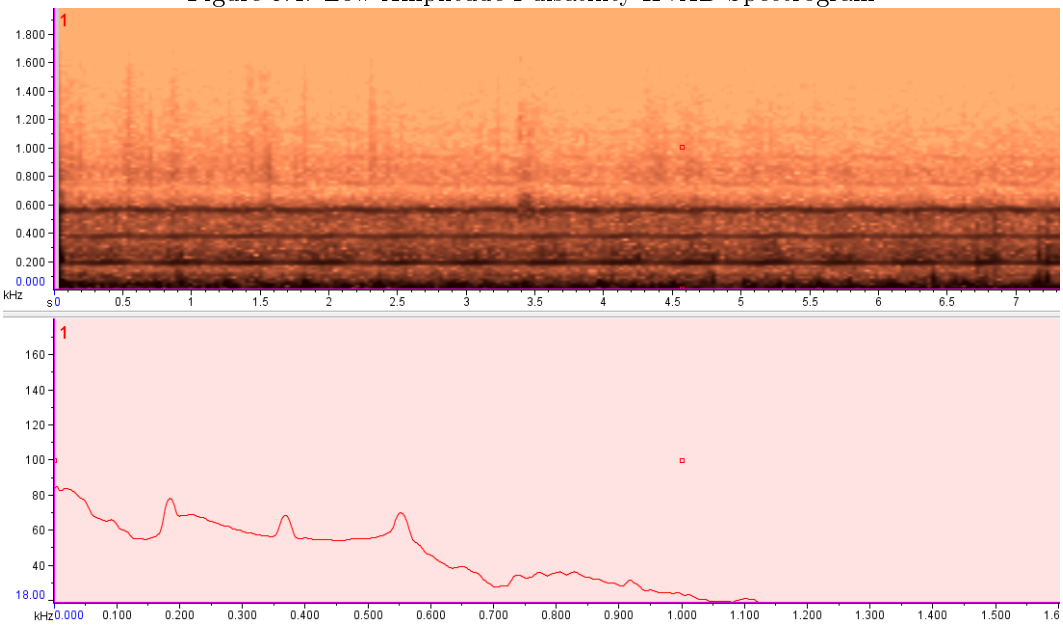

Figure 9.5: Moderate Amplitude Pulsatility HVAD Spectrogram

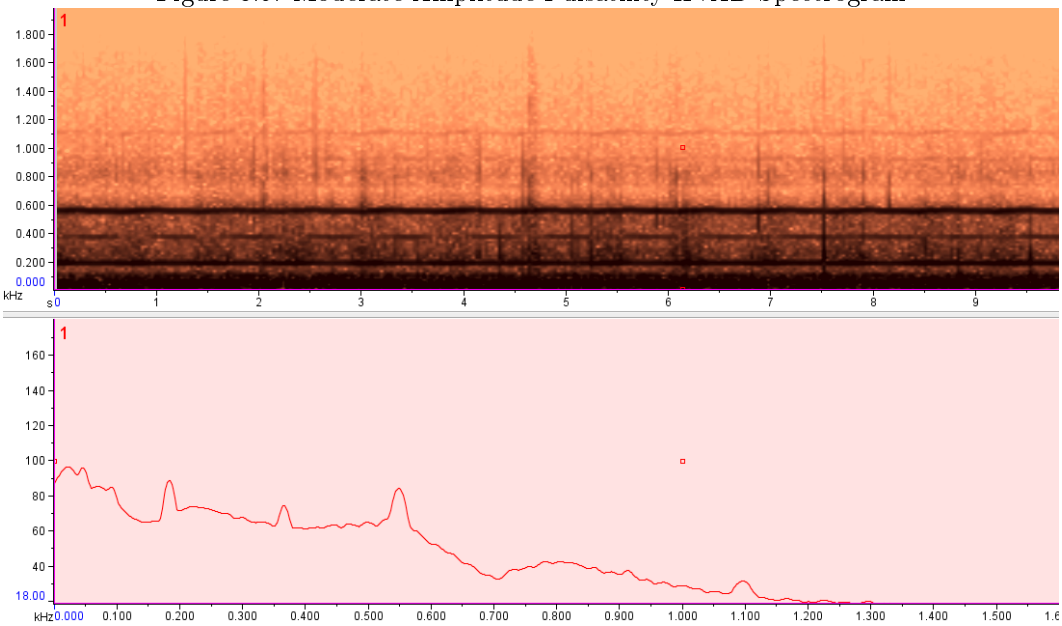

Figure 9.6: High Amplitude Pulsatility HVAD Spectrogram

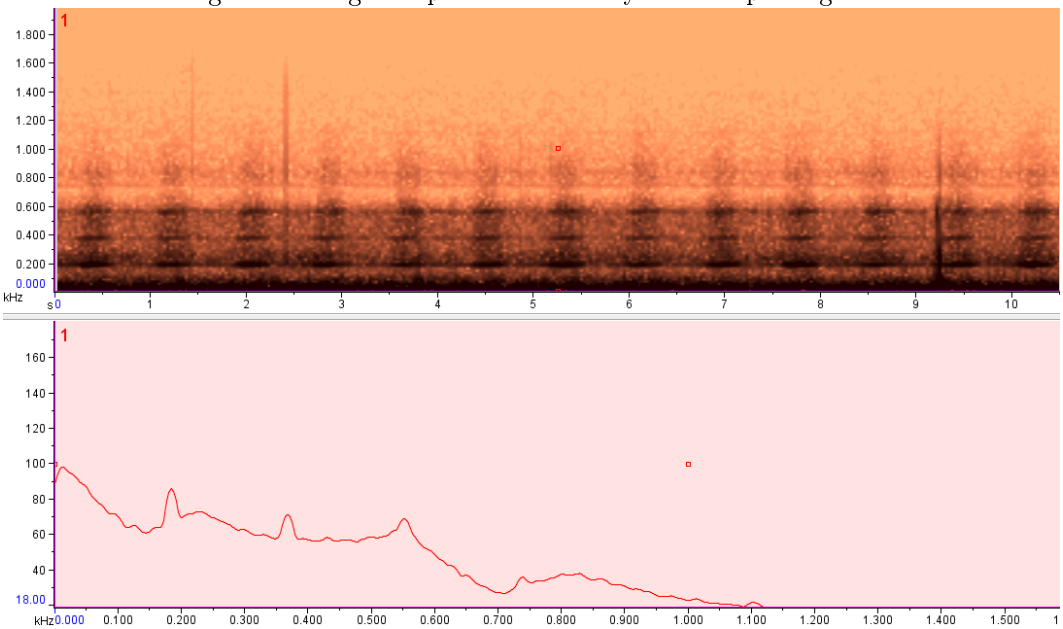

9.4 Thrombosis in an HeartWare HVAD Patient

During the course of this investigation a single patient with a HeartWare HVAD has presented with the need for surgical device exchange due to device thrombus. The clinical events and acoustic signature associated with the episode are presented here.

9.4.1 Clinical Events

An 74 year old Caucasian man who had been stable on HVAD support for approximately 2 years was admitted for dark urine and increasing shortness of breath. Two months prior to this admission the patient had been treated for bacteremia with Enterococcus Faecalis. The patient had been previously implanted at the admitting center (Advocate Christ Medical Center) and followed closely with regularly scheduled clinic visits. The past medical history was significant for ischemic cardiomyopathy, diabetes, hyperlipidemia, previous cerebrovascular accident, and obstructive sleep apnea. At the time of admission, urine was noted to be black in color. He had experienced blood in his urine the previous night and gradually increased fatigue in the preceding weeks. No laboratory or blood chemistry values were able to be drawn due to complications with hemolysis. However, due to evidence of significant hemolysis based on hemoglobinuria and hematuria, as well as elevated device powers and speeds suggesting device thrombosis, the decision was made to take the patient into the operating room for emergent exchange of his HVAD. Though the surgery required intraoperative revision of the aortic graft anastamosis site to effect hemodynamic stability, hemostasis was ultimately obtained. The patient's mediastinal wound was left open to be re-explored the following day. Re-exploration allowed for the control of diffuse oozing from the chest wall. The patient's mediastinal wound was closed subsequently. Postoperative cardiac recovery was unremarkable.

9.4.2 Spectral Analysis

An initial recording was made prior to surgical exchange, while the patient laid supine in the operating room. The patient had been administered complete anesthesia prior to recording and was unconscious. It is not clear if this effects LVAD function. Follow-up recordings to use as comparison against the thrombus recording were made once the patient had become stable postoperatively. Figure 9.7 demonstrates normal

HVAD function at 24 days after the surgical exchange. At this time his LVAD speed was set to 2,800 RPM, generating 4th, 8th, and 12th harmonics at 186.7 Hz, 373.3 Hz, and 746.7 Hz, respectively. Spectrographic analysis reveals peaks at these locations, and is otherwise suggestive of appropriate pump function.

Figure 9.7: Baseline Spectrogram Indicating Proper HVAD Function

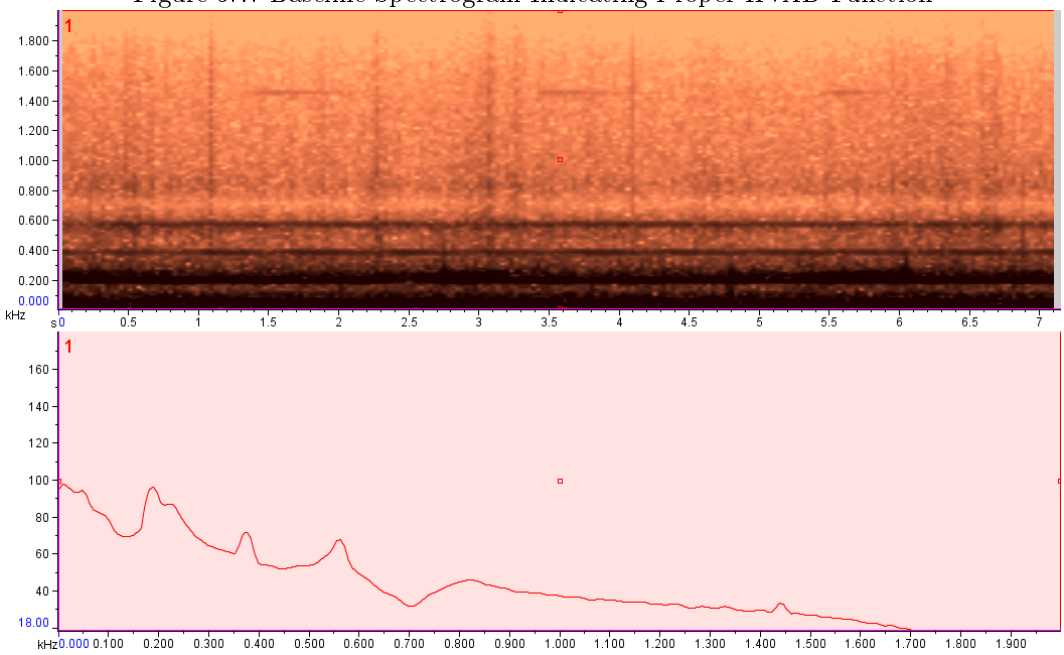

In comparison, Figure 9.8 is the spectrogram and spectrogram slice generated from the measurement taken from the thrombosed HVAD. A unique feature is noted on this spectrogram- the presence of several lower amplitude harmonic bands between 700 and 900 Hz. These bands were not present in the baseline measurement, nor have they been noted in spectrograms generated from any other stable HVAD patient. The bands appear to be four in number and are clustered around the 16th harmonic. These additional bands manifest as 4 smaller peaks in the spectrogram slice between 700-900 Hz. It can be seen that the amplitude of each is less than that of the peaks at the 4th, 8th, and 12th harmonics. However, presuming each peak is an iteration of a larger peak, it also can be seen that their combined amplitude is similar to that of the other peaks.

Figure 9.8: Spectrogram and Spectrogram Slice for Thrombosed HVAD

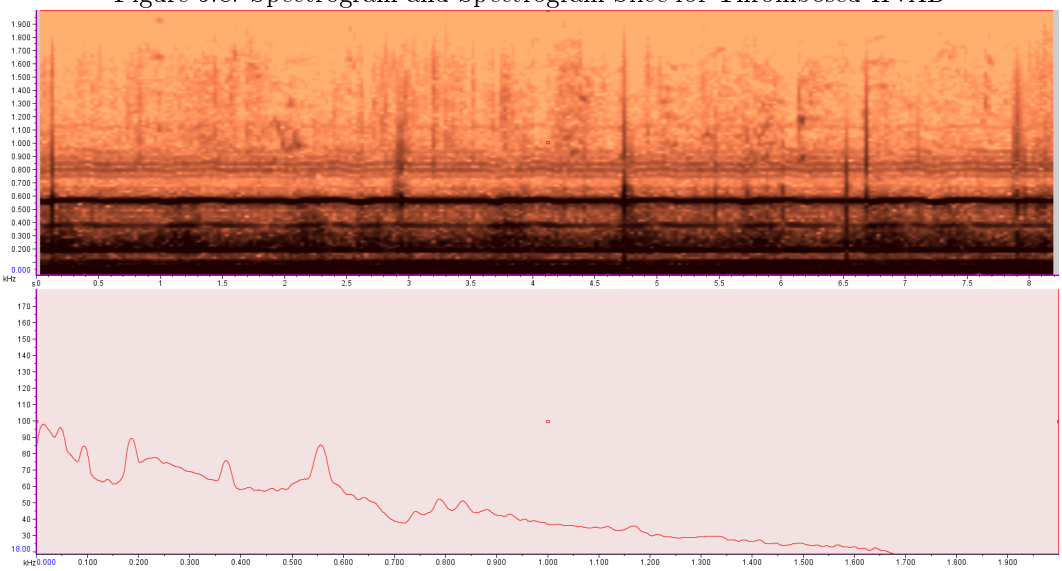

Chapter 10

Results From In Vivo Studies with the Jarvik 2000

10.1 Spectrographic Analysis of the Jarvik 2000

The Jarvik 2000 LVAD is currently undergoing clinical trial for use as destination therapy. The pump investigated in this study was the first implant of a Jarvik 2000 at our center. Accordingly, the results described herein are largely observational and are based on a single patient.

The Jarvik 2000 operates on a similar principal to that of the HeartMate II- an axial flow impeller which is suspended, via mechanical bearings, by fixed inflow and outflow stators and which operates in the range of 8,000 to 12,000 RPM[23]. Despite these similarities in design, the acoustic signature associated with this Jarvik 2000 pump is distinct from those observed in the HeartMate II. Spectrographic analysis reveals the presence of strong harmonic representation at the first, second, and third harmonics, and weak to moderate representation at the fourth and fifth harmonics with subsequent attenuation of signal (Figure 9.10). While frequency localization analysis shows that these harmonics occur within a small range of their predicted frequency, harmonic bands two, three, and four exhibit cyclical modulation of both frequency and amplitude. As discussed in the HVAD, modulation of amplitude has been observed in other pump

designs and is a result of pulsatile flow across the device impeller, however, this is the only instance in which modulation of frequency has been observed in an LVAD spectrogram.

Figure 10.1: Spectrogram and Spectrogram Slice for the Jarvik 2000 LVAD

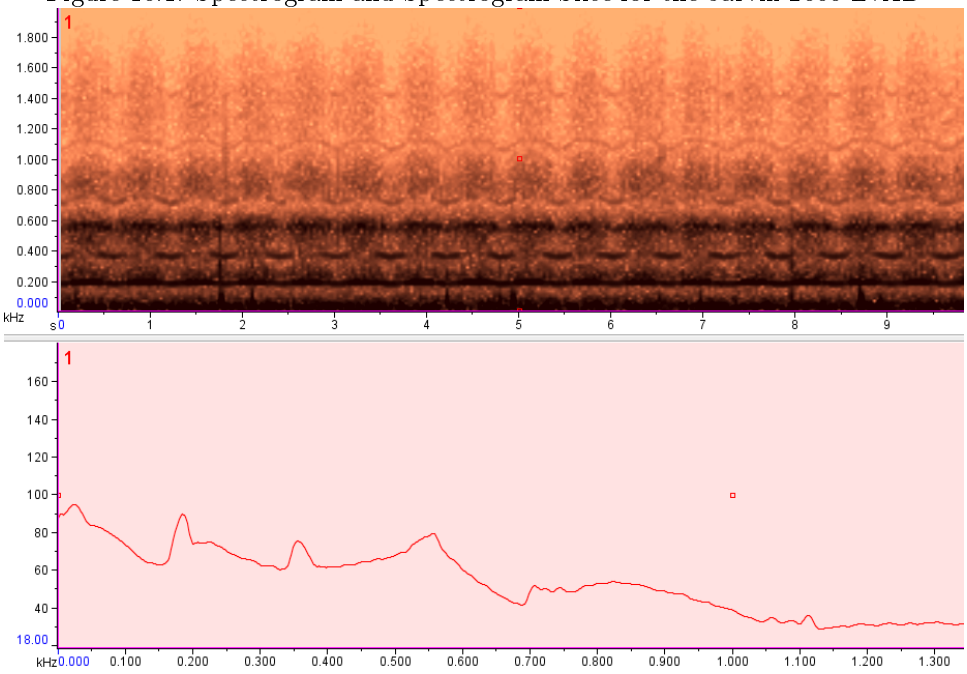

Part V

Discussion and Conclusions

Chapter 11

In Vitro and *In Vivo* Studies in the HeartMate II

Preliminary studies with the HeartMate II (HMII) indicated that acoustic analysis with an electronic stethoscope was practical and was sensitive to LVAD generated noise. Harmonic bands are easily detected using a spectrogram to display acoustic data, and harmonic peaks are evident when data are plotted as spectrogram slices (amplitude versus frequency). See Figures 7.1, 7.2. The lack of variability in the spectrogram over time suggests that acoustics generated by the HeartMate II are not changed during the cardiac cycle. Further, cardiac sounds, including those of valve closure, generally occur at frequencies less than 200 Hz, and are largely distinct from those associated with LVAD function. The relationship between peak harmonic frequency and LVAD speed was expected. Equation 12 was established in theory prior to the execution of *in vitro* studies. The clear linear relationship between peak harmonic frequency at all harmonics and device speed is illustrated by Figure 7.4. This observation led to the hypothesis that acoustic sampling with the Littmann 3200 electronic stethoscope and subsequent post-processing and analysis with Raven Pro and Matlab software is sensitive to LVAD acoustics.

This hypothesis was tested using a Bland-Altman analysis and tests of correlation. Bland-Altman compares two techniques for measuring a continuous variable by plotting the difference of the two measurements

on the y-axis against the mean of the two measurements on the x-axis. The tight clustering of data and small difference (y-axis) values across all frequencies indicates close agreement between the predicted and measured values. Strong r-values at all speeds further indicates agreement between the two measures.

With sufficient evidence for the sensitivity of the methodology to peak harmonic frequency location, *in vitro* experiments investigating the effects of fluid pressure, fluid viscosity, and artificial graft stenosis were undertaken. Though viscosity was increased with serial additions of glycerol, Figure 7.6 indicates no trend in peak harmonic frequency as viscosity rose. Table 7.5 indicates a single significant p-value, but this is likely a result of chance rather than a statistically significant difference between peak harmonic frequency arrays. Correspondingly, amplitude at peak harmonic frequency did not express a trend with increased viscosity, though many p-values assessing significant difference in the peak harmonic amplitude arrays were less than 0.05.

Similar trends were noted in analyses of varied inflow and outflow pressures; peak harmonic frequency showed no pattern with altered pressure nor were differences found to statistically significant, and amplitude at peak harmonic frequency showed no pattern with altered pressure, but many p-values were significant. The results of these experiments with altered viscosity and pressure indicate an independence of device acoustics from fluid viscosity and pressure, and suggest that *in vivo* measurements may be made and compared without correction for blood viscosity or pressure at the inflow and outflow tracts of the HMII.

The purpose of the *in vitro* studies was to inform data collection and analysis *in vivo*. Comparison of peak frequency values measured in 10 stable HMII patients with peak frequency values measured, at corresponding speeds, *in vitro* provided a link between *in vivo* and *in vitro* acoustic analysis. The strong correlations noted between the *in vitro* and *in vivo* arrays indicated that the artificial circulatory system and gel phantom were an appropriate model for the physiological circulatory system and the thoracic cavity. Further, the close agreement between these two models suggests that neither the thoracic cavity nor the experimental acoustic environment caused significant frequency shifts in the measured ranges. Curve morphology, plotted as area under the curve (AUC), is largely preserved between *in vitro* and *in vivo* measurements taken at the same speed (Figure 8.3). However, both amplitude and AUC were lower *in vivo* than *in vitro* for all patients, as demonstrated with Patient 4 in Figure 8.3. This is likely due to amplitude attenuation in the chest where the acoustic environment is considerably more complex than the gel phantom used *in vitro*; muscle, bone,

fibrous tissue, and fluid may reduce the magnitude of acoustic transmission.

Comparison of peak frequency values measured *in vivo* against expected values generated strong correlations, further demonstrating the sensitivity of the methods in live patients. With positive results *in vivo* and *in vitro* we sought to test the sensitivity of the method to device malfunction. Partial occlusion of the HMII outflow graft *in vitro* resulted in a reduction in amplitude with preservation of curve morphology compared to a baseline measurement (Figure 7.12). Similar findings were reported by Hubbert et al. who detected a reduction in spectral amplitude when ball valves were used to occlude the inflow and outflow conduits of a HMII LVAD *in vitro* [31]. Three episodes of device thrombosis requiring surgical exchange provided the opportunity to investigate potential changes in HMII acoustics resulting from thrombus formation *in vivo*. In Patient I the average correlation between predicted peak frequencies and measured peak frequencies was strong (r=0.998). When measured separately, the correlation for measurements taken from the clotted pumps was r=0.999, while the correlation for measurements taken from the patent pump was r>0.999, and the correlation for the hemolyzing pump was r=0.999. Though these results are identical to those found in the 10 stable patients without device thrombosis, they indicate that the frequency of each harmonic peak of the HMII acoustic signal are not significantly altered in the presence of pump thrombosis. Importantly, however, these curves exhibit a similar pattern to that observed in Figure 7.12, showing a reduction of amplitude with mirroring of predominant curve morphology. This trend was again noted when the patient underwent a second exchange for device thrombosis. A second patient, whose HMII LVAD was also exchanged for severe thrombosis of the HMII LVAD again demonstrated the same trend observed in Patient 1- reduction of amplitude with mirroring of curve morphology. Based on these three instances noted *in vivo*, paired with the simulated thrombosis created *in vitro*, we suggest that the presence of thrombus material in the HMII LVAD results in a reduction in the amplitude of noise produced by operation at a given speed. It is unclear, however, whether this is the result of impaired fluid flow through the device or another mechanism such as damping of noise by the clot tissue itself.

Though reduction in amplitude seems to be characteristic of LVAD thrombosis, in each case in which spectra were compared, minimum amplitude separation occurred at the 6th harmonic, between 800 and 1,200 Hz. In all cases of thrombosis in Patient 1 and Patient 2, the curves representing the patent and thrombosed spectral energy distribution overlapped in this frequency range (Figure 11.1). The cause of this trend is not

Figure 11.1: Comparison of Spectral Energy in Clotted and Patent HeartMate II

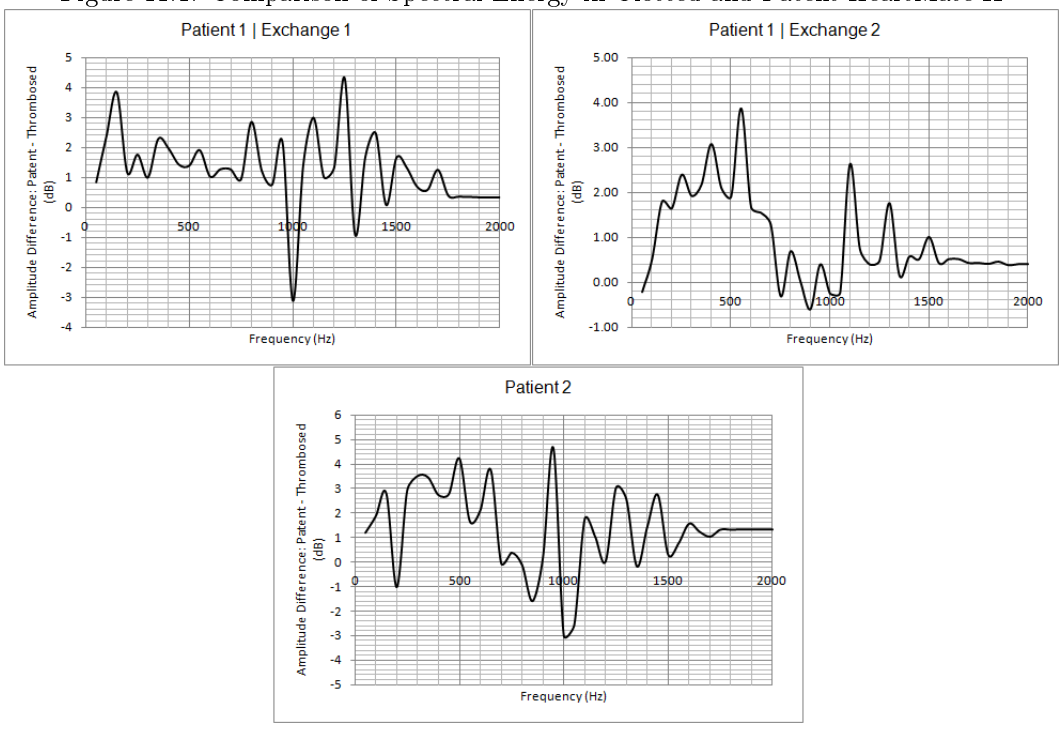

Legend: Difference in amplitude across the measured frequency range 0-2000 Hz is displayed for all exchanges analyzed in Part III. Each graph shows lowest difference in amplitude in the frequency range of the 6th harmonic (between 800 and 1200 Hz).

clear. However, it is possible the difference in spectral energy may reflect a difference in noise generated by flow. Modal analysis did not reveal any inherent resonances in the device housing, leading to the conclusion that all acoustic behavior measured in the sample range 0-2000 Hz is resultant to LVAD operation.

Chapter 12

Comparison of Acoustics in the HeartMate II, HVAD, and Jarvik 2000

12.1 The HeartMate II

The HeartMate II is typically operated in the range of 8400 to 9800 RPM, corresponding to a first harmonic frequency range of 143.3-163.3 Hz. Spectrographic analysis of most patients revealed the presence of harmonic bands at all integer values between 1 and 12 (as demonstrated in Figures 7.1, 8.1, 8.2) with harmonic frequency predicted by equation 11. Additionally, inspection of the spectrogram slices for these figures indicates a trend of decreasing amplitude with increasing frequency. Despite this attenuation, however, the third harmonic, in all *in vitro* and *in vivo* samples is higher in amplitude than harmonics one or two. Amplitude attenuation with increasing frequency is typical in an acoustic signal and is an expected result. The presence of a strong third harmonic, however, is not. We suggest that this is a result of device construction, specifically the HeartMate II impeller's three-bladed design. The dynamic fluctuation created by the rotational motion of the three blades as they spin will occur at three times the frequency of the impeller as a whole, and will add to the amplitude of the extant third harmonic. Any structural defect limiting the patency of the impeller could affect the strength of all of the harmonics. Besides encountering

the three spinning blades of the impeller, blood moving through the HeartMate II LVAD passes across the inflow and outflow stators whose three-vaned structure may also affect the strength of the harmonics. In addition, we suggest that an asymmetric interaction between the impeller and the stator vanes is responsible for the presence of the consistent harmonics observed in the HeartMate II spectrogram. Harmonic presence and strength in the HeartMate II is not only consistent across the measured frequency range but also across the time course of each sample. This is evidenced in the spectrogram by the linear, unbroken bands at each harmonic and indicates that each harmonic is consistent in frequency and amplitude over the course of several cardiac cycles. Again, the acoustic signature of this pump is related to its design and function: as discussed previously, the HeartMate II axial design results in little change in flow through the pump over the course of large pressure changes, as occurs during ventricular systole[51]. Thus, over the time course of acoustic sampling (several cardiac cycles), flow through the pump is relatively constant, impeller speed is unchanged, and subsequently, the frequency and amplitude of all harmonic bands are invariable. This observation is supported by the *in vitro* experiments detailed in sections 5.1.5 and 7.4 in which frequency was found to not modulate with pressure.

12.2 The HeartWare HVAD

The HVAD operates between 1,800 and 4,000 RPM, significantly slower than the speeds typical of HeartMate II or Jarvik 2000 operation. Accordingly, first harmonic frequencies occur between 30 and 66 Hz, a range also occupied by noise from heart valve closure, fluid flow in the heart and large vessels, and air flow in the lungs[58]. Analysis of HVAD spectrograms does not indicate the presence of a first harmonic, potentially due to the low signal-to-noise environment in which it is expected to occur. However, the second and third harmonics are also notably absent in all HVAD spectrograms, both in vivo and in vitro. In fact, only the fourth, eighth, and twelfth harmonics are consistently present, with less frequent occurrence of the 16th and 20th. Consequently, Equation 2, a slight modification of equation 1, predicts the presence of harmonic bands at 4th-integer multiples.

We suggest that the design of the HVAD is responsible for its unique acoustic signature. As previously discussed, the HVAD centrifugal design utilizes a flow path through four radial grooves in the impeller to

generate fluid pressure within the pumping chamber, creating flow and pressure fluctuations at four times its rotational frequency (See Figure 3.3). These fluctuations generate strong dynamic response at the fourth, eighth, and twelfth harmonics that are manifest in spectral analysis (Figure 9.3-9.6). We suggest that a lack of perfect symmetry between the three blades of the impeller and the vanes of the inflow and outflow stators is responsible for the formation of harmonics at all values in the HeartMate II. While it has been shown previously that unstable malrotation in a centrifugal LVAD may be accompanied by characteristic acoustic changes, the relationship between impeller stability and the presence of additional HVAD harmonics has not been investigated[78]. Though further research is needed, we suggest that an imbalance in the finely engineered impeller may result in generation of harmonics not seen in a properly functioning pump. Analysis of HVAD acoustics reveals another trend unique to this pump: the presence of pulsatility over the time sample of the spectrogram with respect to acoustic amplitude (Figure 3.4). This amplitude fluctuation is periodic with ventricular contraction, but does not occur in all patients or in the absence of pressure variations at the inflow conduit. We suggest that amplitude modulation *in vivo* is resultant to changes in head pressure across the HVAD during systole and diastole. As described in section 3.2, flow through the HVAD is highly sensitive to head pressure, and is periodic with the cardiac cycle. It seems that loading and unloading of the pump during systole and diastole causes the amplitude pulsatility demonstrated in Figure 9.6. We suggest, further, that the intensity of amplitude modulation is related to the degree of pump loading during systole, and consequently to the degree of ventricular contraction. Figures 9.4, 9.5, and 9.6 indicate low, moderate, and high pulsatility in three patients. It is likely that reduced left ventricular contractility in the patient with low pulsatility generated more constant pressures at the inflow of the HVAD, while increased contractility in the patient with increased pulsatility generated larger pressure fluctuations with ventricular systole and diastole. As pressure fluctuates with the cardiac cycle, so too does the loading of the device, and the acoustics produced to maintain a constant device speed. *In vitro* experiments in which inflow pressures were cyclically decreased and increased by partial occlusion of the soft tubing above the inflow conduit generated pulsatile flow and wattage waveforms on the HeartWare clinical screen. Subsequent acoustic analysis revealed amplitude pulsatility similar to that observed in vivo. The same effect was not observed following this procedure in the HeartMate II. Thus, while HVAD acoustics are affected by pressures and flows across the pump, the degree to which left ventricular contraction contributes to these acoustic changes

remains unclear.

12.3 The Jarvik 2000

Despite similarities in design, the acoustic signature associated with this Jarvik 2000 pump is distinct from those observed in the HeartMate II. Spectrographic analysis reveals the presence of strong harmonic representation at the first, second, and third harmonics, and weak to moderate representation at the fourth and fifth harmonics with subsequent attenuation of signal. While frequency localization analysis shows that these harmonics occur within a small range of their predicted frequency, harmonic bands two, three, and four exhibit cyclical modulation of both frequency and amplitude (Figure 10.1). As discussed in the HVAD, modulation of amplitude has been observed in other pump designs and is a result of pulsatile flow across the device impeller, however, this is the only instance in which modulation of frequency has been observed in an LVAD spectrogram. Unlike the HeartMate II, which is surgically implanted in a preperitoneal pocket at the level of the diaphragm, the Jarvik 2000 pump housing sits entirely within the cavity of the left ventricle[82]. This implies that, differences in device design aside, the acoustic signals detected at the surface of the chest will likely be fundamentally different between the two LVADs due to pump placement alone. We suggest that the relative lack of acoustic signal at frequencies above 1000 Hz is related to deep imbedding of the Jarvik 2000 within the architecture of the abdomen. Further, mechanical vibrations produced by operation of the Jarvik 2000, instead of passing through the relatively akinetic tissue between an implanted HeartMate II and acoustic detection equipment at the epidermal surface, must also pass through the contractile myocardium. The dynamic stiffness and structural properties of the myocardial tissue change with contraction and relaxation of muscle fibers. It is possible that these properties influence the transmission of sound through the heart and surrounding tissues, causing the frequency modulation observed at the surface of the chest.

Chapter 13

Conclusion and Future Studies

This study establishes the use of an electronic stethoscope with computerized post-processing as a simple, effective, and sensitive means of quantifying LVAD acoustics in the HeartMate II and HeartWare HVAD. An *in vitro* model was used to test the effects of fluid viscosity, fluid pressure, and artificial stenosis on device acoustics. Though viscosity and fluid pressure were not found to significantly alter acoustics, narrowing of the device outflow graft resulted in a reduction of amplitude compared to a baseline measurement. This same trend was noted *in vivo* when acoustics sampled from three clotted HeartMate II LVADs were compared to patent baseline measurements. It appears, based on this data, that it may be possible to non-invasively detect the presence of thrombus formation in the HeartMate II with this method.

Differences in acoustic signature generated by the HeartMate II, HeartWare HVAD, and Jarvik 2000 LVADs were analyzed and appear to be related to impeller size, shape, and rotational speed, as well as surgical placement of the device itself. These observations will inform further development of a diagnostic tool using electronic auscultation. Finally, it was noted that, in a single patient with HVAD thrombosis, the presence of additional harmonic bands to those observed in baseline measurements may be a result of thrombus formation within the pump housing causing impeller malrotation.

This study establishes a methodology and a means for continuing investigation. Future study may inform the relationship between clinical variables like volume status, heart rate, myocardial viability, ventricular strain, and device acoustics. Enrollment of a large cohort tracked over time would allow for an understand-

ing of how device acoustics may change on a day to day level. Further, by establishing a protocol with implementation of transfer of acoustic data by the patient at home, LVAD operation may be monitored with improved resolution. A mobile medicine protocol will allow investigators to analyze device acoustics in the days prior to an admission or the occurrence of device dysfunction to determine if there are detectable changes associated with the onset of that event.

Future study will also need to perform *in vitro* studies using an HVAD. This study was limited to only *in vivo* analysis of HVAD spectra, making it difficult to test and understand the effects of pressure, viscosity, and artificial stenosis on the centrifugal pump's acoustics. Currently the Jarvik 2000 device remains investigational and is used very rarely. If, in the future, the pump becomes more widely implemented, appropriate *in vitro* and *in vivo* studies should be completed. Current thought dictates that the future of mechanical circulatory support will shift towards partial support with much smaller, intravenous or intraarterial pumps. Early trials have begun with these pumps, which operate at higher speeds than current devices (on the order of 20,000 RPM). It will be important to continue to investigate new devices as they become important parts of therapy for advanced heart failure.

Bibliography

[1] A Aggarwal, A Gupta, S Kumar, JA Baumblatt, S Pauwaa, C Gallagher, A Treitman, P Pappas, A Tatooles, and G Bhat. Are blood stream infections associated with an increased risk of hemorrhagic stroke in patients with a left ventricular assist device? *ASAIO J.*, 58(5):509–513, 2012.

[2] A Aggarwal, R Pant, S Kumar, P Sharma, C Gallagher, AJ Tatooles, PS Pappas, and G Bhat. Incidence and management of gastrointestinal bleeding with continuous flow assist devices. *Ann. Thorac. Surg.*, 93(5):1534–1540, 2012.

[3] GH Bardy, KL Lee, and Mark DB. Amiodarone or an implantable cardioverter defibrillator for congestive heart failure. *N. Engl. J. Med.*, 350:2140–50, 2004.

[4] JE Blair, M Huffman, and SJ Shah. Heart failure in north america. *Curr. Cardiol. Rev.*, 9(2):128–146, 2013.

[5] JM Bland and DG Altman. Statistical methods for assessing agreement between two methods of clinical measurement. *Lancet*, 137(8476):307–310, 1986.

[6] JM Brophy, L Joseph, and JL Rouleau. Beta-blockers in congestive heart failure. a bayesian meta-analysis. *Ann. Intern. Med.*, 134(7):550, 2001.

[7] DJ Burke, E Burke, F Parsaie, V Poirier, K Butler, and D. Thomas. The heartmate ii: Design and development of a fully sealed axial flow left ventricular assist system. *Artif. Organs*, 25(5):380–385, 2001.

[8] NS Cheng. Formula for the viscosity of a glycerol-water mixture. *Ind. Eng. Chem. Res.*, 47:3285–3288, 2008.

[9] JG Cleland, JC Daubert, and E Erdmann. The effect of cardiac resynchronization on morbidity and mortality in heart failure. *N. Engl. J. Med.*, 352:772–6, 2005.

[10] LH Cohn. *Cardiac Surgery in the Adult*, chapter Heart Transplantation, pages 1297–1325. McGraw Hill Medical, 4 edition, 2012.

[11] JA Cowger, MA Romano, P Shah, N Shah, V Mehta, JW Haft, KD Aaronson, and Pagani FD. Hemolysis: a harbinger of adverse outcome after left ventricular assist device implant. *J Heart Lung Transplant*, 33(1):35–43, 2014.

[12] S Crow, D Chen, C Milano, W Thomas, L Joyce, V 3rd Piacentino, R Sharma, J Wu, G Arepally, D Bowles, J Rogers, and N Villamizar-Ortiz. Acquired von willebrand syndrome in continuous-flow ventricular assist device recipients. *Ann. Thorac. Surg.*, 90(4):1263–9, 2010.

[13] Z Dai, Y Peng, HA Mansy, RH Sandler, and TJ Royston. Comparison of poroviscoelastic models for sound and vibration in the lungs. *J. Vib. Acoust.*, 136(5):1–11, 2014.

[14] VJ Dzau. Tissue renin-angiotensin system in myocardial hypertrophy and failure. *Arch. Intern. Med.*, 153(8):937, 1993.

[15] J Fang, GA Mensah, JB Croft, and NL Keenan. Heart failure-related hospitalizations in the u.s., 1979 to 2004. *J. Am. Coll. Cardiol.*, 52(6):428–34, 2008.

[16] JC Fang. Rise of the machines- left ventricular assist devices as permanent therapy for advanced heart failure. *N. Engl. J. Med.*, 361:2282–2285, 2009.

[17] GM Felker, RE Williams, and JM. Hare. Underlying causes and long-term survival in patients with initially unexplained cardiomyopathy. *N. Engl. J. Med.*, 342:1077, 2000.

[18] NM Fine, Y Topilsky, JK Oh, T Hasin, SS Kushwaha, RC Daly, LD Joyce, JM Stulak, NL Pereira, BA Boilson, AL Clavell, BS Edwards, and SJ Park. Role of echocardiography in patients with in-

travascular hemolysis due to suspected continuous-flow lvad thrombosis. *JACC Cardiovasc Imaging*, 6(11):1129–40, 2013.

[19] DK Foot, RP Lewis, TA Pearson, and GA Beller. Demographics and cardiology. *J. Am. Coll. Cardiol.*, 35(5):66B–80B, 2000.

[20] GS Francis, JN Cohn, and G Johnson. Plasma norepinephrine, plasma renin activity, and congestive heart failure: relations to survival ian the effects of therapy in v-heft ii: The vehft va cooperative studies group. *Circulation*, 87:VI140, 1993.

[21] OH Frazier, TJ Meyers, S Westaby, and ID Gregoric. Use of the jarvik 2000 left ventricular assist system as a bridge to heart transplant or as destination therapy for patients with chronic heart failure. *Tex. Heart Inst. J.*, 237(5):631–637, 2003.

[22] OH Frazier, TJ Myers, ID Gregoric, T Khan, R Delgado, and M Croitoru. Initial clinical experiences with the jarvik 2000 implantable axial-flow left ventricular assist system. *Circulation*, 105:2855–2860, 2002.

[23] OH Frazier, TJ Myers, S Westaby, and ID Gregoric. Research and development of an implantable, axial-flow left ventricular assist device: The jarvik 2000 heart. *Ann. Thorac. Surg.*, 71:S125–32, 2001.

[24] HJ Fu. Overview of modal analysis. *Modal Analysis*, pages 15–25, 2001.

[25] AH Goenka, H Wang, and SD. Flamm. Cardiac magnetic resonance imaging for the investigation of cardiovascular disorders. part 2: emerging applications. *Tex. Heart Inst. J.*, 41(2):135–143, 2014.

[26] EZ Gorodeski, EC Chu, JR Reese, MH Shishehbor, E Hsich, and RC Starling. Prognosis on chronic dobutamine or milrinone infusions for stage d heart failure. *Circ Heart Failure*, 2(320-4), 2009.

[27] BP Griffith, RL Kormos, HS Borovetz, K Litwak, and JF. Antaki. Heartmate ii left ventricular assist system: From concept to clinical use. *Ann. Thorac. Surg.*, 71:S116–120, 2001.

[28] T Hasin, S Deo, JJ Maleszewski, Y Topilsky, BS Edwards, NL Periera, JM Stulak, L Joyce, R Daly, SS Kushawaha, and SJ Park. The role of medical management for acute intravascular hemolysis in patients supported on axial flow lvad. *ASAIO J.*, 60(1):9–14, 2014.

[29] International Society For Heart and Lung Transplantation Registry Steering Committee. The registry of the international sociey for heart and lung transplantation: Thirtieth annual report. *J. Heart Lung Transplant.*, 32(10):941–950, 2013.

[30] B Hornig, N Arakawa, D Haussmann, and H Drexler. Differential effects of quinaprilat and enalaprilat on endothelial function of conduit arteries in patients with chronic heart failure. *Circulation*, 98(25):2842, 1998.

[31] L Hubbert, P Sundbom, M Loebe, B Peterzén, H Granfeldt, and Ahn H. Acoustic analysis of a mechanical circulatory support. *Artif. Organs*, Epub 2013.

[32] SA Hunt, WT Abraham, and MH Chin. 2009 focused update incorporated into the acc/aha 2005 guidelines for the diagnosis and management of heart failure in adults: a report of the american college of cardiology foundation/american heart association task force on practice guidelines: developed in collaboration with the international society for heart and lung transplantation. *Circulation*, 119(14):e391, 2009.

[33] R John. Current axial-flow devices- the heartmate ii and jarvik 2000 left ventricular assist devices. *Semin. Thorac. Cardiovasc. Surg.*, 20:3–12, 2008.

[34] H Kamada, Y Imai, M Nakamura, T Ishikawa, and T Yamaguchi. Computational study on thrombus formation regulated by platelet glycoprotein and blood flow shear. *Microvasc. Res.*, pages 83–95, 2013.

[35] F Kaufmann, C Hormandinger, A Stepanenko, A Kretzschmar, S Soltani, T Krabatsch, E Potapov, and R Hetzer. Acoustic spectral analysis for determining pump thrombosis in rotary blood pumps. *ASAIO J.*, 60(5):502–507, 2014.

[36] J Kim, ED Feller, W Chen, and V Dilsizian. Fdg pet/ct imaging for lvad associated infections. *JACC Cardiovasc Imaging*, 7(8):839–842, 2014.

[37] JK Kirklin, DC Naftel, FD Pagani, RL Kormos, LW Stevenson, ED Blume, MA Miller, JT Baldwin, and JB. Young. Sixth intermacs annual report: A 10,000-patient database. *J. Heart Lung Transplant.*, 33:555–564, 2014.

[38] B Krishnan, H Yarmohammadi, P Eckman, and S Adatya. Outflow thrombus in a left ventricular-assist device: Visualization by ct angiography. *J Cardiovasc Comput Tomogr.*, 8(6):473–474, 2014.

[39] SH Kubo, TS Rector, AJ Bank, RE Williams, and SM Heifetz. Endothelium-dependent vasodilation is attenuated in patients with heart failure. *Circulation*, 84(4):1589, 1991.

[40] JA LaRose, D Tamez, M Ashenuga, and C Reyes. Design concepts and principal of operation of the heartware ventricular assist system. *ASAIO Journal*, 56:285–289, 2010.

[41] WC Lee, YE Chavez, T Baker, and BR Luce. Economic burden of heart failure: a summary of recent literature. *Heart & Lung J. of Critic. Care*, 33(6):362–371, 2004.

[42] D Levy. Temporal trends in mortality after diagnosis of heart failure for the four decades between 1950 and 1990. *N. Engl. J. Med.*, 347:1397–1402, 2002.

[43] WC Levy, D Mozaffarian, DT Linker, SC Sutradhar, SD Anker, AB Cropp, I Anand, A Maggioni, P Burton, MD Sullivan, B Pitt, PA Poole-Wilson, DL Mann, and M Packer. The seattle heart failure model: prediction of survival in heart failure. *Circulation*, 113(11):1424–33, 2006.

[44] K Lietz, JW Long, AC Kfoury, MS Slaughter, MA Silver, CA Milano, JG Rogers, Y Naka, D Mancini, and LW. Miller. Outcomes of left ventricular assist device implantation as destination therapy in the post-rematch era. *Circulation*, 116:497–505, 2007.

[45] JA López and JF Dong. Shear stress and the role of high molecular weight von willebrand factor multimers in thrombus formation. *Blood Coagul. Fibrinolysis*, 16(1):S11–S16, 2005.

[46] Q Lu, BV Hofferbert, G Koo, and RA Malinauskas. In vitro shear stress-induced platelet activation: sensitivity of human and bovine blood. *Artif. Organs*, 37(10):894–903, 2013.

[47] FA Masoudi, EP Havranek, and HM Krumholz. he burden of chronic congestive heart failure in older persons: magnitude and implications for policy and research. *Heart Fail. Rev.*, 7(1):9–16, 2002.

[48] AL Meyer, C Kuehn, J Weidemann, D Malehsa, C Bara, S Fischer, and M Struber. Thrombus formation in a heartmate ii left ventricular assist device. *The Journal of thoracic and cadiovascular surgery*, 135(1):203–204, 2008.

[49] AL Meyer, D Malehsa, U Budde, C Bara, A Haverich, and M Strueber. Acquired von willebrand syndrome in patients with a centrifugal or axial continuous flow left ventricular assist device. *JACC Heart Fail.*, 2(2):141–5, 2014.

[50] LW Miller, FD Pagani, and SD Russell. Use of a continuous-flow device in patients awaiting heart transplantation. *N. Engl. J. Med.*, 357:885–896, 2007.

[51] N Moazami, F Kiyotaka, M Kobayashi, N Smedira, KJ Hoercher, and A Massiello. Axial and centrifugal continuous-flow rotary pumps: A translation from pump mechanics to clinical practice. *J. Heart Lung Transplant.*, 20:260–272, 2013.

[52] N Moazami, CA Milano, R John, B Sun, RM Adamson, FD Pagani, N Smedira, MS Slaughter, DJ Farrar, OH Frazier, and HeartMate II Investigators. Pump replacement for left ventricular assist device failure can be done safely and is associated with low mortality. *Ann. Thorac. Surg.*, 95(2):500–505, 2013.

[53] GH Mudge, S Goldstein, and LZ Addonzio. Twenty-fourth bethesda conference on cardiac transplantation. task force 3: recipient guidelines. *J. Am. Coll. Cardiol.*, 22(21), 1993.

[54] SS Najjar, MS Slaughter, FD Pagani, RC Starling, EC McGee, and P Eckman. An analysis of pump thrombus events in patients in the heartware advance bridge to transplant and continued access protocol trial. *J Heart Lung Transplant*, 33:23–34, 2014.

[55] Heart Failure Society of America, J Lindenfeld, and NM Albert. Comprehensive heart failure. *J. Card. Fail.*, 16:e1, 2013.

[56] FD Pagani, LW Miller, and SD Russell. Extended mechanical circulatory support with a continuous-flow rotary left ventricular assist device. *J. Am. Coll. Cardiol.*, 54:312–21, 2009.

[57] JT Parissis, P Rafouli-Stergiou, V Stasinos, P Psarogiannakopoulos, and A Mebazaa. Inotropes in cardiac patients: update 2011. *Curr Opin Crit Care*, 16(5):432–41, 2010.

[58] H Pasterkamp, SS Kraman, and GR Wodicka. Respiratory sounds: Advances beyond the stethoscope. *Am. J. Respir. Crit. Care Med.*, 156:974–987, 1997.

[59] CB Patel, JA Cowger, and A Zuckermann. A contemporary review of mechanical circulatory support. *J. Heart Lung Transplant.*, 33(7):667–74, 2014.

[60] RD Patten, MW Kronenberg, CR Benedict, JE Udelson, D Kinan, D Stewart, S Yusuf, JJ Smith, L Kilcoyne, N Dolan, TR Edens, J Metherall, and MA Konstam. Acute and long-term effects of the angiotensin-converting enzyme inhibitor, enalapril, on adrenergic activity and sensitivity during exercise in patients with left ventricular systolic dysfunction. *Am. Heart J.*, 134(1):37, 1997.

[61] D Pereda and JV Conte. Left ventricular assist device driveline infections. *Cardiol. Clin.*, 29(4):515–527, 2011.

[62] SJ Pocock, CA Ariti, JJ McMurray, A Maggioni, L Køber, IB Squire, K Swedberg, J Dobson, KK Poppe, GA Whalley, and RN; Meta-Analysis Global Group in Chronic Heart Failure. Doughty. Predicting survival in heart failure: a risk score based on 39 372 patients from 30 studies. *Eur. Heart J.*, 34(19):1404–13, 2012.

[63] J Puskas, M Gerdisch, D Nichols, R Quinn, C Anderson, B Rhenman, L Fermin, M McGrath, B Kong, C Hughes, G Sethi, M Wait, T Martin, and A; PROACT Investigators Graeve. Reduced anticoagulation after mechanical aortic valve replacement: interim results from the prospective randomized on-x valve anticoagulation clinical trial randomized food and drug administration investigational device exemption trial. *J. Thorac. Cardiovasc. Surg.*, 147(4):1202–1210, 2014.

[64] JS Raval, PD Wearden, RA Orr, and JE Kiss. Plasma exchange in a 13-year-old male with acute intravascular hemolysis and acute kidney injury after placement of a ventricular assist device. *J. Clin. Apher.*, 25(5):274–7, 2012.

[65] VL Roger, AS Go, and DM. Lloyd-Jones. Heart disease and stroke statistics–2012 update: a report from the american heart association. *Circulation*, 125(1):e2–220, 2011.

[66] T Rossing. *Modal Analysis*. Springer-Verlag, 2007.

[67] TJ Royston, Z Dai, R Chaunsali, Y Liu, Y Peng, and RL Magin. Estimating material viscoelastic properties based on surface wave measurements: A comparison of techniques and modeling assumptions. *J. Acoust. Soc. Am.*, 130(6):4126–4138, 2011.

[68] G Sayer and G Bhat. The renin-angiotensin-aldosterone system and heart failure. *Cardiol. Clin.*, 32(21):21–32, 2014.

[69] MP Siegenthaler, OH Frazier, F Beyersdorf, J Martin, H Laks, and J. Elefteriades. Mechanical reliability of the jarvik 2000 heart. *Ann. Thorac. Surg.*, 81:1752–9, 2006.

[70] Mark S. Slaughter, Joseph G. Rogers, Carmelo A. Milano, Stuart D. Russell, John V. Conte, David Feldman, Benjamin Sun, Antone J. Tatooles, Reynolds M. Delgado, James W. Long, Thomas C. Wozniak, Waqas Ghumman, David J. Farrar, and O. Howard Frazier. Advanced heart failure treated with continuous-flow left ventricular assist device. *New England Journal of Medicine*, 361(23):2241–2251, 2009. PMID: 19920051.

[71] MS Slaughter, CR Bartoli, MA Sobieski, GM Pantalos, GA Giridharan, RD Dowling, SD Prabhu, DJ Farrar, and SC Koenig. Intraoperative evaluation of the heartmate ii flow estimator. *J Heart Lung Transplant*, 28:39–43, 2009.

[72] MS Slaughter, MA Sobieski, C Gallagher, J Graham, J Brandise, and R Stein. Fibrinolytic activation during long-term support with the heartmate ii left ventricular assist device. *ASAIO J.*, 54(1):115–119, 2008.

[73] MS Slaughter, MA Sobieski, D Tamez, T Horrell, J Graham, and PS Pappas. Heartware miniature axial-flow ventricular assist device. texas heart inst j. *Tex. Heart Inst. J.*, 36(1):12–16, 2009.

[74] RC Starling, N Moazami, SC Silvestry, G Ewald, JG Rogers, CA Milano, JE Rame, MA Acker, EH Blackstone, J Ehrlinger, L Thuita, MM Mountis, EG Soltesz, BW Lytle, and NG Smedira. Unexpected abrupt increase in left ventricular assist device thrombosis. *New England Journal of Medicine*, 370(1):33–40, 2014.

[75] RF Steinback, M Croitoru, A Hernandez, TJ Myers, Y Wadia, and OH. Frazier. Echocardiographic evaluation of the jarvik 2000 axial-flow lvad. *Tex. Heart Inst. J.*, 32(263-270), 2005.

[76] KS Sundareswaran, SH Reichenbach, KB Masterson, KC Butler, and DJ Farrar. Low bearing wear in explanted heartmate ii left ventricular assist devices after chronic clinical support. *ASAIO J.*, 59(1):41–45, 2013.

[77] LB Tan, SG Williams, DK Tank, and A Cohen-Solal. So many definitions of heart failure: are they all universally valid? a critical appraisal. *Expert Rev. Cardiovasc. Ther.*, 8:217, 2010.

[78] H Tanishiro, A Funakubo, and Y Fukui. Arterial sound based noninvasive malrotation detection of rotary lvad. *ASAIO Journal*, 50:306–10, 2004.

[79] DO Taylor, J Stehlik, and LB Edwards. Registry of the international society for heart and lung transplantation: twenty-sixth official adult heart transplant report-2009. *J. Heart Lung Transplant.*, 28(10):1007–1022, 2009.

[80] JO Taylor, KP Witmer, T Neuberger, BA Craven, RS Meyer, S Deutsch, and KB Manning. In vitro quantification of time dependent thrombus size using magnetic resonance imaging and computational simulations of thrombus surface shear stresses. *J. Biomech. Eng.*, 139(7), 2014.

[81] LB Ware and MA Matthay. Acute pulmonary edema. *N. Engl. J. Med.*, 353:2788, 2005.

[82] S Westaby, OH Frazier, DW Pigott, S Saito, and RK Jarvik. Implant technique for the jarvik 2000 heart. *Ann. Thorac. Surg.*, 81:1752–9, 2002.

[83] CW Yancy, M Jessup, and B Bozkurt. Accf/aha guideline for the managment of heart failure: a report of the american college of cardiology foundation/american heart association task force on practice guidelines. *J. Am. Coll. Cardiol.*, 62:e147, 2013.

[84] TK Yasar, TK Royston, and RL Magin. Wideband mr elastography for viscoelasticity model identification. *Mag. Res. Med.*, 70:479–489, 2013.

Vita

Education

M.S., Bioengineering- May 2015

University of Illinois at Chicago, Chicago, IL & Christ Advocate Hospital, Oak Lawn, IL

B.S., Biology- May 2012

Cornell University, Ithaca, New York

Published Work

1. Yost G, Gregory M, Bhat G. The Clinical Utility of the MNA-SF® in Advanced Heart Failure- A Short Form Nutritional Assessment in Patients Evaluated for Ventricular Assist Device Placement or Cardiac Transplantation. Nutrition in Clinical Practice. 2014 Oct;29(5):686-91

2. Mohamedali B, Bhat G, Yost G, Tatooles A. Survival on Bi-Ventricular Mechanical Support with Centrimag as Bridge to Decision: A Single Center Risk Stratification. Perfusion. 2014 Dec [Epub ahead of print].

3. Mohamedali B, Yost G, Bhat G. Mechanical Circulatory Support Improves Diabetic Control in Patients with Advanced Heart Failure. 2014 Oct;16(10):1120-4

4. Mohamedali B, Yost G, Bhat G. Changes in Spirometry after Left Ventricular Assist Device Implantation. Artificial Organs. 2015 [Epub ahead of print]

Presentation Work- Conference Abstracts

1.Hemolysis: Predictors of Risk Factors Post Left Ventricular Assist Device Implantation Burhan Mohamedali MD, Gardner Yost, Geetha Bhat MD, PhD. Presented at the American College of Cardiology 2015

2. Handgrip Strength Is a Predictor for Length of Stay in Patients Implanted with Left Ventricular Assist Devices Gardner Yost, Mary Gregory RD, LDN, Geetha Bhat MD, PhD. Presented at the American College of Cardiology 2015

3. The Effects of Pre-LVAD Obesity on Post-LVAD Re-Hospitalizations Burhan Mohamedali MD, Gardner Yost, Geetha Bhat MD, PhD. Oral presentation at the American Heart Association annual meeting 2014

4. The Effects of Pre-LVAD Diabetes on Post-LVAD Outcomes Burhan Mohamedali MD, Gardner Yost, Geetha Bhat PhD, MD. Oral presentation at the American Heart Association annual meeting 2014

5. Pulmonary Function is Associated with Length of Stay and Survival in Patients Receiving Permanent Left Ventricular Assist Devices, Gardner Yost, Burhan Mohamedali MD, David Jandura, Gabriel Sayer MD, Geetha Bhat MD, PhD. Presented at The Heart Failure Society of America 2014

6. The MAGGIC Risk Score is Not an Effective Predictor of Outcomes in an Advanced Heart Failure Population Gardner Yost, Burhan Mohamedali MD, Geetha Bhat MD, PhD. Presented at The Heart Failure Society of America 2014

7. The Clinical Utility of the MNA-SF® in Advanced Heart Failure- A Short Form Nutritional Assessment in Patients Evaluated for Ventricular Assist Device Placement or Cardiac Transplantation, Gardner Yost, Mary Gregory RD, LDN, Geetha Bhat PhD, MD. Presented as oral presentation at NATCO The Organization for Transplant Professionals

8. Use of a Single Circuit to Provide Temporary Mechanical Respiratory and Circulatory Support in Patients with LV Apical Thrombus and Cardiogenic Shock, Gardner Yost, Burhan Mohamedali MD, Geetha Bhat MD, PhD, Antone Tatooles MD. Presented at ASAIO 2014, Washington DC

9. Temporary Biventricular Mechanical Support With CentriMag as Bridge to Decision, Gardner Yost, Burhan Mohamedali MD, Sakthi Sundararajan MD, Pat Pappas MD, Geetha Bhat MD, PhD, Antone

Tatooles MD. Presented at ASAIO 2014, Washington DC

10. Pulmonary Function Decreases Significantly Following Left Ventricular Assist Device Placement, David Jandura, Gardner Yost, Burhan Mohamedali MD, Geetha Bhat MD, PhD Presented at ASAIO 2014, Washington DC

11. Changes in Pulmonary Function in Obese Patients Following Left Ventricular Assist Device Placement, Gardner Yost, David Jandura, Burhan Mohamedali MD, Geetha Bhat MD, PhD. Presented at ASAIO 2014, Washington DC

12. Use of Theophylline to Avoid Permanent Pacing in Post Heart Transplant Sinus Node Dysfunction, Gardner Yost BS, Burhan Mohamedali MD, Sakthi Sundararajan MD, Geetha Bhat MD, PhD. Presented at the World Transplant Congress 2014, San Francisco

13. Utility of Liver Biospies in Patients Undergoing Left Ventricular Assist Devices Implantation Hesam Keshmiri MD, Burhan Mohamedali MD, Gardner Yost BS, Geetha Bhat PhD, MD. Presented at the American College of Gastroenterology 2014, Philadelphia

14. Pre-Implant Glomerular Filtration Rate (GFR) as a Predictor of Adverse Outcomes Post Left Ventricular Assist Device Placement. Burhan Mohamedali MD, Gardner Yost BS, Geetha Bhat PhD, MD. Oral presentation at the International Society for Heart and Lung Transplantation, 2015. Nice, France.

Honors

University of Illinois at Chicago Medical Accelerator for Devices Laboratory, engineering and medicine representative

University of Illinois at Chicago Graduate Student Council, President-Bioengineering

University of Illinois at Chicago Bioengineering Graduate Society, Vice-President

University of Illinois Engineering Magazine, UIC's Face of Engineering 2014- student profile for excellence in engineering

University of Illinois Avery Brundage Scholar, for academic and athletic achievement

United States Under 23 National Rowing Team, World Champions at 2012 FISA World's Regatta, Trakai, Lithuania

Cornell University Academic Honor Roll, for academic excellence

Cornell Rowing Charles Courtney Award, excellence in athletics, and leadership on the Cornell Crew

Cornell Rowing Big Stick Award, for greatest athletic achievement

Red Key Athletic Honor Society, Inductee, Newsletter Writer

Distinguished Leader Award Nominee, Cornell University SOAR committee for exceptional leadership capability